SAFETY EVALUATION OF THE CYCLE 9 CORE RELOAD ANALYSIS FOR WOLF CREEK NON-PROPIETARY VERSION

A copy of this submittal, with attachment, is being provided to the designated Kansas State official.

If you have any questions concerning this matter, please contact me at (316) 364-8831, extension 4553, or Mr. Richard D. Flannigan, at extension 4500.

Very truly yours,

Robert C. Hagan

RCH/jra

Attachment

cc: G. W. Allen (KDHE), w/a
L. J. Callan (NRC), w/a
D. F. Kirsch (NRC), w/a
J. F. Ringwald (NRC), w/a
J. C. Stone (NRC), w/a

Executive Summary

The Wolf Creek Nuclear Operating Corporation (WCNOC) has prepared this Safety Evaluation to support our request for Nuclear Regulatory Commission (NRC) approval of the Technical Specification changes associated with implementation of revised nuclear and core thermal-hydraulic design methodologies.

In 1988, WCNOC committed to the development of an in-house reload design capability which encompassed the nuclear, core thermal-hydraulic, and non-LOCA (Loss Of Coolant Accident) safety analyses. Using nuclear and core thermal-hydraulic design technology licensed from the Babcock & Wilcox Fuel Company and additional technology licensed from the Westinghouse Electric Corporation, topical reports describing the reload design process were submitted to and subsequently reviewed and approved by the NRC. The reload design development project culminated in 1991 with the NRC's issuance of a Safety Evaluation Report which approved the reload design safety evaluation methodology submitted by WCNOC. Subsequently, WCNOC completed an in-house reload design for Cycle 7 operation of the Wolf Creek Generating Station (WCGS).

To guarantee the safe and efficient operation of the WCGS, WCNOC continually reviews analysis methodologies employed in the reload design process. To this end, WCNOC has licensed advanced nuclear and core thermal-hydraulic design technology from the Westinghouse Electric Corporation, which will be implemented for the Cycle 9 reload design. This evaluation supports changes to the Technical Specifications required to implement these advanced analysis methodologies.

The Technical Specification changes described herein are required solely to support changes in analysis methodologies. These Technical Specification changes contain no changes to licensed design parameters from previous cycles nor is there a reduction in the margin of safety to any licensed design parameter. The proposed Technical Specification changes have been evaluated and determined to meet all applicable design criteria.

Table of Contents

WCNOC Implementation of Westinghouse Nuclear & Thermal-Hydraulic Design Methods

List of Tables

WCNOC Implementation of Westinghouse Nuclear & Thermal-Hydraulic Design Methods

List of Figures

1. Introduction

1.1 Purpose

This Safety Evaluation is provided in support of Technical Specification changes required for the implementation of revised nuclear and core thermal-hydraulic design methodologies for Cycle 9 operation of the Wolf Creek Generating Station (WCGS).

1.2 Background

The purpose of a reload design safety evaluation is to confirm the conservative nature of existing safety analysis. The existing safety analysis is defined as the reference analysis which is intended to bound all future plant cycles. Thus, safety analysis input parameters for the reference analysis are selected to bound the values expected for future cycles. For a reload evaluation of a given cycle, if all safety analysis input parameters for the cycle being evaluated are bounded by the values used in the reference analysis, the reference analysis remains valid. For reload parameters which are found to not be bounded by the reference analysis, further evaluation is required. The purpose of this further evaluation is to confirm that the margin of safety, as defined in the plant Technical Specifications, is not reduced.

The reload design safety evaluation methodology employed by the Wolf Creek Nuclear Operating Corporation (WCNOC) for reload design at the WCGS then consists of two parts;

1. An evaluation to establish whether the reload parameters are bounded by the values used in the reference safety analysis.
2. A determination of the effects on the reference safety analysis when any reload parameter is not bounded by the value used in the reference safety analysis.

The reload design safety evaluation process insures that subsequent cycle designs will not result in a reduction of the margin of safety and that all specified design bases are met.

In 1988, WCNOC committed to the development of an in-house reload design capability which encompassed the nuclear, core thermal-hydraulic, and non-LOCA (Loss Of Coolant Accident) safety analyses. Using nuclear and core thermal-hydraulic design technology licensed from the Babcock & Wilcox Fuel Company, and additional technology licensed from the Westinghouse Electric Corporation, topical reports describing the reload design process were submitted to and subsequently reviewed and approved by the Nuclear Regulatory Commission (NRC). The reload design development project culminated in 1991 with the NRC's issuance of a Safety Evaluation Report approving the reload design safety evaluation methodology submitted by WCNOC. Subsequently, WCNOC completed an in-house reload design for Cycle 7 operation of the Wolf Creek Generating Station.

To guarantee the safe and efficient operation of the WCGS, WCNOC continually reviews analysis methodologies employed in the reload design process. To this end, WCNOC has licensed advanced nuclear and core thermal-hydraulic design technology from the Westinghouse Electric

Corporation which will be implemented for the Cycle 9 reload design. This evaluation supports changes to the Technical Specifications required to implement these advanced analysis methodologies.

The Technical Specification changes described herein are required solely to support changes in analysis methodologies. These Technical Specification changes contain no changes to licensed design parameters from previous cycles, nor is there a reduction in the margin of safety to any licensed design parameter. The proposed Technical Specification changes have been evaluated and determined to meet all applicable design criteria.

The analytical methods used to establish the core operating limits are an integral part of the plant Technical Specifications[1]. Specifically, these methods are referenced in the Core Operating Limits Report (COLR, Technical Specification 6.9.1.9). The implementation of Westinghouse nuclear and core thermal-hydraulic analysis methodologies necessitates a revision to Technical Specification 6.9.1.9 and consequently, a revision to Specification 3/4.2.2, "Heat Flux Hot Channel Factor (F_Q)" and Specification 3/4.2.3, "Nuclear Enthalpy Rise Hot Channel Factor ($F^N_{\Delta H}$)."

This document presents a detailed Safety Evaluation defining the nuclear and core thermal-hydraulic analysis methodologies, system models, and integration of these methods into the reload design process. Revisions to the plant Technical Specifications, implementing the revised analysis methodology, follow the Safety Evaluation.

2. Safety Evaluation

2.1 Core Design Methods

The NRC-approved methodology[2] which was used by WCNOC for core design and reactor physics calculations for Cycle 7 and Cycle 8 at WCGS will be replaced. Starting with Cycle 9, this work will be done only with the NRC-approved ALPHA/PHOENIX/ANC (APA) nuclear code system from Westinghouse[3,4].

The Westinghouse APA code system is now installed at WCGS. The primary physics codes included in this sytem are PHOENIX-P, ANC, and APOLLO. APOLLO is a two-group 1-D neutron diffusion code. PHOENIX-P is a 2-D multi-group assembly transport code for Pressurized Water Reactor (PWR) lattice physics constants. ANC is a nodal code used mainly for 3-D core design calculations. ANC is based on nodal expansion methodology, group theory for fuel pin power reconstruction, and the equivalence theorem for homogenization.

WCNOC will use the Westinghouse APA codes without modifications and in accordance with Westinghouse training and approved methods. Benchmarking of APA calculation results for previous cycles at WCGS against measured data has provided further assurance of proper operation of and use of the Westinghouse APA code system.

Westinghouse has provided training in the proper use of the APA code system to the WCNOC core design staff. The WCNOC core design staff has used the APA code system to create core models for WCGS Cycles 1-8. Training has been continuous through regular exchange of information between the WCNOC core design staff and Westinghouse personnel, and through Westinghouse review of the core models of WCGS Cycles 1-8 generated by the WCNOC core design staff.

Performance of these core models of Cycles 1-8 has been benchmarked against plant measurements in the cycles of most interest, Cycles 6, 7 and 8. These cycles are more significant for benchmarking purposes since in several key areas they are closer to the conditions of future WCGS cycles than were Cycles 1-5. These key areas include fuel management (low leakage), fuel design type, burnable poisons, rated thermal power, and moderator temperatures. The benchmarks include rod worths, critical boron concentrations, and moderator temperature coefficients from startup. Also included are the boron letdown curve from core follow, and power distributions from flux maps. These benchmarks are discussed later in this section. From these comparisons, WCNOC has concluded that the reliability (uncertainty) factors used by WCNOC and previously approved by the NRC remain applicable to calculations produced using the Westinghouse APA code system.

2.1.1 Codes

The core physics model is based on the standard NRC-approved set of computer codes from Westinghouse. This set includes the lattice code PHOENIX-P and the nodal code ANC. These codes are used as obtained from Westinghouse without modification and used with methods prescribed by Westinghouse and approved by the NRC. The core modeling flow is shown in Figure 2-1.

A brief description of the major codes and their major applications follows.

ALPHA

ALPHA (Automated Linkage of PHOENIX-P and ANC) is a computer program that automates the generation of PHOENIX-P models and accesses the resulting data banks to generate all cross section information required by ANC.

ALPHA has two major functions. The first is to simplify and standardize the generation of input to the PHOENIX-P code. The second is to build a skeleton ANC depletion deck including the punched cross section data.

ALPHA contains standardized fuel geometry and material information including standard Westinghouse fuel and burnable absorber data. This use of standardized data greatly decreases the probability of individual user input error and speeds the process of assembling a PHOENIX-P input deck. ALPHA also interfaces with the FIGHTH code to generate fuel and clad temperatures.

ALPHA also has the capability to access PHOENIX-P depletion data banks and punch the fuel cross sections in ANC input format. This feature greatly reduces the need for hand-transfer of data and speeds the process of generating an ANC input deck.

PHOENIX-P

The PHOENIX-P code is a two-dimensional, multi-group transport theory code used to generate few-group physics constants as a function of burnup for PWR lattices. These constants include all the data required by ANC; macroscopic cross sections, feedback parameters, microscopic cross sections, discontinuity factors, pin power factors, burnable absorber constants and control rod constants. PHOENIX-P is used most frequently in the unit assembly mode. It can also perform a one-dimensional calculation to generate baffle/reflector constants.

PHOENIX-P solves the neutron transport equation through the use of a nodal method, based on transmission probabilities and response fluxes which preserves the heterogeneity of pin, clad, moderator, and of a standard discrete ordinates method which models the interaction between pin cells and assemblies.

In application, a [

]^{b}.

PHOENIX-P can also be executed in a restart or branch calculation mode. These cases recover unit assembly fuel data from a depletion data bank (geometry, nuclide concentrations, etc.) and branch to a different set of conditions. An example would include "restarting" at cold conditions to generate few-group constants at a reduced temperature. Control rods can be inserted in a restart to generate cross section data for ANC rodded models.

ANC

ANC (Advanced Nodal Code) is a multi-dimensional nodal code for all nuclear core design calculations. It predicts core reactivity, assembly power, rod power, thimble flux and other relevant core parameters.

Three major components form the basis for ANC methodology: a nodal expansion method for nodal solution, the equivalence theory for homogenization, and a group theory for pin power recovery. These techniques coupled within an explicit reflector model make ANC a stand alone code, without reference to a fine mesh discrete calculation.

ANC's accuracy and reasonable run times in three-dimensional calculations make it the model of choice for the bulk of core physics calculations. All the cycle-specific reactivity calculations are performed with ANC, including the boron letdown curve, moderator temperature coefficients, Doppler coefficients/defects, control rod worth, and power coefficients/defects. ANC is also utilized for the full range of pin power distribution calculations. ANC uses a procedure of superposition of the average power, the form factor, and a precalculated pin factor to reconstruct pin-by-pin power distributions. The assembly and pin power calculations are used to confirm F_Q and $F^N_{\Delta H}$ Technical Specification compliance, along with verification that safety analysis local pin power design constraints are satisfied.

APOLLO

APOLLO is a one-dimensional, two-group steady state neutron diffusion theory program. The code utilizes an axial slab geometry. Space-dependent feedback effects due to xenon, samarium, rod position, boron, fuel temperature, and water density are included.

The basic APOLLO model parameters and cross section data as a function of burnup are written onto an APOLLO data bank by collapsing a 3-D model. Accurate one dimensional models can be developed with the APOLLO code by utilizing the 3-D-1-D collapse methodology in ANC.

This quick running code is used for analyses which require large numbers of calculations. The Relaxed Axial Offset Control (RAOC) analysis is a major application of APOLLO where thousands of core configurations are analyzed. APOLLO can also be used to generate integral and differential rod worth shapes.

ALPS

The Automated Loading Pattern Search (ALPS) code is a fuel management tool used to search quickly and reliably for loading patterns. The core physics models and depletion model are sufficiently accurate to provide reasonable estimates of enrichment requirements, cycle length, power distribution and moderator temperature coefficient. The ALPS model can be run independent of any other design code.

ALPS is used as a self-contained fuel management tool to set initial batch size, enrichment, and loading pattern candidates. It has a built-in master library of group constants for current fuel assembly and burnable absorber designs. ALPS obtains information about burned fuel assemblies to be considered for reinsertion from user input or from an ANC data bank. ALPS can also generate its own data banks for use in considering multiple cycle fuel management strategies.

ALPS scans through a large number of loading pattern alternatives quickly, with each pattern being analyzed and depleted. The output to the user contains a variety of loading patterns. From these options the user can select one or more candidates for further analysis. For this stage the user can shuffle loading patterns manually, which are then depleted and analyzed by ALPS.

ALUCARD

The ALUCARD code is used to automatically generate analytic constants for the INCORE code. These constants are calculated directly from a three-dimensional ANC data bank file.

The code generates fuel assembly and fuel rod power constants, fast and thermal fluxes in the instrumentation thimble locations, and constants for rodded planes. ALUCARD also edits values and location of the hot channel and highest power node.

INCORE

INCORE is a data analysis code used to process information obtained by in-core flux mapping. The results are used to verify compliance with power distribution Technical Specifications.

The code compares measured to predicted reaction rates, converts measured reaction rate to local power, and calculates relative quadrant powers, tilts and axial offsets. INCORE also applies the W(Z) factors in determining the available F_Q margin.

Figure 2-1 : Core Physics Methodology Flowchart

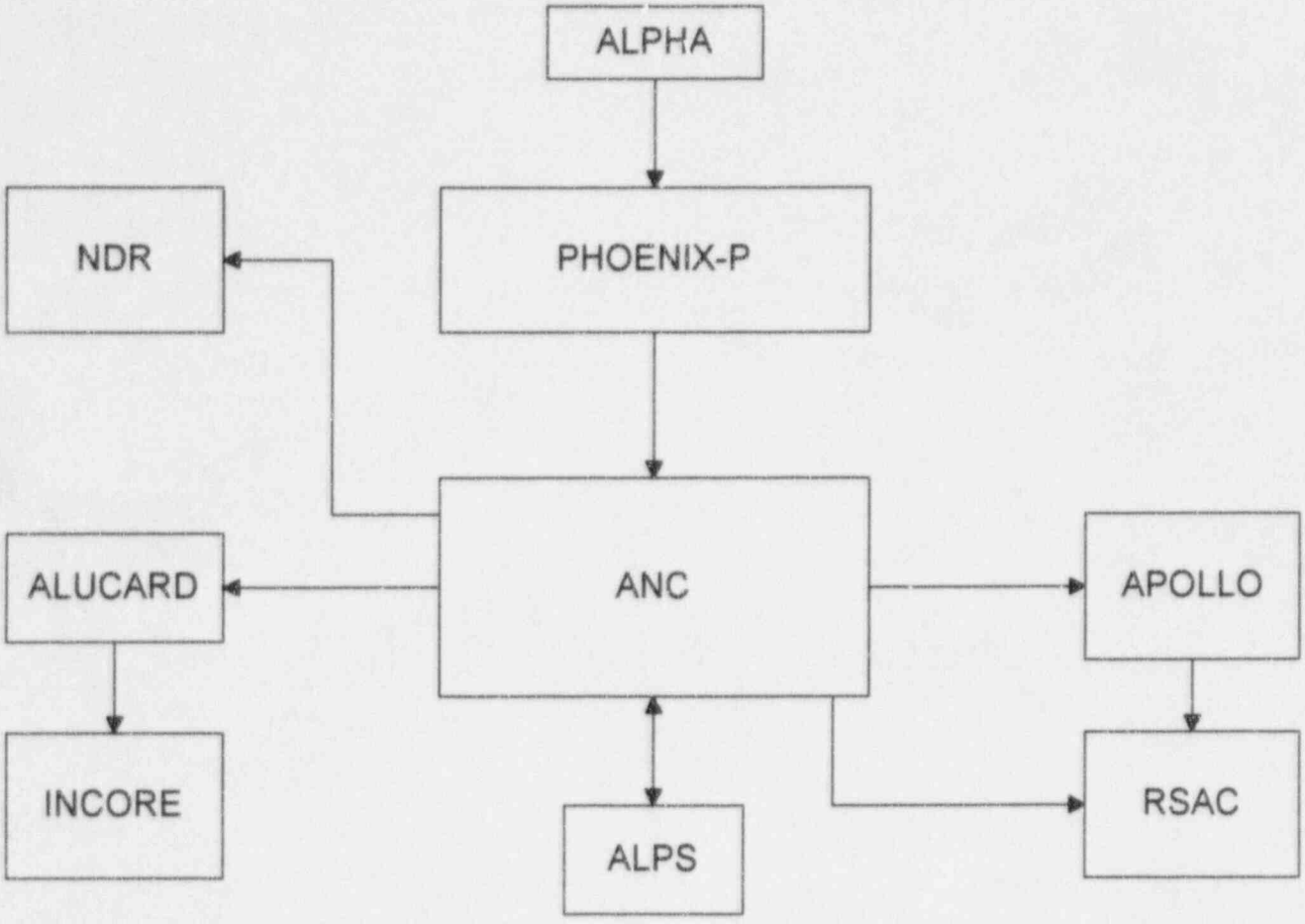

2.1.2 Benchmarks

2.1.2.1 Startup Benchmarks

2.1.2.1.1 Rod Worths

Rod worth measurements at startup of Cycles 6, 7 and 8, using the Rod Exchange method, are compared to results from calculations with ANC in Table 2-1. The data in this table clearly shows that the WCNOC acceptance criteria for control rod bank worths, listed below, were met with substantial margin in all cases.

Acceptance Criteria for Control Rod Bank Worth Uncertainty

1. Absolute value of the percent difference between measured and predicted integral bank worth for the reference bank (maximum worth bank) is less than or equal to 10%. For each test bank, absolute value of the percent difference between the measured (inferred) test bank worth and the predicted worth is less than or equal to 15%, or less than or equal to 100 pcm, whichever is greater.
2. The sum of the measured (inferred) bank worths for all banks must be less than or equal to 110% of the sum of all the predicted bank worths.

2.1.2.1.2 HZP Critical Boron Concentration

Critical boron concentration measurements at startup are compared to results from calculations with ANC in Table 2-2. WCNOC acceptance criterion requires that the measured boron concentration and predicted boron concentration at startup differ by no more than +/- 100 ppm. The results in Table 2-2 indicate acceptable agreement between measured and predicted values.

2.1.2.1.3 HZP Moderator Temperature Coefficient (MTC)

MTC values inferred from Isothermal Temperature Coefficient (ITC) measurements at startup are compared to results from calculations with ANC in Table 2-3. The WCNOC acceptance criterion requires that the measured/inferred MTC values differ from predicted values by no more than 2.0 pcm/°F. As shown in Table 2-3, this standard was adequately met for each cycle; significantly, the ANC-calculated MTC is more positive than the measured/inferred MTC.

2.1.2.2 Cycle Depletion Benchmarks

2.1.2.2.1 Boron Letdown Curve

The measured and ANC-calculated boron letdown curves are compared for Cycles 6, 7 and 8 in Figure 2-2, Figure 2-3, and Figure 2-4, respectively. The WCNOC Measurement and Acceptance Criteria are, for critical boron concentration predictions, a difference of no more than 50 ppm, plus a difference of no more than 1000 pcm-equivalent of the predicted boron concentration. These figures show that the agreement is good and the criteria are met.

2.1.2.2.2 Power Distribution

WCNOC has an ANC-based model to monitor the power distribution in Cycle 8. A "measured" $F_{\Delta H}^{N}$ is inferred from flux maps obtained during monthly surveillances. The "measured" $F_{\Delta H}^{N}$ is based on the measured in-core detector signal at the thimble location in the fuel assembly. This signal is modified by assembly power-to-thimble flux and pin-to-assembly power factors from ANC to convert it to $F_{\Delta H}^{N}$.

The first several Cycle 8 comparisons between the "measured" and calculated $F_{\Delta H}^{N}$ are shown in Figure 2-5 through Figure 2-8. The results show good agreement. The largest difference between measurement and prediction occurs in peripheral, low power assembly locations in the core. The uncertainty factor of 5% used by WCNOC is satisfied.

Table 2-1 : Rod Worths at HZP (BOC, Xe=0, Peak Sm)

a

Cycle	Bank	Measured (pcm)	Predicted (pcm)	(M-P)/P (%)	M-P (pcm)	Remark
6	D					
	C					
	B					
	A					
	SE					
	SD					
	SC					
	SB					Reference
	SA					
	Total					
7	D					
	C					
	B					
	A					
	SE					
	SD					
	SC					
	SB					Reference
	SA					
	Total					
8	D					
	C					
	B					
	A					
	SE					
	SD					
	SC					
	SB					Reference
	SA					
	Total					

Prediction: ANC
Measurement method: Rod Exchange

Table 2-2 : Critical Boron Concentration at HZP (BOC, Xe=0, Peak Sm)

Cycle		Measured (PPM)	Predicted (PPM)	(M-P)/P (%)	M-P (PPM)	Remark
6						D at 203 steps*
7						D at 204 steps
8						D at 201 steps

* Bank completely withdrawn = 228 steps

Table 2-3 : Moderator Temperature Coefficient at HZP (BOC, Xe=0, Peak Sm)

Cycle		Measured (pcm/ °F)	Predicted (pcm/ °F)	M-P (pcm/ °F)	Remark
6					D at 203 steps* D at 207 steps
7					D at 204 steps
8					D at 202 steps

"Measured" MTC = Measured ITC - Calculated DTC (Doppler Temperature Coefficient)

* Bank completely withdrawn = 228 steps

Figure 2-2 : Cycle 6 Boron Letdown Curve

Figure 2-3 : Cycle 7 Boron Letdown Curve

Figure 2-4 : Cycle 8 Boron Letdown Curve

Figure 2-5 : Measured and Predicted $F_{\Delta H}^{N}$

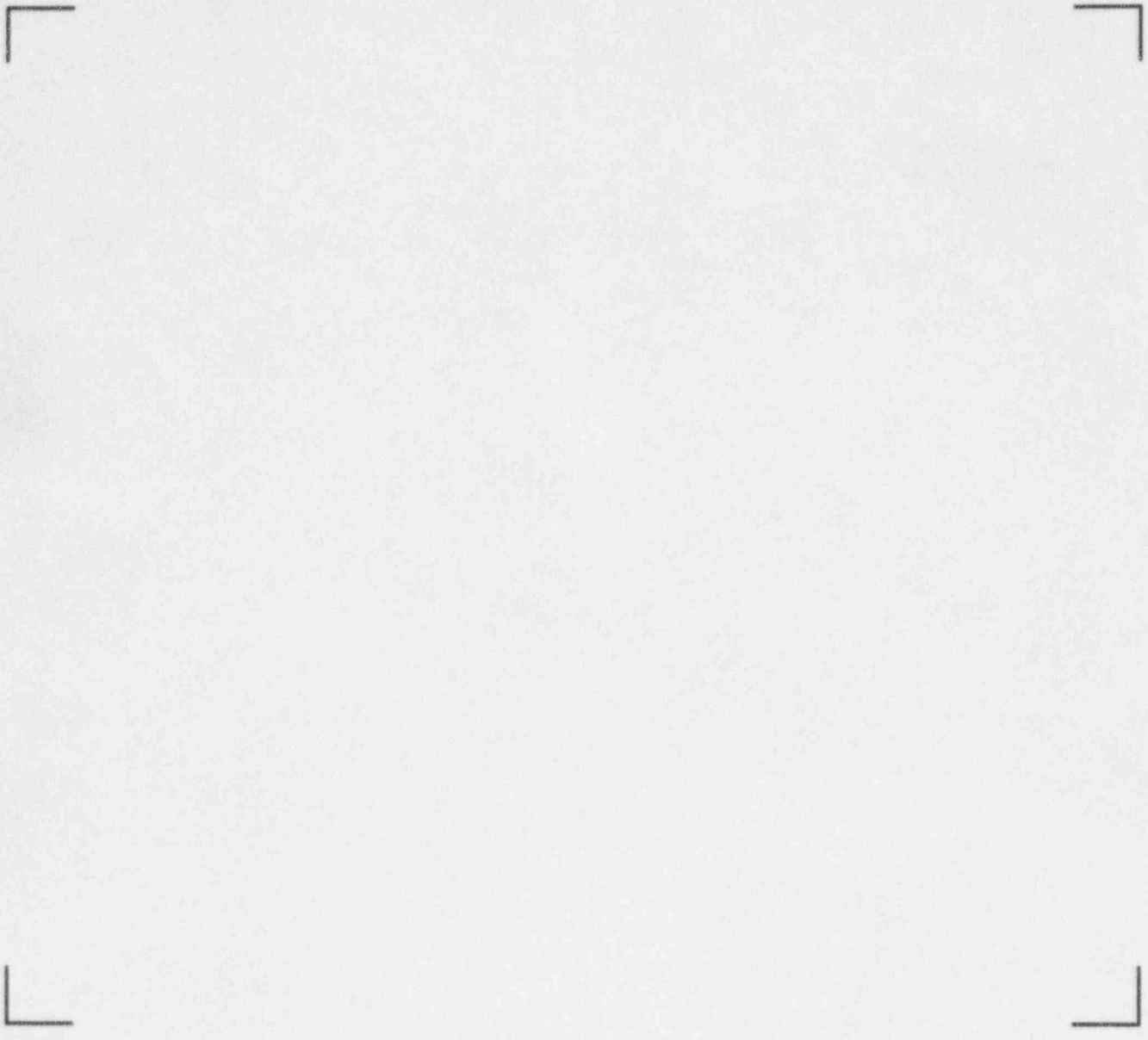

Figure 2-6 : Measured and Predicted $F_{\Delta H}^{N}$

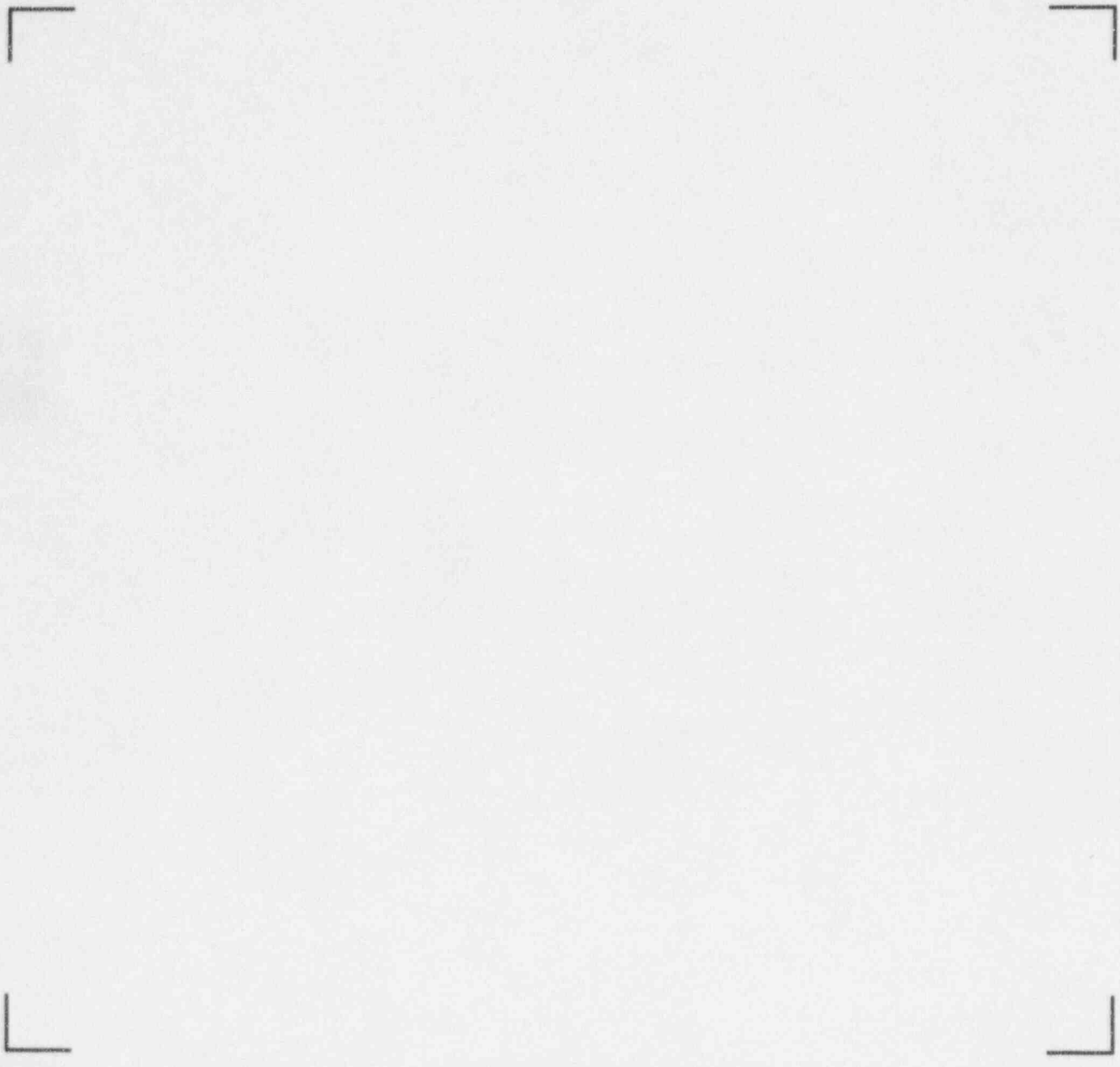

Figure 2-7 : Measured and Predicted $F^N_{\Delta H}$

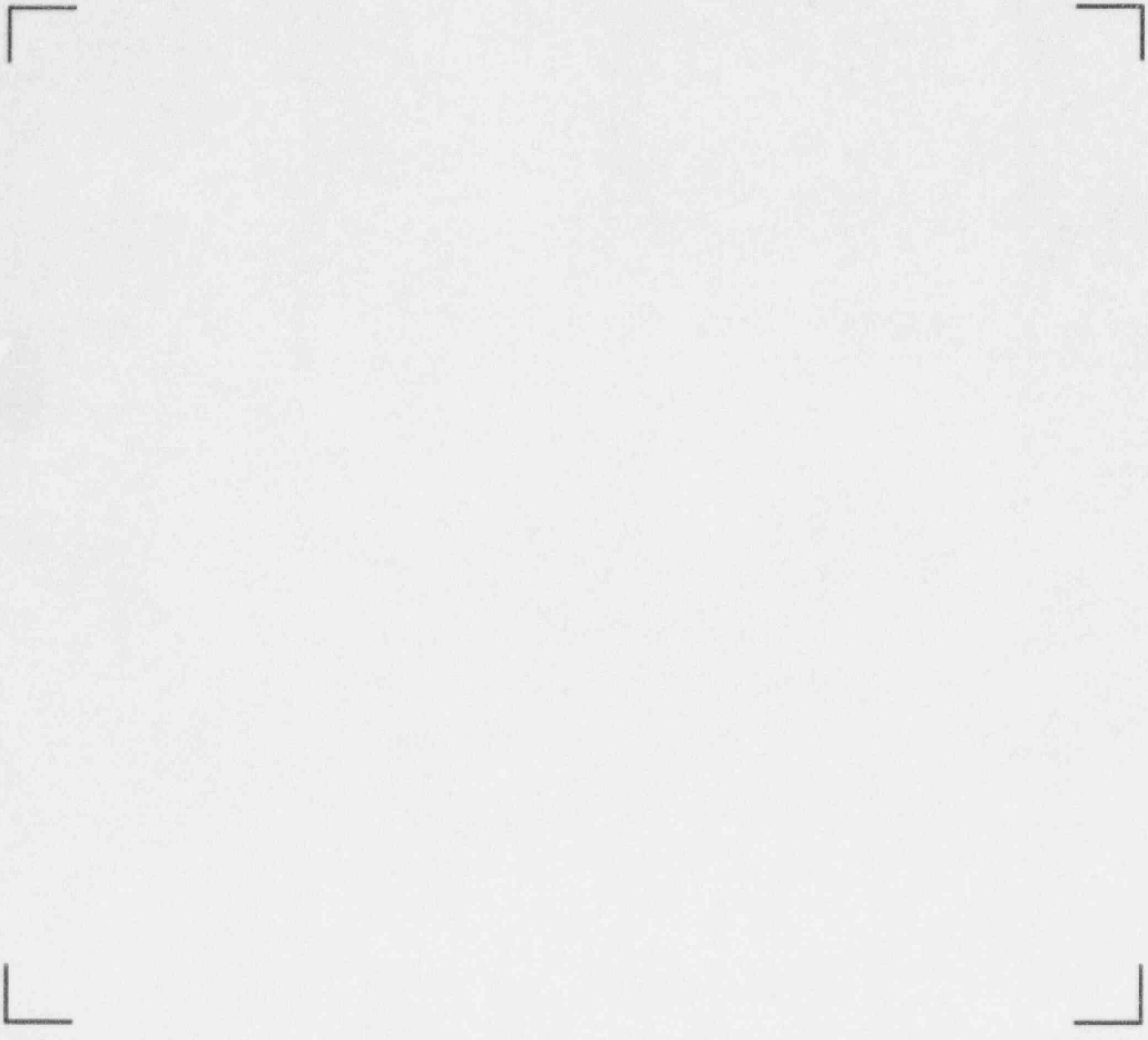

Figure 2-8 : Measured and Predicted $F_{\Delta H}^{N}$

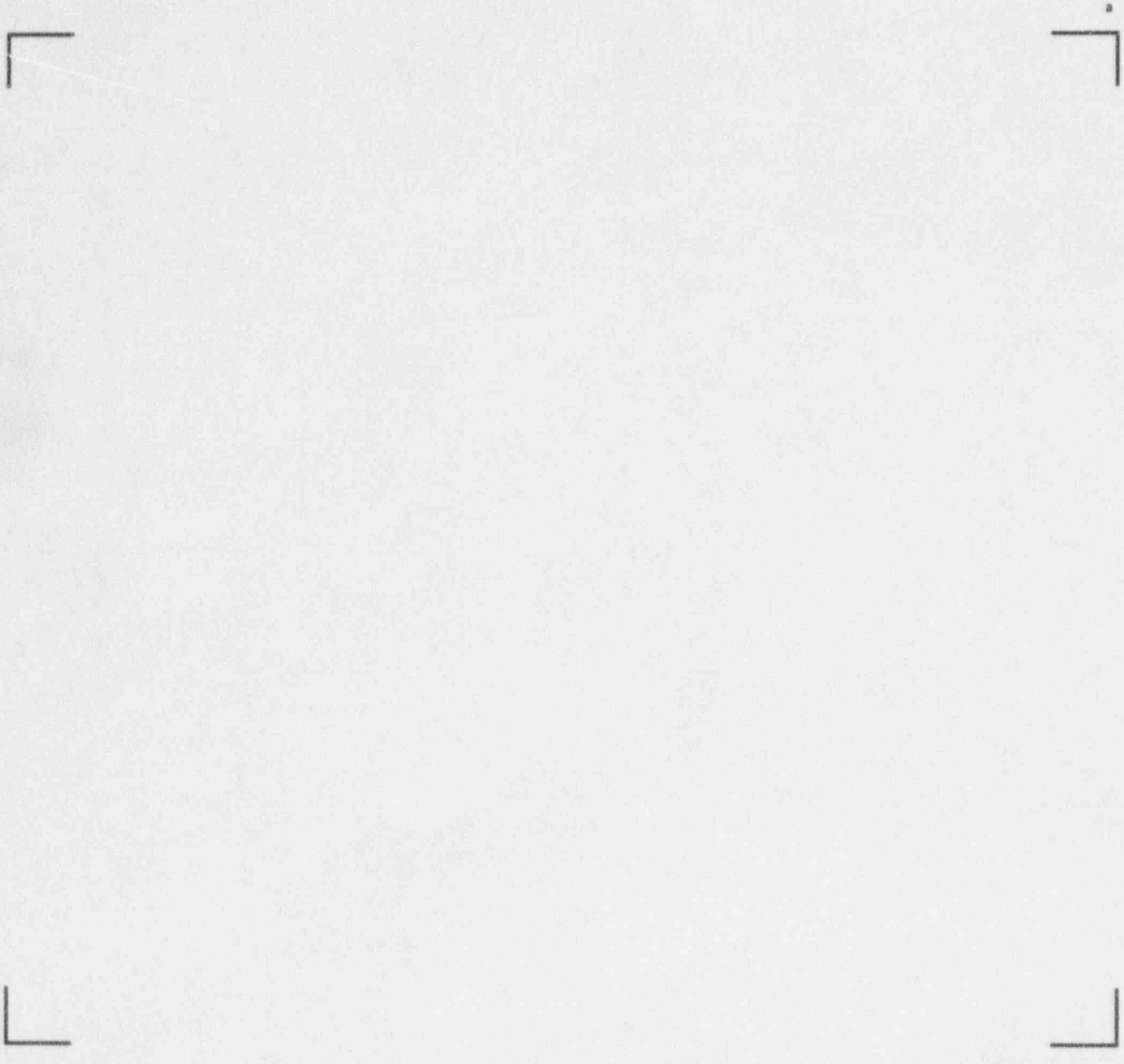

2.1.3 Relaxed Axial Offset Control (RAOC)

WCGS currently utilizes the Babcock and Wilcox methodology for Westinghouse PWRs to verify Technical Specification compliance for the heat flux hot channel factor, F_Q, and the nuclear enthalpy rise hot channel factor , $F^N_{\Delta H}$. The decision to transition to Westinghouse computer design codes and methodology for performing core physics and thermal hydraulics analysis necessitates the implementation of compatible F_Q and $F^N_{\Delta H}$ monitoring Technical Specifications. The analysis methods for setting operational limits (ΔI, Rod Insertion Limits or RIL) and implementation techniques for monitoring power distributions are set forth in extensive detail in WCAP-10216-PA, "Relaxation of Constant Axial Offset Control-F_Q Surveillance Technical Specification."[5] An abbreviated discussion of the analysis methods and monitoring techniques, known as "RAOC Analysis" in Westinghouse terminology, is presented here.

The three major outputs from the RAOC Analysis are: 1) normal operation power shapes, 2) Condition II power shapes, and 3) W(Z) factors. The power shapes from items one and two are transmitted electronically for thermal hydraulic analysis to verify that Departure from Nucleate Boiling (DNB) criteria are satisfied. The W(Z) factors, used for verification of power distribution Technical Specification compliance, are transmitted via the Core Operating Limits Report (COLR) to Reactor Engineering.

It is important to note that the power shapes are dependent upon normal operating restrictions (ΔI, RIL) and also safety settings (OTΔT , OPΔT). This relational dependence dictates an iterative approach to RAOC Analysis. Specifically, if the power shapes generated in the RAOC Analysis do not meet DNB or F_Q criteria, then the operating limits and/or safety settings would be adjusted and the power shapes regenerated.

An outline showing the iterative relationships between physics calculations and other disciplines is shown in Figure 2-9. For purposes of demonstration, the following discussion of RAOC methods will ignore the iterative aspect of the calculation. The RAOC Analysis is divided into the following major steps, 1) Xenon Library, 2) Normal Operation Analysis, 3) Condition II Analysis, and 4) RAOC Limit Determination.

Xenon Library

The xenon reconstruction library contains bounding xenon parameters which enable reconstruction of axial xenon shapes which encompass the entire ΔI band. The validity of Xe(z) is demonstrated by reconstruction which yields axial offsets (AOs) within about [ ]^b and F_z within [ ]^b. The agreement is satisfactory for the enveloping calculations which the reconstruction model performs.

Xenon transient calculations are performed to encompass the ΔI band. The following sequence is executed to generate transient xenon shapes:

[ ]^b

The control rod insertion limits are not violated during the xenon transient calculations.

The allowed bounding combinations of xenon reconstruction parameters from the above transients constitute the xenon library. Additionally, a range of bounding xenon concentrations is chosen using the [ ]^b xenon concentration from the above xenon transients.

These parameters, combined with the xenon concentrations, comprise the xenon reconstruction library. This xenon library is used as the beginning point in the normal operation analysis.

Normal Operation Analysis

In the RAOC analysis of normal operation shapes the simulated transient core configurations are not allowed to violate control rod insertion limits. An outline of the entire normal operation analysis is shown in Figure 2-10. The following steps are used to generate power distributions.

b

Performance of these steps results in a large set of power distributions bounding the ΔI/Power space. This set of power distributions is used for the LOCA and Loss Of Flow Accident (LOFA) analysis, which comprises the normal operation analysis.

Additionally, for use in monitoring F_Q Technical Specification compliance, the W(Z) factors are generated based on the normal operation transient power distributions. The W(Z) factors are the ratio of normal operation transient local power to the nominal local power as a function of height. The W(Z) factors represent the local pin peaking increase resulting from a possible normal operation transient.

Each normal operating power shape generated as described above is analyzed to determine if LOCA constraints are met or violated. The total peaking factor, as a function of height, is checked against LOCA constraints. At each power level, a range of ΔI in which there are no violations is determined. This bounding ΔI limit, as a function of power, is the preliminary ΔI/Power space, pending the outcome of the LOFA and Condition II analyses.

The LOFA analysis is a thermal-hydraulic calculation used to analyze the cycle specific power shapes. Normal operation power shapes are evaluated relative to the assumed limiting power distribution used in the accident analysis. Limits of ΔI/Power from this analysis are combined with the results of the LOCA analysis and the most restrictive limits determined. A typical ΔI/Power operating envelope from this portion of the RAOC analysis is shown in Figure 2-11.

Condition II Analysis

The objectives of the RAOC analysis for Condition II events are:

1. Determine if the consequences of Condition II events satisfy the safety analysis requirements for the transient in terms of maximum power density and design basis axial power shape used in the Departure from Nucleate Boiling Ratio (DNBR) evaluation.
2. Determine the conservatism of the f(ΔI) penalty function in the OTΔT setpoint equation. This analysis verifies that power shapes which do not meet design criteria are precluded.

The Condition II analysis flow path is shown in Figure 2-12. Any Condition II transient analyzed must begin from an acceptable normal operating condition. These restrictions include control rods above RIL and ΔI within the limits. Starting from these normal operating conditions, the following accidents are simulated.

Overcooling Accident (Rods in Manual)

This transient simulates a reduction in the inlet temperature of the primary coolant. The specific method of the temperature reduction is not considered. The control rods are assumed to remain in the initial rod configuration. The maximum amount of inlet temperature reduction considered is [ ]^{b}. Credit is taken for the high flux trip function.

Control Rod Withdrawal

This accident simulates control rod withdrawal independent of the mechanistic cause. Boron concentration remains unchanged. The control rod is withdrawn in [ ]^{b} steps from the initial RIL position to full out. This analysis also considers overcooling conditions. Credit is taken for the [ ]^{b} function.

Boration/Dilution (Automatic Rod Control)

An uncontrolled boration/dilution accident is simulated. The reactivity change at constant power with the boration/dilution is compensated by automatic control rod motion. [

]^{b}.

The Condition II simulations all begin from normal operation preconditions. From these normal power distributions and configurations, the following simulations are executed:

b

The power distributions generated in these transient simulations are analyzed for peak power density and DNB concerns.

Core peaking factors are obtained using a [
]^{b}. Typically, peak power density will exceed the safety analysis limits only at very large ΔI values. These regions are protected by operator action and the f(ΔI) function on OTΔT. The f(ΔI) function on OTΔT can also be used to protect areas limited by OPΔT concerns.

The Condition II power distributions are transmitted to thermal-hydraulics to verify that the power shapes used in the DNB analysis and resultant OTΔT setpoints are bounding.

RAOC Limit Determination

After the normal operation and Condition II power distributions have been converted to allowable ΔI, the final determination of allowed ΔI/Power can be made. The limiting LOCA and LOFA are compared and the most limiting operating space allowed by these two normal operation concerns is set. The resultant operating space is then compared to the trip setpoints of OTΔT , f(ΔI), and OPΔT, to verify that the normal operating space is within the trip setpoints. Typical final Δ I/Power and trip setpoints and the relationship between them is shown in Figure 2-13

Figure 2-9 : Flow Diagram of RAOC Analysis Process

b

Figure 2-10 : Condition I Analysis - LOCA/ LOFA

b

Figure 2-11 : Typical Axial Flux Difference Limits

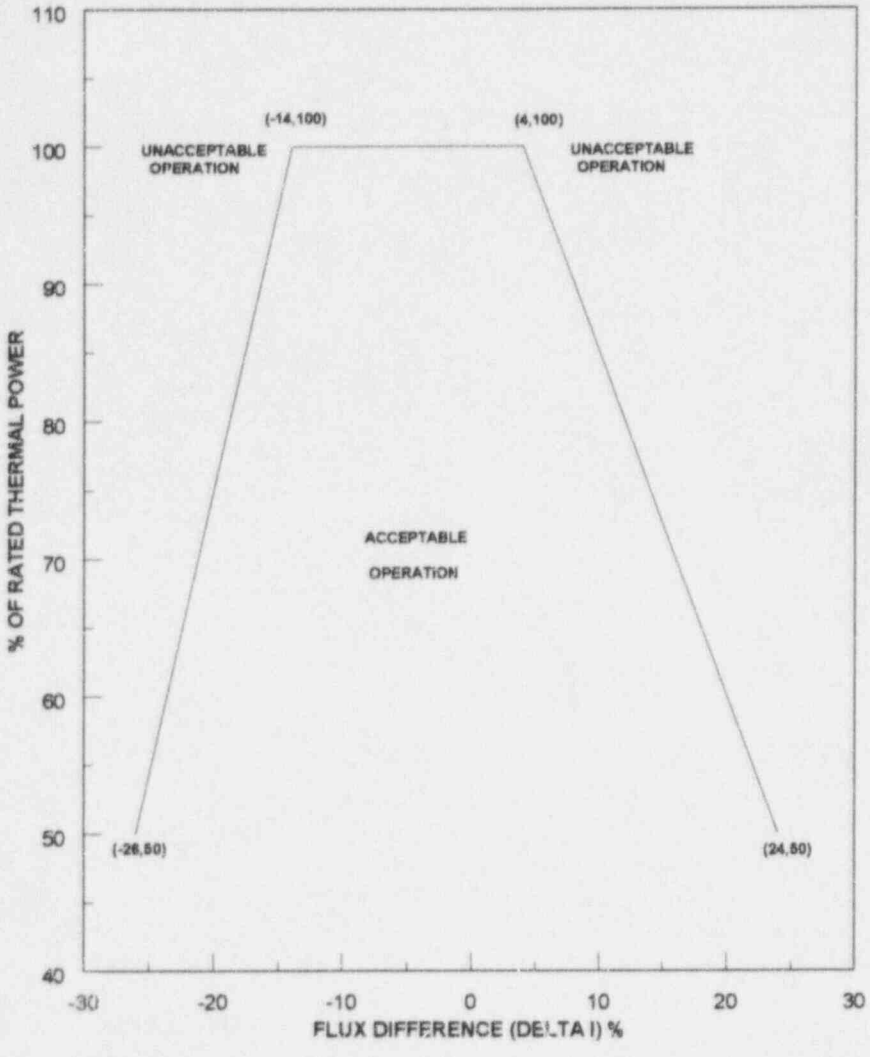

Figure 2-12 : Condition II Analysis - OPΔT/OTΔT

b

Figure 2-13 : Typical Normal Operation AFD Band and Trip Setpoints

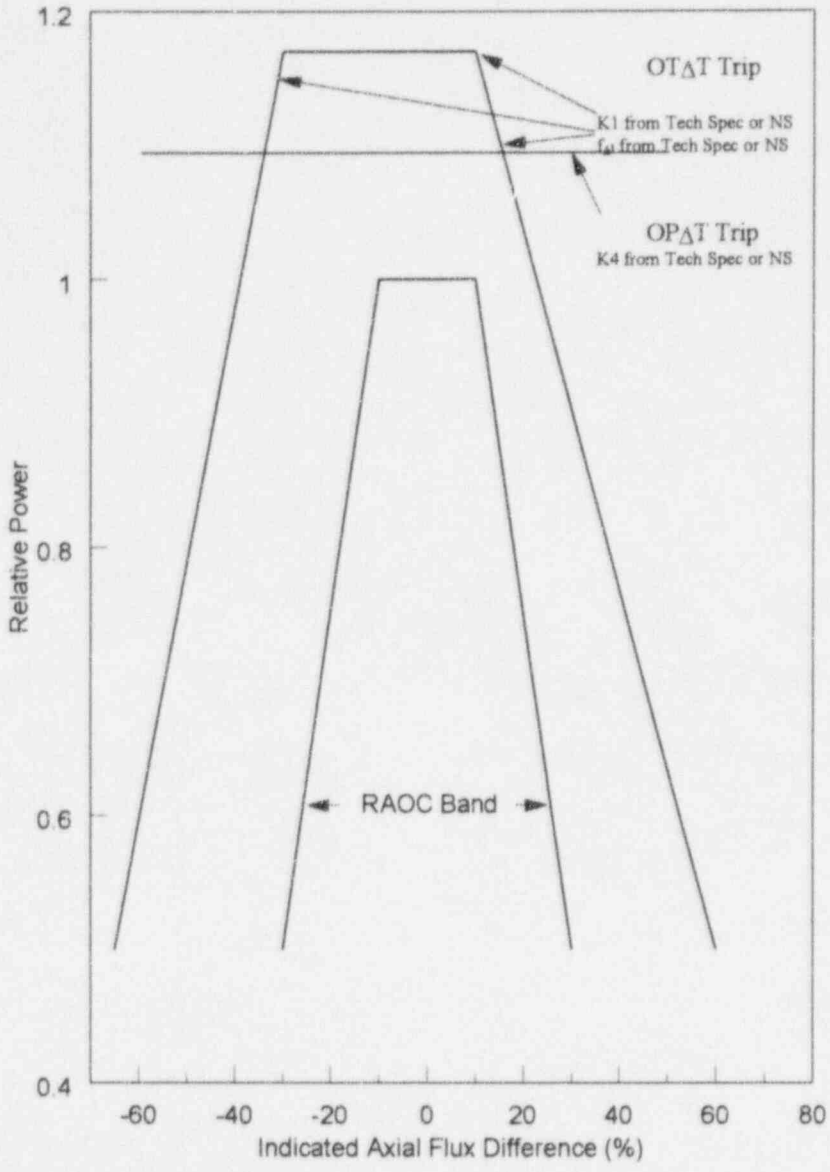

2.1.4 Reload Safety Analysis Integration

At issue in the core model applications is whether the cycle specific loading pattern meets all limits and requirements for safety-related nuclear and thermal-hydraulic parameters. A reload core can affect nuclear related key safety parameters in three basic areas: core kinetic characteristics, control rod worths, and core power distributions. The analysis of these three areas is formally detailed in an interface document, the Reload Safety Analysis Checklist (RSAC).

The RSAC contains two sets of parameters. The first set is provided by transient analysis consisting of limiting values assumed in the existing accident analysis for the plant. The second set of parameters, provided by core physics, is based on analyses for the specific cycle. (Thermal-Hydraulic calculations for the current reload are also performed, but not discussed in this section.)

Several nuclear-related key safety parameters calculated for the RSAC are discussed below. The following discussion will describe the methods and applicable uncertainty factors to be applied to the reload key safety parameter calculations. The uncertainty factors to be applied are summarized in Table 2-4.

2.1.4.1 Core Kinetics Parameters and Reactivity Coefficients

The kinetic characteristics of the reactor core determine the response of the core to changing plant conditions or to operator actions made during normal operation, as well as the core response during abnormal or accidental transients. These characteristics are quantified in terms of point kinetics parameters and reactivity coefficients. The reactivity coefficients reflect the changes in the neutron population due to varying plant conditions such as changes in power, moderator or fuel temperatures, and boron concentration.

Each of the reload reactivity parameters and coefficients are evaluated to determine the most negative or the most positive (least negative) value to ensure the RSAC parameters are bounding. Considerations to find the limiting plant configuration include time in core life, power level ranging from zero to full power, and allowable rod insertion. Additionally, consideration is given to the impact on safety parameters as a result of the previous cycle minimum and maximum burnup window. The key safety reactivity parameters and coefficients are discussed below.

2.1.4.2 Delayed Neutron Fraction

Delayed neutrons play an important role in determining the transient response of the core. The delayed neutrons are emitted from fission products, called precursors, a short time after a fission event. The effective delayed neutron fraction, β_{eff}, for point kinetics will be calculated based on PHOENIX-P concentrations coupled with ANC core-wide assembly burnup distributions and power sharings. The effective delayed neutron fraction for different precursor groups is obtained by weighting by fractional regionwise fissions for each isotope. The calculation of these

parameters is performed at beginning of core (BOC) and end of core (EOC) for rodded and unrodded configurations. The conservatism factor, [ ]^a, will be applied to increase/decrease the calculated value, depending on the application.

2.1.4.3 Prompt Neutron Lifetime

Values of the prompt neutron lifetime (l*) are obtained by weighting regionwise power sharings in a manner similar to the calculation of effective delayed neutron fraction. The fissionable isotope concentrations are obtained from PHOENIX-P and weighted with power sharings from ANC. The conservatism factor, [ ]^a, will be applied to increase/decrease the calculated value, depending on the application.

2.1.4.4 Moderator Temperature Coefficient

The Moderator Temperature Coefficient (MTC) is a measure of the change in core reactivity due to a change in coolant density corresponding to a coolant temperature change. The value of this coefficient is sensitive to changes in the moderator density, moderator temperature, soluble boron concentration, fuel burnup, and the presence of control rods/burnable poisons. The MTC is calculated with a three-dimensional ANC model at various plant conditions by varying the moderator temperature by several degrees about the temperatures of interest. Depending on the safety analysis accident under consideration the least negative or the most negative MTC may be limiting. The most negative MTC is usually found at EOC. The most positive MTC is found at the most reactive time in core life which, for integral fuel bundle absorber (IFBA) cores, is not necessarily at BOC. The reliability factor, [ ]^a, will be added to/subtracted from the calculated value, depending on the application.

2.1.4.5 Doppler Coefficients

The Doppler coefficients are a measure of the change in the core reactivity associated with a change in the fuel temperature. The reactivity is changed because of the broadening of the resonance absorption (U238 and Pu240, mainly) with increasing fuel temperature. Doppler depends on fuel temperature and core burnup. The reactivity effect of the corresponding change in moderator temperature is specifically excluded.

2.1.4.6 Doppler Power Coefficient

The Doppler power coefficient gives the change in reactivity for a percentage change in core power level. The Doppler power coefficient is calculated directly with a 3-D ANC model by varying core power (fuel temperature) while holding moderator temperature constant. The reliability factor, [ ]^a, will be added to/subtracted from the calculated value, depending on the application.

2.1.4.7 Doppler Temperature Coefficient

The Doppler temperature coefficient is a calculation of the reactivity change due to the change in fuel temperature. The Doppler temperature coefficient is calculated by subtracting the moderator temperature coefficient from the isothermal temperature coefficient, at the same power, burnup, boron concentration and xenon condition.

The least negative and most negative values are considered for the RSAC. The reliability factor, [ ]^{a}, will be applied on the Doppler temperature coefficient, both the least negative and the most negative, in the same manner as for the Doppler power coefficient.

2.1.4.8 Differential Boron Worth

The differential boron worth is a calculation of the reactivity change associated with a change in soluble boron concentration. The value of this parameter depends on the boron concentration, on the moderator temperature, and the presence of control rods/burnable poisons. It is calculated at various plant conditions with a 3-D ANC model by varying the boron concentration about the reference concentrations of interest. The reliability factor, [ ]^{a}, will be applied in a conservative manner.

2.1.4.9 Rod Worths

2.1.4.9.1 Application of Rod Worth Uncertainty

Full length rod cluster control assemblies (RCCA's) are used to compensate for relatively rapid reactivity variations. The RCCA's are designated by function as control banks or shutdown banks. Control banks may be present in the core during power operation and are used to compensate for reactivity changes associated with changes in operating conditions such as coolant temperature, power level, boron concentration, or xenon concentration. The shutdown banks, together with the control banks, are used to provide the required shutdown reactivity at all operating and hot zero power conditions.

A reload core can significantly alter RCCA worths. These changes can be attributed to the power distribution (reactivity importance) produced by the loading pattern of fresh and burned fuel. Rod worths also change with fuel depletion which occurs during the operation of the cycle. Changes in rod worth affect trip reactivity, differential rod worths, and shutdown rod worth.

Rod worths are calculated with a three-dimensional ANC model at various plant conditions. The reliability factor, the larger of [ ]^{a} for a single rod or bank, [ ]^{a} for a sum of banks, will be added to/subtracted from the calculated value, depending on the application.

For example, accidents where the calculated rod worth will be increased [ ]^{a} include: (a) the Rod Withdrawal from Subcritical (maximum differential rod worth of two sequential control banks moving together at hot zero power (HZP), 100% overlap, at specified maximum speed); and (b) the Rod Withdrawal at Power (maximum differential rod worth of control banks moving with normal overlap).

The calculated rod worth will be decreased [ ]^{a} in the determination of the shutdown margin and the scram reactivity. The procedure for these calculations is discussed below.

2.1.4.9.2 Shutdown Margin

Safe shutdown of the core at any time must be considered in the RSAC. The shutdown margin is defined as the amount by which the core would be subcritical at hot shutdown conditions following a reactor trip, assuming that the highest worth control rod remains fully withdrawn, and assuming no changes in xenon and boron concentration.

The shutdown margin calculation is performed ensuring that the required excess rod worth is available after compensating for the reactivity insertion that results when taking the core from hot full power (HFP) to HZP, all rods in - strongest rod out (ARI-SRO). Below HZP, the shutdown margin (SDM) is preserved by maintaining a soluble boron concentration necessary to ensure the required SDM. The SDM verification is based on calculations performed with ANC. The calculation process is as follows:

[ ]^{a}

2.1.4.9.3 Trip Reactivity

Trip reactivity is the rod worth inserted versus rod position after a trip signal with the most reactive rod assumed to be stuck out of the core. The minimum trip reactivity and the trip reactivity shape initiated from full power conditions are evaluated for each reload core. Conservatism in this analysis for evaluating total worth is assumed to occur with control rods at the insertion limit and xenon skewed towards the bottom to maximize inserted rod worth. In contrast to the total worth calculation, the shape of the trip reactivity is based on an initial all-rods-out position.

The total integral rod worth minus the most reactive rod is calculated with a 3-D ANC model for various core conditions designed to minimize available rod worth. Although the worth calculation is a 3-D simulation, the calculation to identify the most reactive stuck rod can be performed with a 2-D ANC rod search. The total available rod worth from the 3-D calculation is reduced by a [ ][a] conservatism factor before comparison to the RSAC limit.

In addition to the total available control rod worth, the trip reactivity shape is calculated to confirm the adequacy of the RSAC trip reactivity shape as a function of control rod position. The reload trip shape is determined from a 1-D APOLLO model simulation initialized from an all-rods-out configuration.

To initiate the APOLLO shape calculation, an EOC statepoint with equilibrium xenon is established. The equilibrium APOLLO model is maneuvered to the negative RAOC ΔI limit at HFP to delay the reactivity insertion upon trip. From this adverse xenon condition the trip is simulated as a series of core calculations at HFP with feedback frozen, each time inserting the rods approximately 5%.

2.1.4.10 Power Peaking Factors

The reload core must meet local hot channel factor heat flux, F_Q, and nuclear enthalpy (or integral) heat flux, $F_{\Delta H}$, limits, as specified in the RSAC. The RSAC limits on steady state integral heat flux must be preserved to validate the initial conditions assumed in the safety analysis for DNB limited Condition I transients, specifically the LOFA. The RSAC limits on local heat flux must be preserved to validate the initial condition assumed in the Emergency Core Cooling System (ECCS) evaluation of LOCA. In addition to these two steady state RSAC peaking limits there are several specific accidents, such as single rod withdrawal, rod ejection, and steamline break, which have accident-specific peaking limits.

For most RSAC applications the F_Q and $F_{\Delta H}$ will be calculated using the 3-D ANC model for conservatively selected core configurations. ANC calculates local pin powers in a stand-alone mode using pin power reconstruction based on nuclear constants imported from the PHOENIX-P lattice calculations.

2.1.4.10.1 Application of F_Q Uncertainty

Based on the 3-D ANC model, the maximum value of F_Q is included in the RSAC for the peak F_Q value for normal operation (LOCA). This analysis contains conservatism based on the previous cycle burnup window, a wide range of control rod insertions, xenon distributions, and calculation uncertainty.

The reliability factor, [ ]^{a,b}, will be applied as follows:

Design F_Q = Calculated F_Q x [ ]^{a,b}.

2.1.4.10.2 Application of $F_{\Delta H}$ Uncertainty

The allowable $F_{\Delta H}$, as a function of power, must be checked to be below the allowable value to demonstrate compliance with the RSAC limits. The calculations are performed with 3-D ANC simulations with consideration for burnup windows, rod insertion limits, and allowance for calculation uncertainty.

The reliability factor, [ ]^{a,b}, will be applied as follows:

Design $F_{\Delta H}$ = Calculated $F_{\Delta H}$ x [ ]^{a,b}.

Table 2-4 : Reliability Factors for Wolf Creek Reload Evaluation

a,b

Parameter	RF
F_Q	
$F_{\Delta H}$	
Rod Worth	
Boron Worth	
Moderator Temperature Coefficient(pcm/°F)	
Doppler Power Coefficient	
Doppler Temperature Coefficient	
Doppler Defect	
Effective Delayed Neutron Fraction	
Prompt Neutron Lifetime	

2.1.5 Continuing Model Verification and Validation

Measurements of physics parameters and related data during initial cycle startup and during cycle operation will continue to be compared to the core model. Examples of measured physics parameters include critical boron concentrations, rod worths, isothermal temperature coefficients and differential boron worths. Measured power distributions from the flux mapping process are also a significant indicator of core model accuracy.

The purpose of comparing measured data to core model predictions is to verify that the uncertainties on the reload safety parameters remain valid and that the physics predictions used for plant operation are accurate. This comparison is performed by WCNOC for WCGS models and data as part of the core follow program. Additionally, the Westinghouse code package is widely used and benchmarked against measurements from a wide database of plants. This extensive benchmarking program provides good assurance that the codes/methods and reload uncertainties are applicable.

This extensive benchmarking can also identify specific areas for modeling improvement. These improvements may take the form of computer code modifications or changes to the methods employed for a specific reload calculation. WCNOC, under a "living license" agreement with Westinghouse, receives notification of any alterations to the reload methods and current versions of the computer codes used in the reload technology. These aspects of the agreement ensure that WCNOC reload technology remains state-of-the-art and consistent with the vendor.

2.2 Core Thermal-Hydraulic Methods

The thermal-hydraulic analysis of a nuclear reactor core must confirm that, for each reload design, design criteria for minimum departure from nucleate boiling ratio (MDNBR), core peaking limits, core thermal margin, and allowable operating limits are satisfied.

2.2.1 VIPRE-01 Models for Thermal-Hydraulic Design

One of the principle prerequisites for the performance of a reload safety analysis for a nuclear plant is the ability to predict the DNBR in the high power channels in the core. Calculations to predict DNBR are accomplished through the use of a thermal-hydraulic analysis code such as the VIPRE-01 code[6]. However, in issuing the Safety Evaluation Report for the VIPRE-01, Mod 1 code, the NRC mandated that, "...Each organization using VIPRE-01 for licensing calculations should submit separate documentation describing how they intend to use VIPRE-01 and provide justification for their specific modeling assumptions, choice of particular two-phase flow models and correlations, heat transfer correlations, CHF correlations and DNBR limit, input values of plant specific data such as turbulent mixing coefficient, slip ratio, grid loss coefficient...."[7] WCNOC has received NRC approval of modeling methodologies, correlation selection, and DNBR limit for VIPRE-01 models of the WCGS core[8].

The changes made to the base thermal-hydraulic model to facilitate a transition to Westinghouse nuclear and thermal-hydraulic design methodologies affect only the radial detail of the model (i.e., number of channels and rods). Axial features of the model, such as the elevation of grids, are

unchanged from the Cycle 8 model. Further, modeling philosophies adopted during the development of the WCNOC thermal-hydraulic analysis methodology, reviewed and approved by the NRC, were observed in the development of the Cycle 9 VIPRE-01 model[9].

Three changes were made to the Cycle 8 base thermal-hydraulic model. First, the number of flow channels included in the model was increased from seventeen (17) to thirty (30). Second, the number of rod models used to simulate heat transfer from the fuel to the coolant was increased from nineteen (19) to thirty-two (32). Finally, the thermal diffusion coefficient, which defines the coolant exchange between subchannels due to natural eddy diffusion, was adjusted to reflect the model channel layout. Further discussion, providing the basis for and implementation details of these changes, is provided below.

The WCNOC VIPRE-01 Cycle 9 thermal-hydraulic model of the WCGS core represents a full core load of the Westinghouse Vantage 5 Hybrid (V5H) with Intermediate Flow Mixers (IFM) fuel design[10]. This fuel design features a debris resistance bottom nozzle, a removable top nozzle, 0.374 inch O.D. fuel rods, two (2) Inconel, non-mixing vane support grids, six (6) Zircaloy mixing vane grids, and three (3) low pressure drop intermediate mixing vane grids. A summary of the design features of the V5H with IFMs is provided in Table 2-5. The WCNOC thermal-hydraulic model of this fuel type is intended to be a fuel cycle independent model suitable for future licensing applications, as applicable.

WCNOC has performed detailed sensitivity studies of the effects of changes in radial modeling detail on critical heat flux predictions[11]. These studies have demonstrated that calculations of minimum DNBR are insensitive to changes in radial noding when the following modeling guidelines are followed;

- The hot channel and the limiting channel for DNB must be surrounded by at least one (1) row of subchannels.
- The subchannel noding should be selected so that changes in the hot assembly peaking distribution can be adequately represented.
- The number of VIPRE-01 fuel rod models included in the model should provide a balance between calculational detail and demand on computing resources.

Therefore, extensive qualification studies of the radial detail of the Cycle 9 thermal-hydraulic model were not required. Rather, performance studies of the revised model were performed to demonstrate the adequacy of the model and to provide a complete understanding of model behavior.

Table 2-5 : Vantage 5H with IFM Design Data - Cycle 9

Number of Fuel Rods	264
Rod Array	17 x 17
Rod-to-Rod Pitch (inches)	0.496
Assembly Dimensions	8.426 x 8.426
Type of Fuel Spacers	Grids
Active Fuel Length (inches)	144.0
Number of Instrumentation Tubes	1
Number of Guide Tubes	24
Fuel Rod Diameter, O.D. (inches)	0.374
Guide Tube Diameter, O.D. (inches)	0.474
Guide Tube Diameter, O.D. dashpot (inches)	0.430
Assembly Pitch	8.466
Flow Area (in^2)	38.259

2.2.1.1 Base Model Development

This section describes the development of the VIPRE-01 base thermal-hydraulic model for Cycle 9. Included in this section are a general description of the WCGS core, channel selection, calculation of all physical dimensions required to construct the VIPRE-01 model and the definition of a base radial power distribution.

The VIPRE-01 thermal-hydraulic model for the WCGS, simulates the thermal-hydraulic conditions in a 1/8 core section of symmetry of the reactor core. Figure 2-14 shows the WCGS core layout and identifies the section represented by the WCNOC VIPRE-01 model. Selection of the section for modeling is arbitrary since the core is 1/8 core symmetric both physically and nuclear. The 1/8 core section encompasses 24.125 fuel assemblies representing 6,369 fuel rods, 579 guide tubes, and 24.125 instrument tubes. Figure 2-15 shows an exploded view of the 1/8 core section of symmetry modeled in the WCNOC thermal-hydraulic model.

As described earlier, a typical V5H with IFM fuel assembly is comprised of 264 fuel rods, 24 guide tubes, and 1 instrument tube. A graphical representation of the typical V5H fuel assembly is shown in Figure 2-16.

Figure 2-14 : WCGS Core

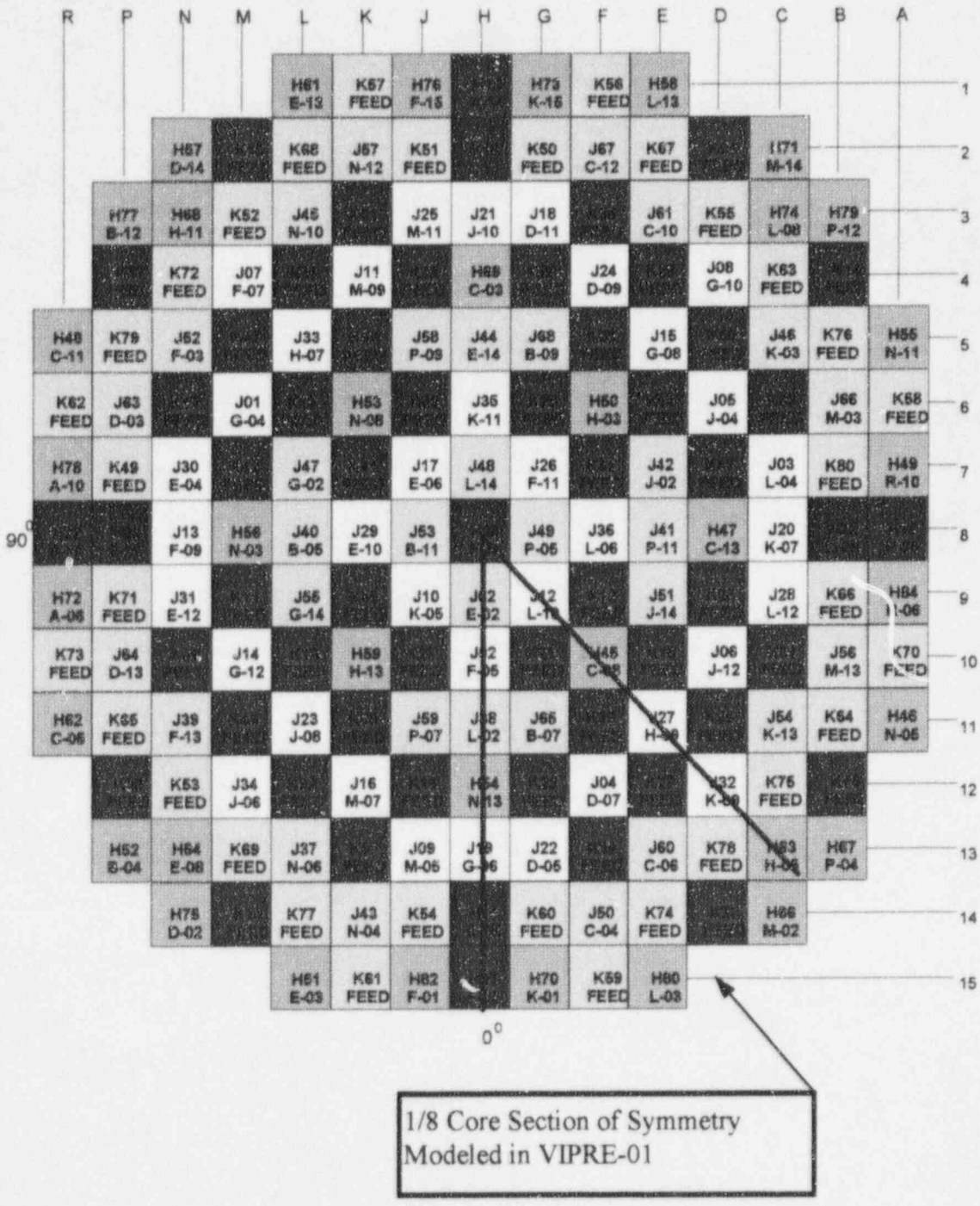

Figure 2-15 : 1/8 Core Section of Symmetry

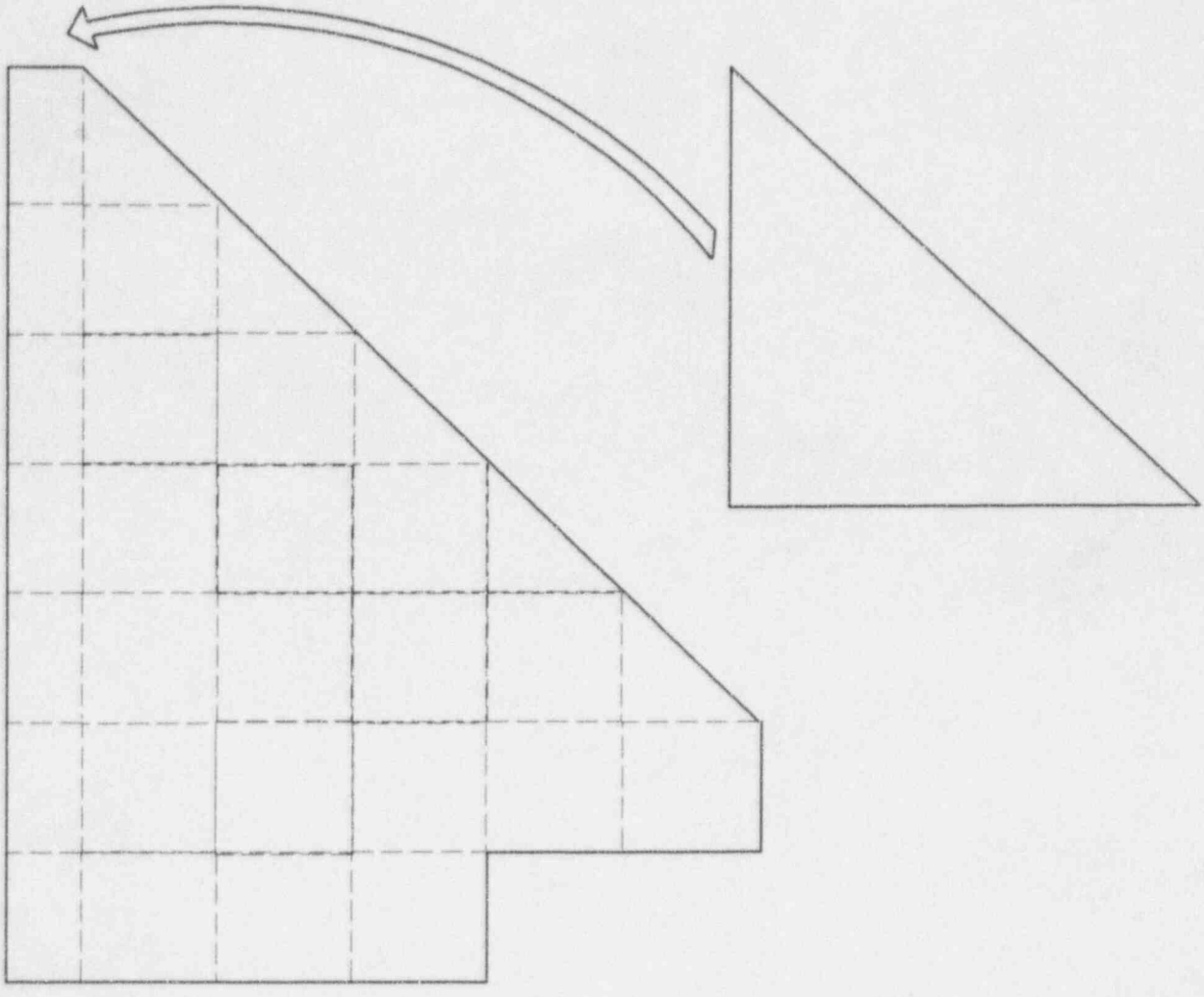

Figure 2-16 : Cross Section of V5H Fuel Assembly

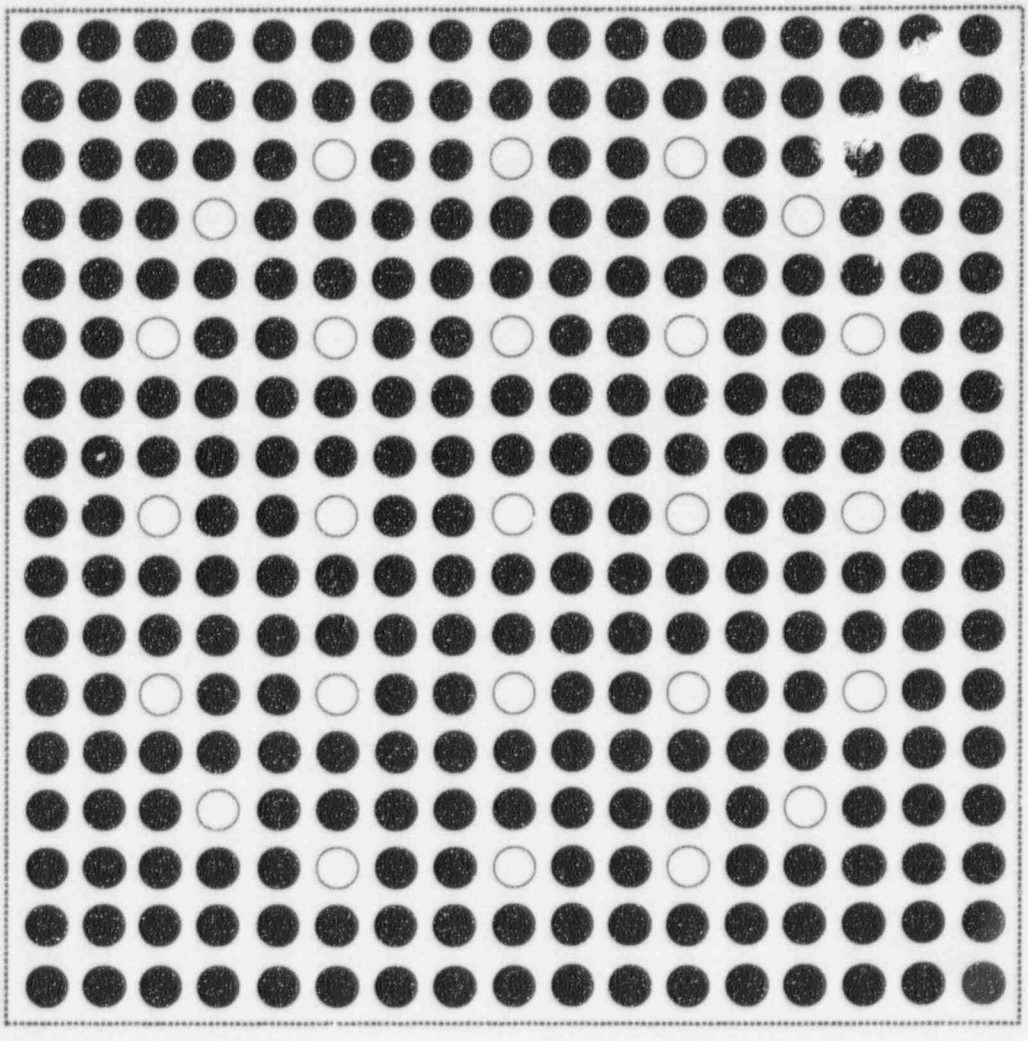

2.2.1.1.1 Base Radial Power Distribution

This section provides the derivation of a limiting radial power distribution for use in core thermal-hydraulic analyses which are performed using Westinghouse thermal-hydraulic design procedures.

Average core parameters or parameters in the core average flow channel (heat flux, coolant temperature, etc.) can be readily determined from a knowledge of the total heat output, core flow rate, geometry, etc. However, the core performance is not limited by the average conditions, but rather by the most severe conditions in the core. Therefore, in core thermal-hydraulic design, it is useful to define several hot channel factors which relate local to average core conditions.

Total hot channel factors for heat flux, F_Q, and nuclear enthalpy rise, $F_{\Delta H}$ are defined as the maximum-to-average ratios of these quantities in the reactor core. Each of the total hot channel factors is the product of a nuclear hot channel factor and an engineering hot channel factor. F_Q considers the local maximum at a point and defines the hot spot. $F_{\Delta H}$ involves the maximum integrated value along a channel and defines the hot channel. The total hot channel factors are used in establishing the thermal limits of the core with respect to fuel temperatures and DNB. These thermal limits are then used to establish core power capability and reactor protection system setpoints. The nuclear enthalpy rise hot channel factor, $F^N_{\Delta H}$, defines the limiting radial power distribution within the core.

The nuclear enthalpy rise hot channel factor is used by core thermal-hydraulic design to perform DNBR calculations. Westinghouse has derived a generic limiting $F^N_{\Delta H}$ distribution for use in designs with 17 x 17 fuel. This power distribution, shown in Figure 2-17, features a maximum pin power of [ ]^b and a pin-to-box factor of [ ]^b. However, since the current licensed peak $F^N_{\Delta H}$ for the WCGS is 1.65, the generic Westinghouse distribution must be adjusted. The adjustment was performed such that the relative intra-bundle peaking distribution was preserved (i.e., pin-to-box factor). This approach has been reviewed and approved by the NRC[12]. For each pin shown in the reference distribution, the pin powers were increased according to the expression;

$$\left[\qquad\qquad\right]^{a,b}$$

The resulting distribution, shown in Figure 2-18, features a peak pin power of 1.65, a pin-to-box factor of [ ]^b, and bundle average power of [ ]^a.

The WCGS core thermal-hydraulic analysis employs a statistical approach for consideration of correlation, nuclear, and plant processes. Cycles 7 and 8 were designed using the Babcock & Wilcox *Statistical Core Design*[13] (SCD) methodology. Beginning with Cycle 9, the core thermal-hydraulic portions of future reload designs for the WCGS will be based on the Westinghouse *Revised Thermal Design Procedure* (RTDP)[14]. Under RTDP, the design $F_{\Delta H}^{N}$ is determined by taking the license limit (i.e. 1.65) and dividing it by the measurement uncertainty (i.e., 4%). Thus, the design $F_{\Delta H}^{N}$ distribution for core thermal-hydraulic design of the WCGS, Cycle 9 operation is established by modifying the pin factors shown in Figure 2-18 according to the expression;

[ ]^{a}

The resulting design, hot assembly power distribution is shown in Figure 2-19.

Figure 2-17 : Westinghouse Reference Radial Power Distribution

[b]

Peak-to-Average = [ ]b
Bundle Average Power = [ ]b

Figure 2-18 : Limiting Power Distribution - WCGS Cycle 9

a,b

[ ]

Peak-to-Average = [ ]^{a,b}
Bundle Average Power = [ ]^{a,b}

Figure 2-19 : Hot Assembly Design Power Distribution

a,b

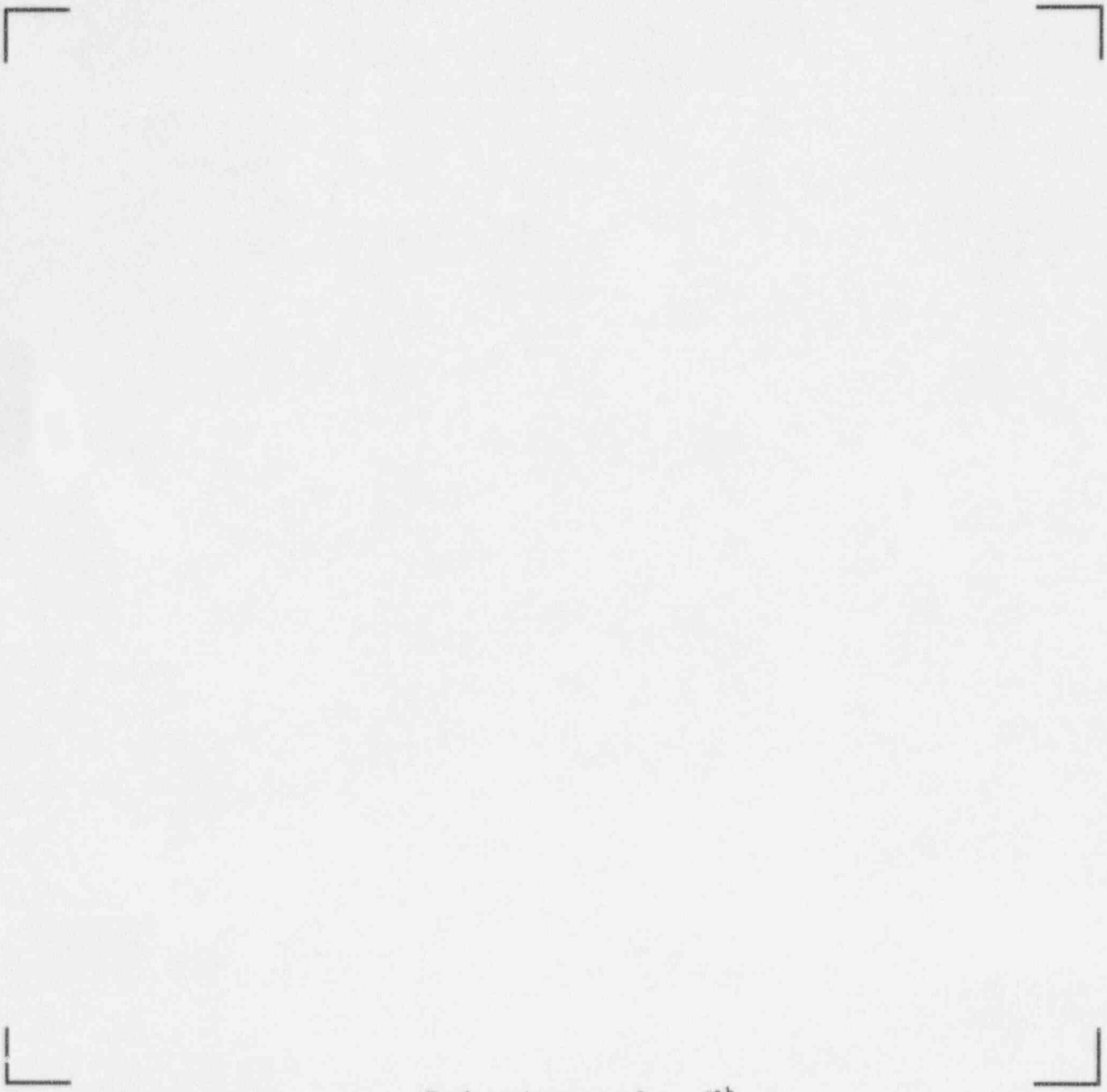

Peak-to-Average = [ ]^{a,b}
Bundle Average Power = [ ]^{a,b}

2.2.1.1.2 Base Model Layout

This section describes the layout and derivation of channel dimensions for the base VIPRE-01 thermal-hydraulic model for the WCGS core, Cycle 9. The base model is a 30 channel model based on nominal cold dimensions for the Westinghouse V5H with IFMs fuel design. The noding for the base model was selected based on the following guidelines;

- The hot channel and the limiting channel for DNB must be surrounded by at least one (1) row of subchannels.
- The subchannel noding should be selected so that changes in the hot assembly power distribution can be accommodated.
- The number of channels should be minimized to reduce the computing resources required to run the model.
- The number of VIPRE-01 fuel rod models included in the model should provide a balance between calculational detail and reduction of computation time.

Using the guidelines outlined above, guidance provided in the VIPRE-01, Mod 1 modeling guidelines[15], and using engineering judgment based on WCNOC experience, the noding for the WCNOC VIPRE-01 base thermal-hydraulic model for Cycle 9 was selected. This noding, shown in Figure 2-20, is a 30 channel model utilizing 28 subchannels and 2 lumped channels. Channels 1 through 29 are located in the hot assembly with channel 30 representing the remainder of the 1/8 section of symmetry of the core.

Figure 2-21 provides an expanded view of the noding used in the hot assembly for the base thermal-hydraulic model. The hot assembly has 29 channels comprised of 28 subchannels and 1 lumped channel. As is shown in the figure, 31 fuel rod modes are required to model heat transfer with the hot assembly. The noding selected for the base model can accommodate a wide variety of radial peaking distributions while meeting the requirement that the limiting channel be surrounded by a row of channels modeled at the subchannel level.

Figure 2-20 : Cycle 9 Base Thermal-Hydraulic Model Channel Layout

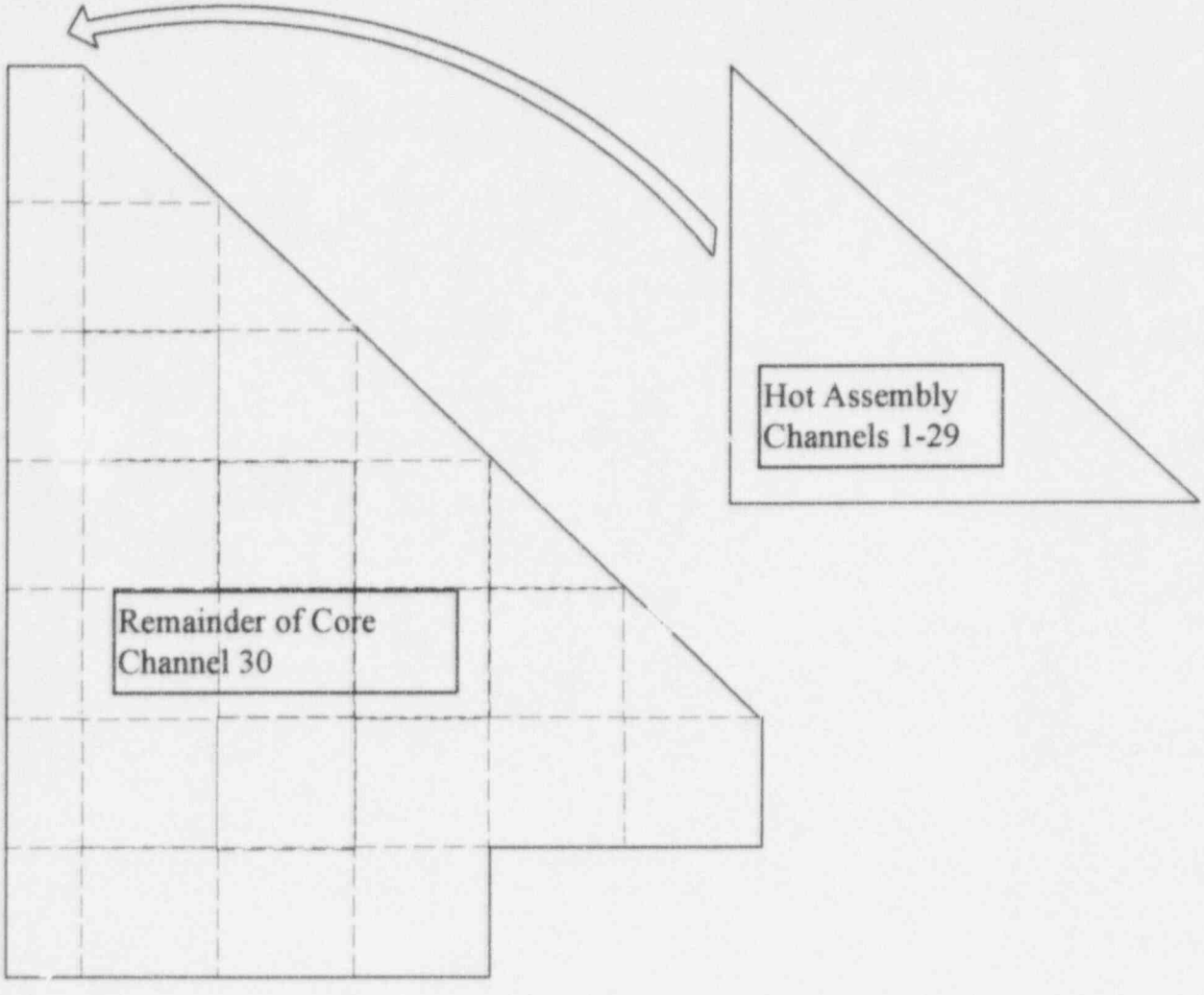

Figure 2-21 : Hot Assembly Noding

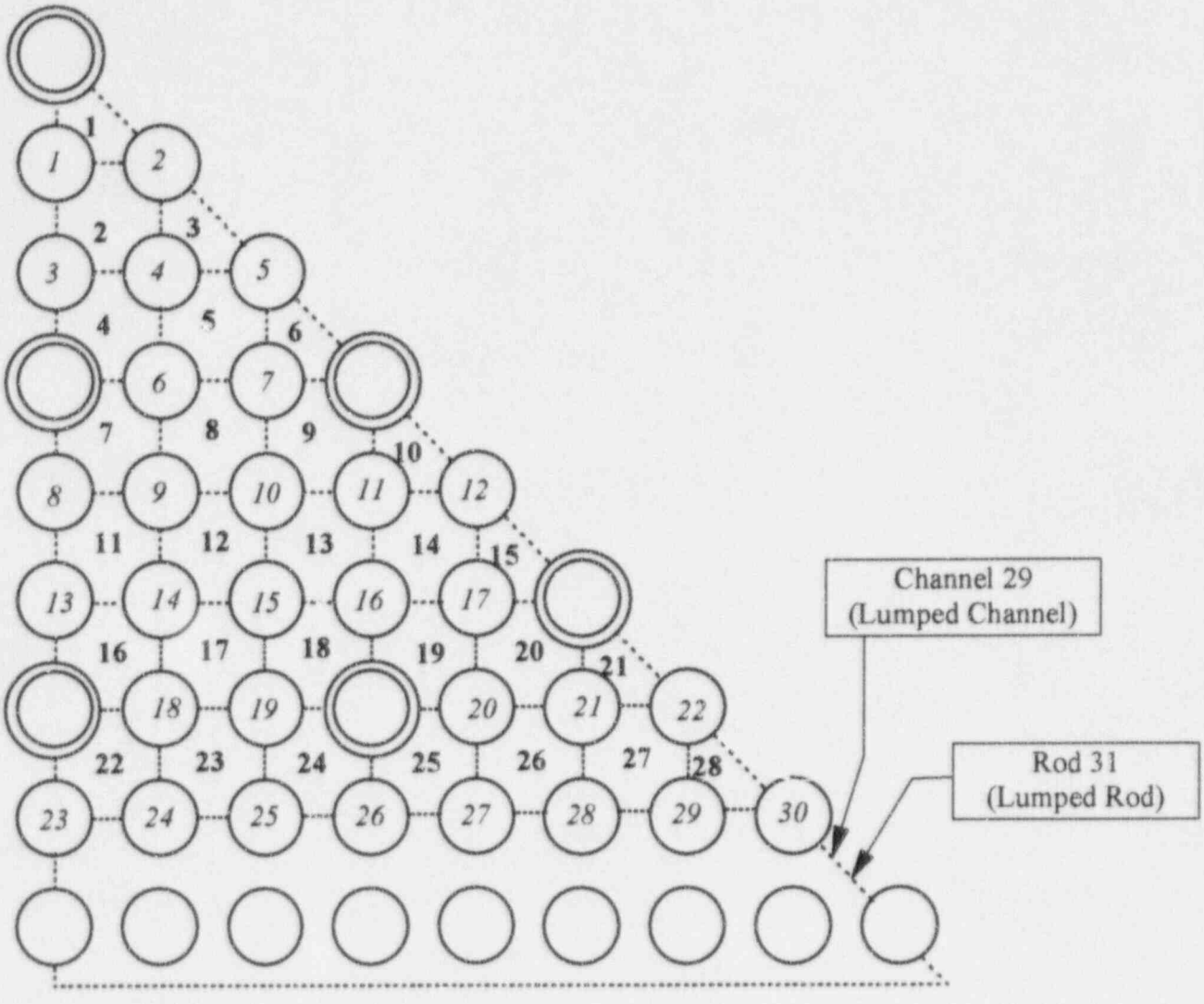

2.2.1.1.2.1 Subchannel Gap & Centroids

To define a VIPRE-01 model, the user must provide the rod-to-rod gap and the subchannel-to-subchannel centroid distance. These parameters are used in the code to calculate crossflow between subchannels. The product of gap width, S, and the axial node length, ΔX, define the area for crossflow between channels[16]. The centroid distance, ℓ, is used to define the lateral pressure gradient in the crossflow momentum equation for mass exchange between channels. Since the existence of a pressure gradient between subchannels is the driving force for crossflow, the centroid distance has a direct impact on the subchannel mass and energy exchange.

In a typical subchannel, the subchannel gap width is simply the distance between adjacent fuel rods. For a unit cell in the V5H design, this distance is

$$\begin{aligned} S &= \text{Pitch - Rod Diameter} \\ S &= 0.496 \text{ in. - } 0.374 \text{ in.} \\ S &= 0.122 \text{ in.} \end{aligned}$$

For gaps between a guide tube and a fuel rod, the gap width may be expressed as;

$$\begin{aligned} S_{g.t.} &= \text{Pitch - } 1/2(\text{Rod Diameter + G. T. Diameter}) \\ S_{g.t.} &= 0.496 \text{ in. - } 1/2(0.374 \text{ in.} + 0.474 \text{ in.}) \\ S_{g.t.} &= 0.072 \text{ in.} \end{aligned}$$

Choice of a value for the centroid distance between subchannels is not as straightforward as the calculation of the gap width. Ideally, the centroid distance (or more correctly 1/2 the centroid distance) would represent the distance into a subchannel at which flow through the gap ceases to influence the local flow field. Due to the complex nature of crossflow through a gap between subchannels, it is not possible to calculate an exact value for the centroid distance based on first principles. In the early version of the COBRA code, the centroid distance was omitted from the flow solution and a uniform gap-to-length ratio (i.e., $\frac{S}{\ell}$) was used instead[17]. VIPRE-01 retains the capability to utilize a uniform gap-to-length ratio but it is more realistic to specify a centroid length for each gap defined in the model. For most thermal-hydraulic analyses, the use of the distance between geometric centroids of adjacent subchannel is appropriate.

The centroid distance for unit channels in the V5H fuel design is the same as the fuel pitch. For V5H, this distance is 0.496 inches. [

]^{a}. The error in the unit channel to guide tube channel centroid length

introduced by this assumption will be less than 10 percent. Variations in centroid length of this magnitude have an insignificant impact on VIPRE-01 results[18]. Therefore, for all gaps connecting adjacent subchannels, the centroid distance to be used in the base thermal-hydraulic model is simply the subchannel pitch or;

$$\ell = 0.496 in.$$

When defining the centroid distance for subchannels cut by a line of symmetry, the centroid distance should be determined as if the entire channel were present[19].

2.2.1.1.2.2 Lumped Channel Gap & Centroids

The use of lumped channels in VIPRE-01 significantly reduces the number of channels, and subsequently, the computer run time. VIPRE-01 lumped channels represent the total flow areas, wetted perimeters, and heated perimeters of the individual subchannels represented. However, since VIPRE-01 assumes uniform conditions exist across each channel defined[20], the use of lumped channels presents special problems when determining crossflow.

To insure that correct crossflows are predicted for lumped channel geometries, the gap width, centroid distance, and lateral form loss coefficient must be modified to represent the physical situation. That is, the gap width should be increased to represent the sum of all the gaps along the channel interface. The centroid length should be adjusted to account for the number of rod rows between the geometric centroids of the lumped channel, and the lateral friction coefficient must be adjusted.

In general, the centroid distance and lateral form loss coefficient should be increased from the nominal subchannel values in proportion to the number of rod rows between the lumped channel centroids[21]. This approach was utilized in the development of WCNOC's thermal-hydraulic analysis methodology and it is preserved in the current model.

2.2.1.1.2.3 Channel Mixing Coefficients

The turbulent mixing correlations available in VIPRE-01 are empirical correlations designed to model the effect of turbulent mixing on lateral momentum exchange between subchannels. Several correlations are available in VIPRE-01 for modeling turbulent mixing. The turbulent mixing correlation selected for use in the WCNOC base model is[22];

$$[\qquad\qquad]^{a}$$

Equation 2.1

Where,

W'	=	turbulent crossflow.
β	=	an empirically derived subchannel turbulent mixing coefficient.
S	=	gap width.
$\overline{G}$	=	average of mass velocities in the adjacent channels.

Turbulent mixing is generally considered to be a subchannel phenomena and is not directly applicable to lumped channel analyses[23]. To assure that the turbulent mixing effect is correctly calculated for lumped channels in a VIPRE-01 model, the mixing coefficient, β, should be reduced from the nominal subchannel value in proportion to the number of rod rows separating adjacent lumped channel centroids. For the WCNOC base thermal-hydraulic model, the effect of turbulent mixing between lumped channels was modeled by reducing the subchannel turbulent mixing coefficient according to the expression[24];

$$\beta_K = A_{sub} * \frac{Dist_{sub}}{Dist_K}$$

Equation 2.2

Where,

β_K	=	turbulent mixing coefficient for Gap K.
A_{sub}	=	subchannel turbulent mixing coefficient (0.038 for V5H).
$Dist_{sub}$	=	subchannel pitch (i.e. 0.496 in.).
$Dist_K$	=	centroid length for gap K.

Application of Equation 2.2 to the base model yields the gap turbulent mixing coefficient. For gaps involving adjacent channels modeled at the subchannel level, Equation 2.2 reduces to yield the nominal subchannel value of the turbulent mixing coefficient. For gaps connecting to a lumped channel, the equation will reduce the turbulent mixing coefficient to account for the number of rod rows separating the centroids of the relevant channels.

2.2.1.1.2.4 VIPRE-01 Rod Definition

The rod models in VIPRE-01 are used to represent the physical structures in the core which transfer energy to the coolant. VIPRE-01 has the capability to define a heat flux boundary condition (i.e., dummy rod option) or to specify a conduction model in which the conduction equation is solved to determine the rod internal and surface temperatures. Since the conduction rod model imposes a significant increase in computing resource requirements, the WCNOC base thermal-hydraulic model was developed utilizing the VIPRE-01 dummy rod option. The conduction rod option will be implemented in those analyses in which the effects of stored energy in the fuel has a significant impact on analysis results.

The base thermal-hydraulic model of the WCGS core contains 32 fuel rod models. Of these, thirty (30) are single rods and two (2) are lumped rods (see Figure 2-21). Since rods 1 through 30 represent single rods, the radial power factors for these rods will be the same as the power factors shown in the design hot assembly power distribution (see Figure 2-19). For rod 31 of the base model, the radial power factor is the average of the rods represented.

The radial power factor for rod 32, which represents the remainder of the 1/8 section of the core, was calculated such that the total normalized core power, in the radial direction, would equal one (1.0). The perimeter factors for the two lumped rods used in the base thermal-hydraulic model are equal to the total number of rods represented in each lumped rod.

The axial power distribution chosen for use in the base model is a 1.55 symmetric cosine shape.
[

]^{b}

2.2.1.1.2.5 Channel Dependent Grid Form Loss Coefficients

Grid spacer form loss coefficients should be modeled in a manner consistent with their treatment in the derivation of the critical heat flux correlations to be used in the model[25]. That is, if a given critical heat flux correlation was developed using subchannel dependent form loss coefficients, the base thermal-hydraulic model should also use subchannel dependent form loss coefficients. This approach should be adhered to even if an alternative method would yield a more "correct" representation of the physical system modeled. The rational for this restriction follows.

A critical heat flux correlation is essentially an empirical fit to the correlation data base. Therefore, a critical heat flux correlation does not correlate the "correct" flow field; rather, it correlates the flow field supplied by the models and methods employed during correlation development. The use of models or methods other than those used in the correlation development, even if the other models produce a more "correct" flow field, would result in predictions for critical heat flux which were suspect.

[

]^{b} These channel specific grid loss coefficients were used to define the grid loss coefficients for channels 1 through 28 in the base model. However, grid form loss coefficient (FLC) for channels 29 and 30 were derived by area weighting the loss coefficients for individual subchannels represented in the lumped channels according to the expression[28],

[ ]^{b}

Equation 2.3

Where,

K_T = Total grid form loss coefficient for lumped channel.
A_T = Total flow area for lumped channel.
K_i = Grid loss coefficient for subchannel i within lumped channel.
A_i = Flow area of subchannel i.

The two Inconel, non-mixing vane grids in the V5H fuel design were not modeled using subchannel specific loss coefficients. Rather, the bundle average loss coefficients for the non-mixing vane grids were uniformly applied, at the appropriate axial elevations, to all channels in the base model. This approach is consistent with Westinghouse methodology.

2.2.1.1.2.6 Inlet Flow Distribution

One of the conservatisms used in the thermal-hydraulic design of nuclear steam supply systems is a [ ]^{a} in inlet flow to the hot assembly[29]. This conservatism has traditionally been applied to NSSS design work to account for uncertainties in the measurement of the inlet velocity distribution in a reactor core. While the advent of thermal-hydraulic analysis codes with single pass analysis capabilities has shown that flow redistribution in the lower region of the core largely offsets the effects of inlet flow mal-distributions, a [ ]^{a} to the hot assembly is incorporated into the WCNOC base model to maintain consistency with Westinghouse analysis methodology. The flow to the remainder of the core must then be slightly increased if conservation of the mass flux is to be preserved.

2.2.1.1.2.7 Miscellaneous Model Input Data

The remaining parameters required to define a VIPRE-01 model, such as axial noding, flow correlations, heat transfer correlations, friction factor correlations, water property options, and numerical solution/convergence criteria are unchanged from the previously licensed model[30].

2.2.1.2 Model Sensitivities

A number of sensitivity studies were performed to demonstrate that the modeling assumptions and empirical correlations utilized in the WCGS base thermal-hydraulic model are sufficient to yield accurate and conservative results for licensing grade design analyses.

2.2.1.2.1 Selection of Sensitivity Study Boundary Conditions

This section describes the selection of a set of boundary conditions for use in sensitivity studies on the base model. The boundary conditions were selected on the following basis;

1. The full range of applicability of the model critical heat flux correlation should be exercised with an emphasis on conditions which result in a DNBR at or near the expected design limit.
2. Conditions expected to occur during normal operation of the WCGS should be included in the study.

Based on the above guidelines, seven different boundary conditions were selected. These conditions are;

1. Nominal Operating Case
2. High Power Case (130%)
3. Intermediate Flow Case (55% Flow)
4. Low Pressure Case (1440 psia)
5. Low Pressure & Intermediate Flow Case
6. Low Pressure, Low Flow, & Intermediate Power Case
7. High Inlet Temperature Case

A summary of the seven boundary conditions and the associated VIPRE-01 input may be found in Table 2-6.

Nominal Operating Case

The nominal operating case, identified as case one (1), was based on minimum measured flow (384,000 GPM) and best estimate bypass (6.61% with thimble plugs removed), nominal system pressure (≈ 2270 psia), nominal rated full power (3565 MW_{th}), and nominal inlet temperature (554.8 °F). Using these parameters, the VIPRE-01 input is;

Parameter		VIPRE-01 Input Value
Q	=	5.8428 kW/ft
P	=	2270.0 psia
T	=	554.8 °F
G	=	2.612 $MLb_m/hr\text{-}ft^2$

High Power Case

The high power case, identified as case two (2), was intended to test performance of the model at moderately high exit qualities. For this case, the power was set to 130% of rated thermal power while the remaining core variables were held at their nominal case values. Thus, the VIPRE-01 input for the high power case is;

Parameter		VIPRE-01 Input Value
Q	=	7.5956 kW/ft
P	=	2270.0 psia
T	=	554.8 °F
G	=	2.612 $MLb_m/hr\text{-}ft^2$

Intermediate Flow Case

The intermediate flow case, identified as case number three (3), was designed to examine performance of the model under conditions of intermediate flow. The flow for this case was set to 55% of nominal inlet flow while the remaining core parameters were held at their nominal case values. Thus, the VIPRE-01 input for the intermediate flow case is;

Parameter		VIPRE-01 Input Value
Q	=	5.8428 kW/ft
P	=	2270.0 psia
T	=	554.8 °F
G	=	1.4366 $MLb_m/hr\text{-}ft^2$

Low Pressure Case

The low pressure case, identified as case number four (4), examines the performance of the model below the low pressure trip setpoint for the WCGS (i.e. 1900 psia). System pressure was set to 1440 psia (the lower bound of the WRB-2 range of applicability) while the remaining input parameters were held at their nominal case values. Note that the reduction in coolant density associated with the lower system pressure results in a change in inlet mass flux even though the volumetric flow rate was held constant. Thus, the VIPRE-01 input for the low pressure case is;

Parameter		VIPRE-01 Input Value
Q	=	5.8428 kW/ft
P	=	1440.0 psia
T	=	554.8 °F
G	=	2.5631 $MLb_m/hr\text{-}ft^2$

Low Pressure & Intermediate Flow Case

The low pressure and intermediate flow case, identified as case number five (5), was designed to examine performance of the model under low pressure conditions with moderately high quality. The case is defined with a system pressure of 1900 psia and an inlet mass flux of 60% of nominal. Note that the density effect of the reduction in system pressure is included in the calculation of inlet mass flux. Thus, the VIPRE-01 input for the low pressure and intermediate flow case is;

Parameter		VIPRE-01 Input Value
Q	=	5.8428 kW/ft
P	=	1900.0 psia
T	=	554.8 °F
G	=	1.5581 $MLb_m/hr\text{-}ft^2$

Low Pressure, Low Flow, & Intermediate Power Case

The low pressure, low flow, and intermediate power case, identified as case number six (6), was designed to examine model performance with several core state parameters at values adverse to DNB. Channel exit qualities for this case are expected to be very high. The case is defined as a system pressure of 1900 psia, inlet flow of 1.0 $Mlb_m/hr\text{-}ft^2$ (lower range of WRB-2 correlation), and core power of 80% of nominal. Thus, the VIPRE-01 input for this case is;

Parameter		VIPRE-01 Input Value
Q	=	4.6742 kW/ft
P	=	1900.0 psia
T	=	554.8 °F
G	=	1.0 $MLb_m/hr\text{-}ft^2$

High Inlet Temperature Case

The high inlet temperature case, identified as case number seven (7), examines model performance with the inlet temperature increased to 110% of nominal. The remaining core parameters were held at their nominal conditions values. Note that the change in inlet density associated with the higher inlet temperature is included in the calculation of inlet mass flux. Thus, the VIPRE-01 input for the high inlet temperature case is;

Parameter		VIPRE-01 Input Value
Q	=	5.8428 kW/ft
P	=	2270.0 psia
T	=	610.3 °F
G	=	2.3709 $MLb_m/hr\text{-}ft^2$

Table 2-6 : Summary of Sensitivity Study Boundary Conditions

Case	System Pressure (psia)	Inlet Temp (°F)	Inlet Mass Flux ($Mlb_m/hr\text{-}ft^2$)	Power (kW/ft)
1	2270.0	554.8	2.612	5.8428
2	2270.0	554.8	2.612	7.5956
3	2270.0	554.8	1.4366	5.8428
4	1440.0	554.8	2.5631	5.8428
5	1900.0	554.8	1.5581	5.8428
6	1900.0	554.8	1.0000	4.6742
7	2270.0	610.3	2.3709	5.8428

2.2.1.2.2 Base Model Performance : Case 1

Table 2-7 provides a summary of the results from the base deck run. As is shown in the table, the minimum DNBR predicted for the nominal operation case (i.e., case 1) is 2.530; occurring in channel 10, rod 11, at an axial elevation of 69.0 inches. This places the limiting channel for DNB under these conditions in a guide tube channel with MDNBR occurring just prior to the third (3) mixing vane grid.

Figure 2-22 shows the predicted DNBR as a function of axial position in channel number 10 for case number 1 (i.e., nominal conditions). The figure reveals the dependence of the predicted DNB ratio on the [ ]^{a,b}
The predicted DNBR is observed to approach a local minimum value prior to each spacer grid. The DNBR then rises sharply just after each grid. This phenomena has been confirmed in critical heat flux testing where the point of critical heat flux is usually observed at an axial location just upstream to mixing vane grids. The DNB ratio increases downstream from the grid because of the increased turbulence and consequently, the increased subchannel crossflow, that occurs when the coolant encounters the grid.

Table 2-8 provides a summary of the channel exit conditions for the base thermal-hydraulic model, case 1. As indicated in the table, channel 3 has the highest exit enthalpy. Mass flow in the model is distributed as expected. Generally, channel exit flow mass is observed to [ ]^{a} towards the center of the core. This effect is caused by the [ ]^{a} in flow assumed for the hot assembly and by the increased flow resistance due to presence of two phase fluid conditions at some elevations in the high power, interior channels. In addition, exit mass flux for guide tube channels are observed to be less than the mass flux in neighboring unit cells. This effect is a result of the increased flow resistance of the spacer grids for a guide tube cell and the increase in axial drag long the rods in the guide tube cell due to the larger wetter perimeter.

The local equilibrium quality for a guide tube channel, channel 10, and the adjacent unit cell, channel 14, is plotted as a function of axial position in Figure 2-23. This plot indicates that the local quality for the two channels is [ ]^{a} in the lower regions of the core. However, in the high power region, the quality in the unit cell is [ ]^{a} than in the adjacent guide tube cell. This occurs because of the higher linear heat rate in the unit cell associated with the larger heated perimeter.

The local mass flux in channels 10 and 14 is plotted in Figure 2-24. This figure indicates that the local mass velocity in the guide tube channel is less than the mass flux in the adjacent unit cell. This is expected behavior since the form loss in the guide tube channel, due to spacer grids and axial drag, is larger than in the unit cell. The figure also reveals the effect of spacer grids on subchannel mass flux. The mass flux in the guide tube channel is observed to [ ]^{a} at the locations corresponding to the spacer grids while the mass flux in the adjacent unit cell is observed to [ ]^{a} at these same locations. The larger form loss of the spacer grids in the guide tube channel drives flow to the unit channels. Further, the figure indicates that the mass flux in the unit cell is generally [ ]^{a} in the regions between the spacer grids giving the unit cell mass flux profile a "sawtooth" effect. Further insight into the mechanism for this phenomenon may be gained by examination of the crossflow patterns between these two channels.

The net crossflow at each axial node for channels 10 and 14 is shown in Figure 2-25 (note: positive crossflow in this figure represents flow into the channel and negative values indicate flow out of the channel). Examination of the crossflow for channel 10, the guide tube channel, reveals the influence of the grids on crossflow within a channel. In the guide tube channel, there are [ ]^{a} crossflow dominates. These elevations correspond to the locations of the six mixing vane grids and the three intermediate flow mixer grids. This behavior is expected as the grid form loss coefficient is larger in the guide tube channels than in surrounding unit cells. Again referring to Figure 2-25, the crossflow for channel 14, the unit cell adjacent to channel 10, also features [ ]^{a}. However, in the unit cell, crossflow at the grid elevations is [ ]^{a}

Crossflow in the unit channel (i.e., channel 14), is dominated by two mechanisms. First, there is a relatively [ ]^{a} occurring at axial elevations corresponding to the locations of the grids. The second mechanism apparent in the unit cells is the [ ]^{a} occurring in the regions between the spacer grids. This pattern is the result of the increased linear heat rate and higher void fraction in the unit cells as compared to the neighboring guide tube channels. The increased linear heat rate, associated with the larger heated perimeter (1.1750 in. for a unit cell versus 0.8812 in. for a guide tube cell) causes the fluid in the unit cell channel to heat up and expand faster than the fluid in the guide tube channels. Also, higher void fractions in the unit channel result in an increase in axial drag due to the [ ]^{a} on axial drag. This increased heatup and fluid expansion, coupled with the increase in flow resistance under [ ]^{a} between the spacer grids.

Examination of the net crossflow for channel 30, the lumped channel representing the remainder of the core outside of the hot assembly, yields additional insight into the model performance (see Figure 2-26). Recall that a [ ]^{a} was applied to the inlet mass flux for the hot assembly. In the lower region of the core, [ ]^{a} Thus, the effect is to redistribute the flow, offsetting much of the effect of the [ ]^{a} However, as flow enters the high power region of the core, with respect to axial elevation, the high power in the hot assembly causes the fluid flowing in the hot assembly to expand faster than fluid in the remainder of the core (i.e., channel 30). The higher equilibrium quality in the hot assembly also increases axial drag in the hot assembly [ ]^{a}

The two Inconel non-mixing vane grids, located at the top and bottom of the V5H fuel assembly, do not induce large crossflow between the various channels in the model because the grid loss coefficient for these grids was applied [ ]^{a} to all subchannels.

Table 2-7 : Base Thermal-Hydraulic Model Results Summary

Table 2-8 : Base Model Results - Channel Exit Summary : Case 1

Channel	Enthalpy (BTU/lb_m)	Temp. (°F)	Density (lb_m/ft^3)	Quality	Void Fraction	Flow (lb_m/sec)	Mass Flux ($MLb_m/hr\text{-}ft^2$)
1	698.13	652.45	36.918	.000	.0000	.285	2.4739
2	698.20	652.49	36.913	.000	.0000	.654	2.4876
3	698.22	652.50	36.910	.000	.0000	.327	2.4917
4	697.94	652.35	36.934	.000	.0000	.570	2.4741
5	697.98	652.37	36.931	.000	.0000	.654	2.4879
6	697.76	652.25	36.949	.000	.0000	.285	2.4745
7	697.31	652.01	36.986	.000	.0000	.571	2.4754
8	697.44	652.08	36.975	.000	.0000	.654	2.4889
9	697.16	651.93	36.998	.000	.0000	.571	2.4752
10	696.61	651.62	37.044	.000	.0000	.285	2.4744
11	696.54	651.58	37.049	.000	.0000	.654	2.4907
12	696.59	651.61	37.045	.000	.0000	.655	2.4946
13	696.43	651.52	37.058	.000	.0000	.654	2.4896
14	696.00	651.29	37.094	.000	.0000	.653	2.4862
15	695.39	650.95	37.143	.000	.0000	.286	2.4757
16	694.93	650.70	37.180	.000	.0000	.572	2.4796
17	694.92	650.69	37.182	.000	.0000	.655	2.4931
18	695.01	650.74	37.174	.000	.0000	.571	2.4784
19	694.61	650.52	37.207	.000	.0000	.570	2.4748
20	693.83	650.09	37.270	.000	.0000	.571	2.4774
21	692.79	649.51	37.354	.000	.0000	.287	2.4849
22	691.32	648.69	37.474	.000	.0000	.573	2.4846
23	692.18	649.17	37.405	.000	.0000	.656	2.4966
24	692.18	649.17	37.404	.000	.0000	.572	2.4815
25	692.33	649.26	37.392	.000	.0000	.572	2.4805
26	692.52	649.36	37.376	.000	.0000	.656	2.4964
27	692.14	649.15	37.407	.000	.0000	.658	2.5027
28	691.60	648.85	37.450	.000	.0000	.329	2.5081
29	686.21	645.81	37.885	.000	.0000	8.594	2.5117
30	643.67	619.94	41.079	.000	.0000	4627.606	2.6126

Figure 2-22 : Base Model Results - Predicted DNBR in Limiting Channel : Case 1

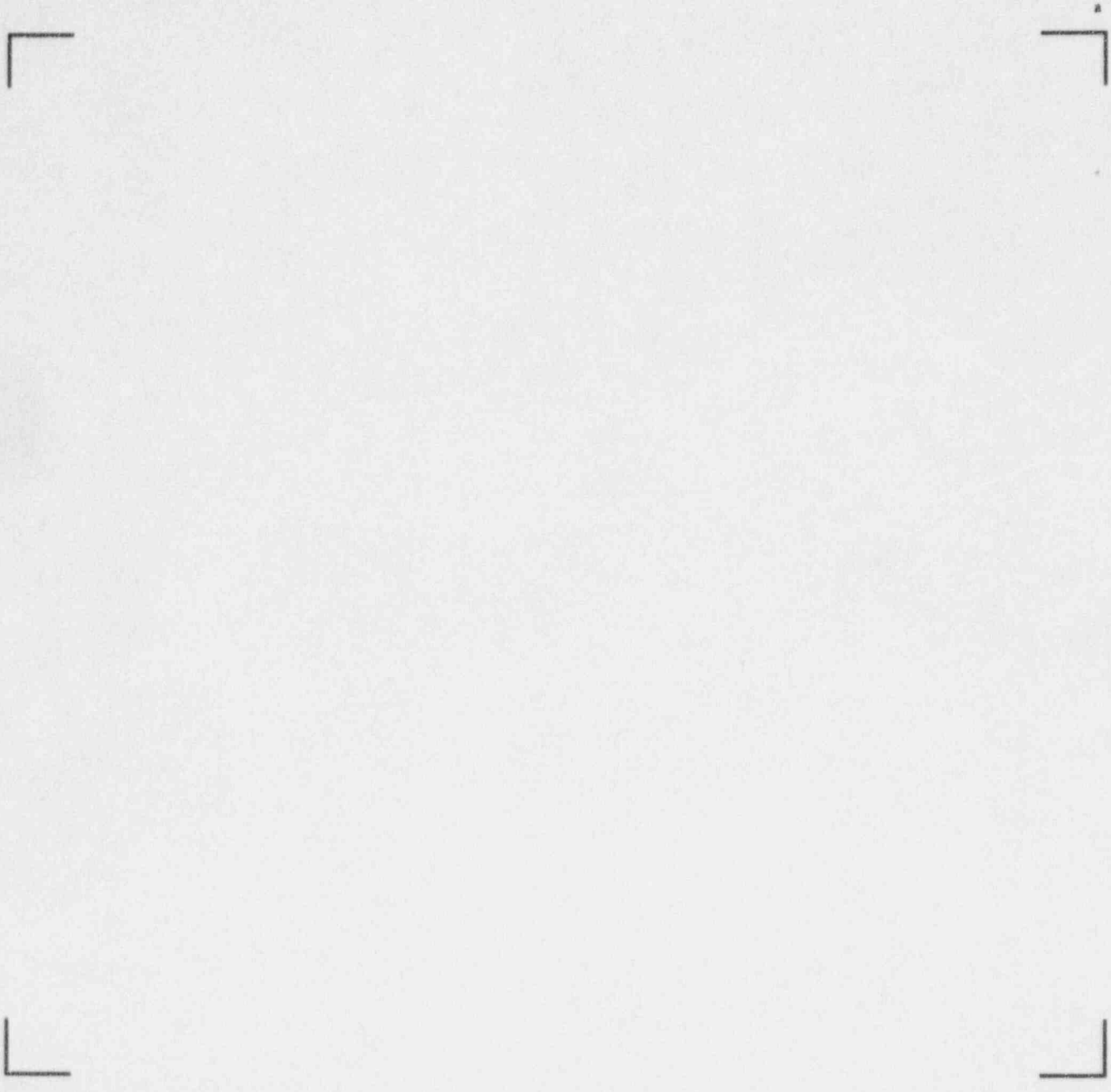

Figure 2-23 : Base Model Results - Equilibrium Quality Vs. Height : Channels 10 & 14

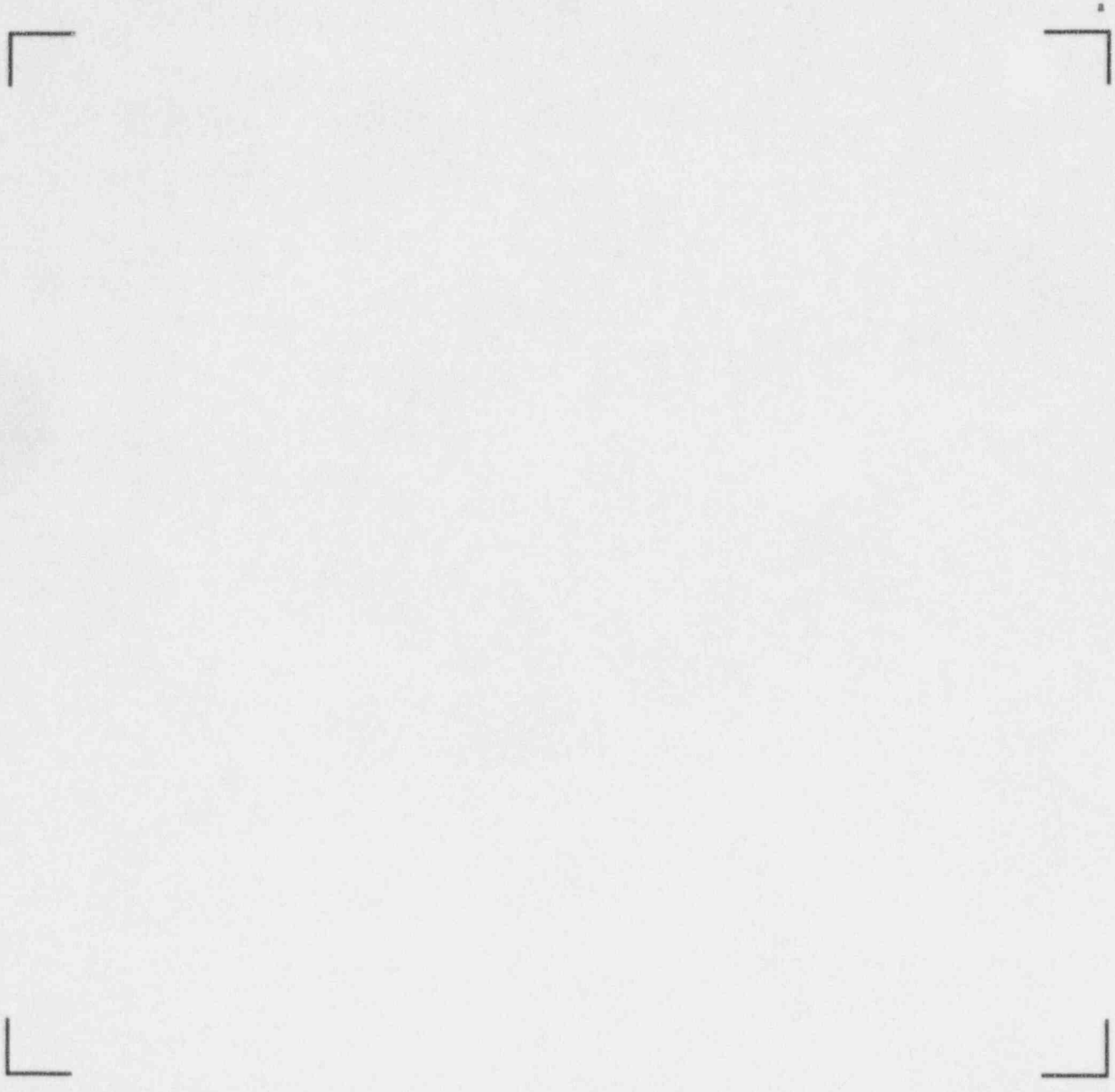

Figure 2-24 : Local Mass Flux Vs. Axial Position - Channels 10 & 14

Figure 2-25 : Net Crossflow - Channels 10 & 14 : Case 1

Figure 2-26 : Net Crossflow - Channel 30 : Case 1

2.2.1.2.3 Base Model Performance : Case 2

Table 2-7 indicates that the predicted minimum DNBR for the high power case run of the base model was 1.712. The limiting channel was channel 4. Channel 4 is also a guide tube channel but it is located interior to the hot assembly from the limiting channel in the nominal conditions run. The axial position of minimum DNBR shifted higher in the rod bundle for the high power case, occurring at 110.1 inches versus 69.0 inches in the nominal case. This places MDNBR just prior to the 5th mixing vane grid.

A summary of channel exit conditions for case 2 is shown in Table 2-9. This table indicates that channel one (1) has the highest exit enthalpy, 748.70 BTU/lb_m. Bundle exit flow is distributed in a manner similar to the base case. That is, channel exit mass flux [ ]^a in channels closer to the center of the core. As indicated in the table, the high power case results in significant voiding in the hot assembly with exit conditions in all hot assembly channels at saturation temperature.

The predicted DNBR in the limiting channel, channel 4, and the adjacent unit cell, channel 5, is plotted as a function of axial height in Figure 2-27. Again, the dependence of the predicted DNBR on the [ ]^a is apparent. While channel 4 is the limiting channel for DNB, there is very little difference between predicted DNBRs for channel 4 and channel 5.

The local mass flux in channels 4 and 5 are plotted as functions of axial elevation in Figure 2-28. As was seen in case 1, the mass flux in the guide tube channel is less than that in the adjacent unit cell. Again, this behavior is attributed to the larger form loss at the spacer grids and the increased axial drag. However, comparison of the results from case 2, Figure 2-28, with those from case 1, Figure 2-24, indicate that the difference between unit cell and guide tube cell mass flux is smaller for the high power case. This is attributed to the larger influence of the [ ]^a on axial drag at the high quality conditions associated with case 2. Since the unit cell has a higher linear heat rate, and consequently higher void fraction, the [ ]^a serves to equalize the form loss between the unit and guide tube cells. This behavior is consistent with previous model performance.

Table 2-9 : Channel Exit Summary - Case 2

Channel	Enthalpy (BTU/lb_m)	Temp. (°F)	Density (lb_m/ft^3)	Quality	Void Fraction	Flow (lb_m/sec)	Mass Flux ($MLb_m/hr\text{-}ft^2$)
1	748.70	653.94	24.996	.109	.3811	.240	2.0772
2	748.48	653.94	25.032	.109	.3799	.550	2.0917
3	747.99	653.94	25.115	.108	.3772	.276	2.0991
4	747.53	653.94	25.196	.107	.3745	.481	2.0851
5	746.74	653.94	25.330	.105	.3700	.553	2.1036
6	745.15	653.94	25.610	.101	.3607	.242	2.1015
7	745.97	653.94	25.465	.103	.3656	.483	2.0958
8	745.02	653.94	25.632	.100	.3600	.556	2.1155
9	742.26	653.94	26.133	.094	.3434	.489	2.1215
10	737.83	653.94	26.982	.083	.3152	.248	2.1528
11	745.11	653.94	25.615	.101	.3605	.556	2.1151
12	744.04	653.94	25.808	.098	.3542	.559	2.1265
13	741.60	653.94	26.255	.092	.3393	.562	2.1388
14	738.61	653.94	26.827	.085	.3203	.567	2.1568
15	738.33	653.94	26.883	.084	.3185	.248	2.1477
16	743.42	653.94	25.920	.097	.3504	.487	2.1139
17	742.68	653.94	26.055	.095	.3459	.560	2.1320
18	741.28	653.94	26.317	.091	.3373	.491	2.1281
19	739.04	653.94	26.745	.086	.3230	.493	2.1403
20	738.84	653.94	26.783	.085	.3218	.494	2.1426
21	739.03	653.94	26.746	.086	.3230	.248	2.1465
22	739.21	653.94	26.711	.086	.3242	.494	2.1427
23	739.92	653.94	26.573	.088	.3288	.565	2.1503
24	739.26	653.94	26.702	.086	.3245	.493	2.1407
25	738.46	653.94	26.857	.085	.3193	.495	2.1458
26	738.71	653.94	26.809	.085	.3209	.567	2.1594
27	738.87	653.94	26.776	.086	.3220	.568	2.1638
28	738.68	653.94	26.814	.085	.3208	.285	2.1699
29	732.68	653.94	28.040	.071	.2801	7.562	2.2103
30	670.85	636.86	39.080	.000	.0000	4630.788	2.6144

Figure 2-27 : MDNBR vs. Elevation : Case 2

Figure 2-28 : Mass Flux Vs. Elevation - Channels 4 & 5 : Case 2

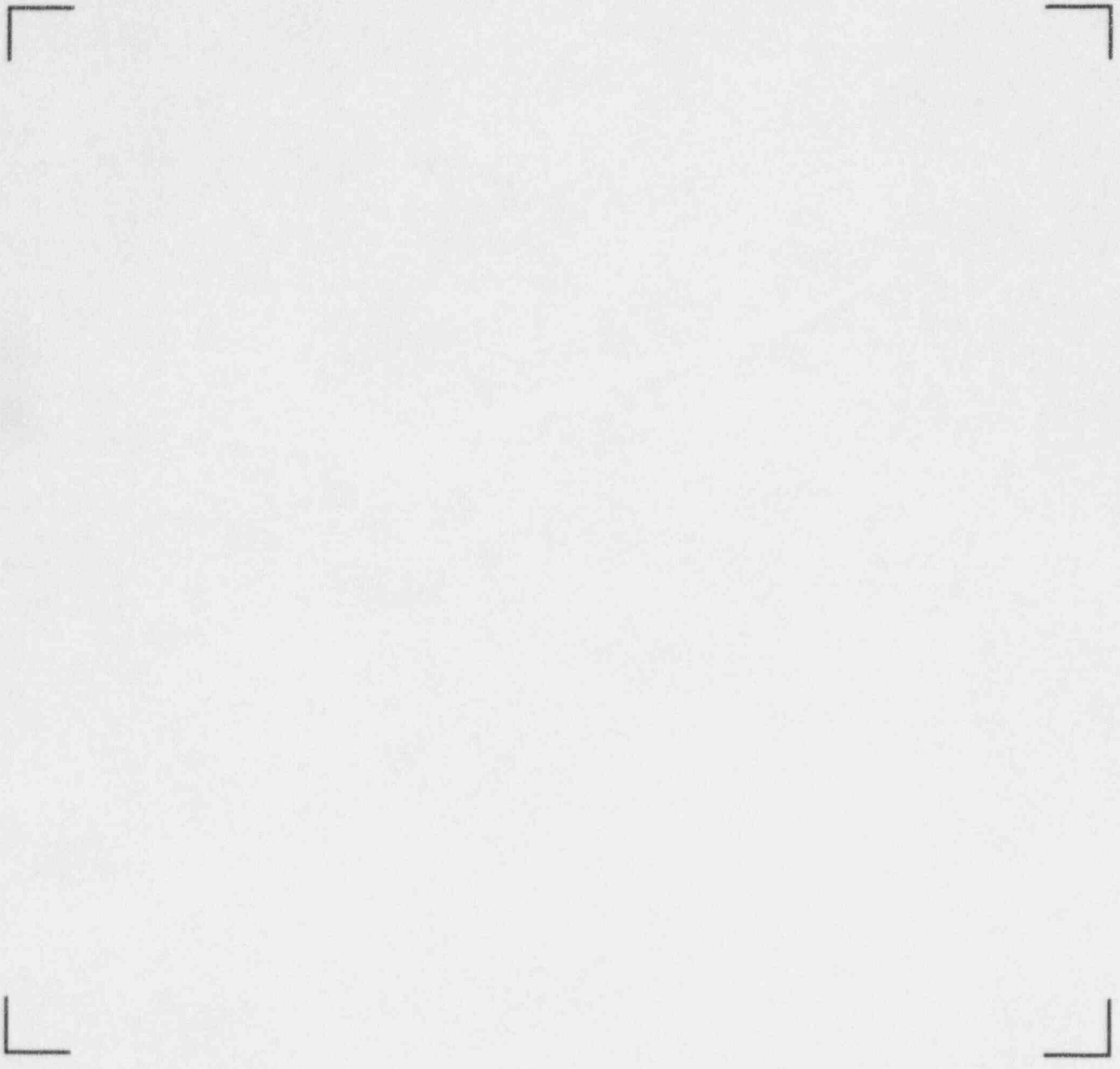

2.2.1.2.4 Base Model Performance : Case 3

Tabie 2-7 indicates that the predicted minimum DNBR for the low flow case run of the base model was 1.390. The limiting channel was channel 14. Channel 14 is a unit cell channel between the two hot rods in the design radial power distribution. The axial position of minimum DNBR shifted higher in the rod bundle for the low flow case; occurring at 110.1 inches versus 69.0 inches in the nominal case. This places MDNBR just prior to the 5th mixing vane grid.

A summary of channel exit conditions for case 3 is shown in Table 2-10. This table indicates that channel 15 has the highest exit enthalpy, 838.63 BTU/lb_m. The limiting channel for DNB, channel 14, has an exit enthalpy of 837.50 BTU/lb_m. While bundle exit flow is generally distributed in a manner similar to the base case that is, channel exit mass flux [ ]^a in channels closer to the center of the core, the extremely low flow used in this case results in a slightly different crossflow distribution pattern as compared to the base case. Specifically, channel exit enthalpies are highest in those channels [ ]^a as opposed to the base case where the highest exit enthalpies occur in channels [ ]^a As indicated in the table, the high power case results in significant voiding in the hot assembly with exit conditions in all hot assembly channels at saturation temperature.

The predicted DNBR in the limiting channel, channel 14, and the adjacent unit cell, channel 15, is plotted as a function of axial height in Figure 2-29. Again, the dependence of the predicted DNBR on the [ ]^a is apparent. While channel 14 is the limiting channel for DNB, there is very little difference between predicted DNBRs for channel 14 and channel 15.

The local mass flux in channels 14 and 15 are plotted as functions of axial elevation in Figure 2-30. As was seen in previous cases, the mass flux in the guide tube channel is less than that in the adjacent unit cell. Again, this behavior is attributed to the larger form loss at the spacer grids and the increased axial drag. However, comparison of the results from case 3, Figure 2-30, with those from case 1, Figure 2-24, indicates that the difference between unit cell and guide tube cell mass flux is smaller for the high power case. This is attributed to the larger influence of the [ ]^a on axial drag at the high quality conditions associated with case 3. Since the unit cell has a higher linear heat rate, and consequently higher void fraction, the [ ]^a serves to equalize the form loss between the unit and guide tube cells. This behavior is consistent with previous model performance.

Table 2-10 : Channel Exit Summary - Case 3

Channel	Enthalpy (BTU/lb_m)	Temp. (°F)	Density (lb_m/ft^3)	Quality	Void Fraction	Flow (lb_m/sec)	Mass Flux ($MLb_m/hr\text{-}ft^2$)
1	804.17	653.94	18.398	.244	.6001	.127	1.0983
2	804.98	653.94	18.328	.246	.6025	.290	1.1048
3	808.54	653.94	18.028	.254	.6124	.144	1.0983
4	806.82	653.94	18.173	.250	.6076	.252	1.0916
5	813.28	653.94	17.645	.266	.6251	.285	1.0843
6	818.41	653.94	17.251	.278	.6382	.123	1.0638
7	820.21	653.94	17.116	.283	.6427	.244	1.0597
8	823.25	653.94	16.892	.290	.6501	.279	1.0614
9	828.49	653.94	16.524	.303	.6623	.240	1.0412
10	835.17	653.94	16.076	.319	.6772	.118	1.0261
11	828.05	653.94	16.553	.302	.6614	.276	1.0509
12	830.55	653.94	16.382	.308	.6671	.275	1.0480
13	834.02	653.94	16.149	.316	.6748	.273	1.0377
14	837.50	653.94	15.924	.325	.6822	.270	1.0281
15	838.63	653.94	15.853	.327	.6846	.117	1.0186
16	831.34	653.94	16.329	.310	.6688	.239	1.0354
17	833.21	653.94	16.203	.314	.6730	.273	1.0399
18	835.17	653.94	16.075	.319	.6772	.237	1.0268
19	837.49	653.94	15.926	.325	.6822	.235	1.0195
20	837.66	653.94	15.914	.325	.6826	.235	1.0198
21	836.63	653.94	15.980	.323	.6804	.118	1.0250
22	829.39	653.94	16.462	.305	.6644	.239	1.0389
23	831.42	653.94	16.323	.310	.6690	.274	1.0429
24	832.51	653.94	16.251	.313	.6714	.238	1.0312
25	834.55	653.94	16.117	.317	.6759	.237	1.0265
26	835.74	653.94	16.037	.320	.6785	.272	1.0339
27	835.42	653.94	16.057	.320	.6778	.273	1.0377
28	834.35	653.94	16.127	.317	.6755	.137	1.0427
29	821.62	653.94	17.010	.286	.6462	3.650	1.0663
30	717.78	653.94	31.624	.034	.1611	2548.185	1.4386

Figure 2-29 : MDNBR Vs. Elevation - Case 3

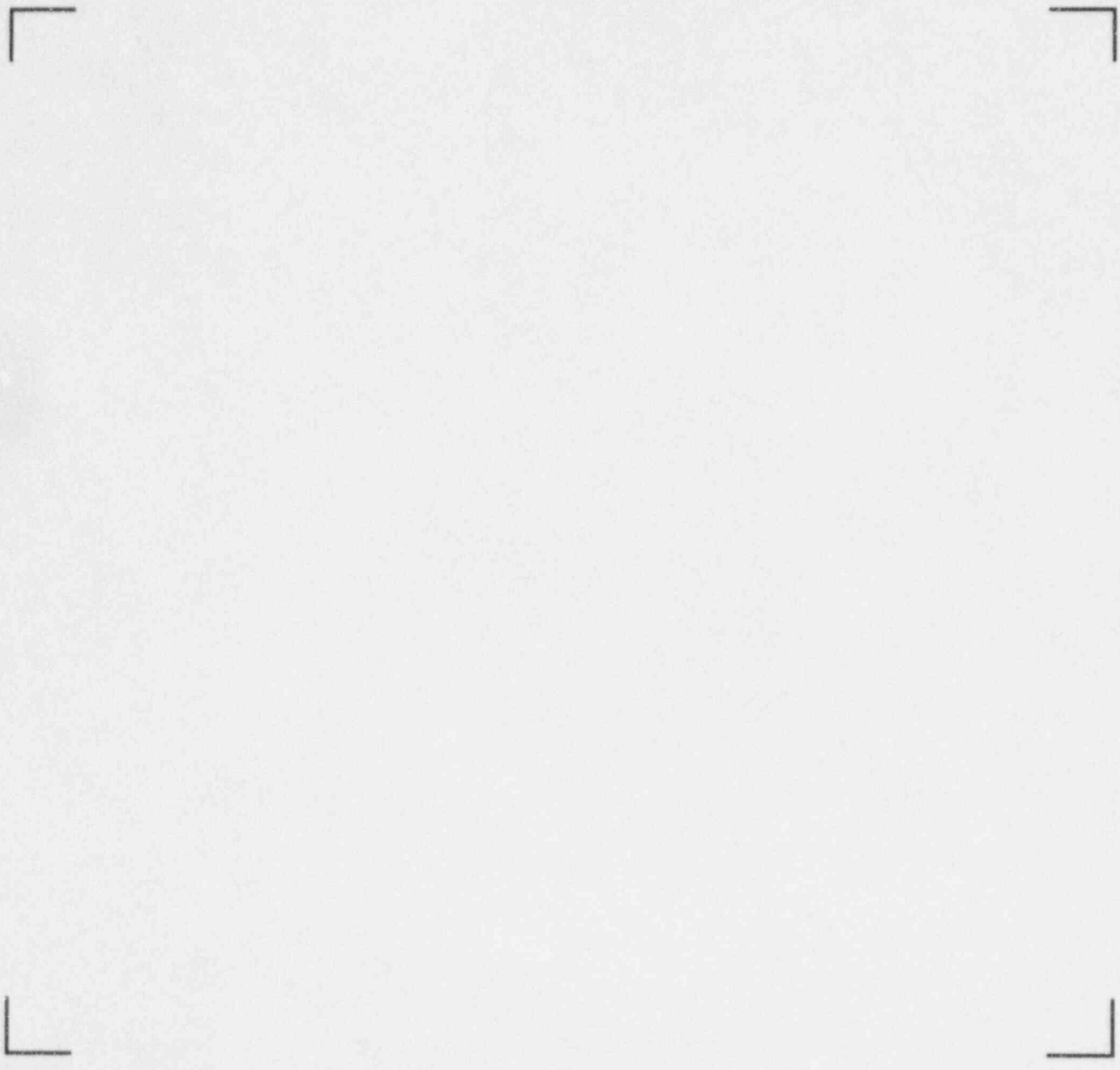

Figure 2-30 : Local Mass Flux Vs. Elevation - Channels 14 & 15 : Case 3

2.2.1.2.5 Base Model Performance : Case 4

Table 2-7 indicates that the predicted minimum DNBR for the low pressure case run of the base model was 1.790. The limiting channel was channel 5. Channel 5 is a unit cell channel located interior to the hot assembly from the highest power rods. The axial position of minimum DNBR for the low pressure case was 69.0 inches. This places MDNBR just prior to the 3rd mixing vane grid.

A summary of channel exit conditions for case 4 is shown in Table 2-11. This table indicates that channel 1 has the highest exit enthalpy, 723.71 BTU/lb_m. The limiting channel for DNB, channel 5, has an exit enthalpy of 719.62 BTU/lb_m. Bundle exit flow is generally distributed in a manner very similar to the base case. That is, channel exit mass flux [ ]^a in channels closer to the center of the core. As indicated in the table, the low pressure case results in significant voiding in the hot assembly with exit conditions in all hot assembly channels, as well as the remainder of the core (i.e., channel 30), at saturation temperature.

The predicted DNBR in the limiting channel, channel 5, and the adjacent guide tube channel, channel 4, is plotted as a function of axial height in Figure 2-31. Again, the dependence of the predicted DNBR on the [ ]^a is apparent. While channel 5 is the limiting channel for DNB, there is very little difference between predicted DNBRs for channel 5 and channel 4.

The local mass flux in channels 4 and 5 are plotted as functions of axial elevation in Figure 2-32. As was seen in previous cases, the mass flux in the guide tube channel is less than that in the adjacent unit cell. Again, this behavior is attributed to the larger form loss at the spacer grids and the increased axial drag. However, comparison of the results from case 4, Figure 2-32, with those from case 1, Figure 2-24, indicates that the difference between unit cell and guide tube cell mass flux is smaller for the high power case. This is attributed to the larger influence of the [ ]^a on axial drag at the high quality conditions associated with case 4. Since the unit cell has a higher linear heat rate, and consequently higher void fraction, the [ ]^a serves to equalize the form loss between the unit and guide tube cells. This behavior is consistent with previous model performance.

Table 2-11 : Channel Exit Summary - Case 4

Channel	Enthalpy (BTU/lb_m)	Temp. (°F)	Density (lb_m/ft^3)	Quality	Void Fraction	Flow (lb_m/sec)	Mass Flux ($MLb_m/hr\text{-}ft^2$)
1	723.71	590.61	14.998	.210	.7070	.227	1.9695
2	723.05	590.61	15.046	.209	.7058	.522	1.9876
3	721.95	590.61	15.129	.207	.7037	.262	1.9978
4	721.29	590.61	15.180	.206	.7024	.457	1.9818
5	719.62	590.61	15.308	.203	.6991	.527	2.0052
6	716.84	590.61	15.528	.198	.6936	.231	2.0049
7	718.16	590.61	15.423	.201	.6962	.461	1.9979
8	716.16	590.61	15.582	.197	.6922	.532	2.0233
9	711.19	590.61	15.995	.188	.6818	.469	2.0348
10	703.24	590.61	16.706	.174	.6638	.240	2.0783
11	716.47	590.61	15.557	.198	.6928	.531	2.0218
12	713.83	590.61	15.772	.193	.6874	.536	2.0402
13	708.39	590.61	16.237	.183	.6757	.542	2.0645
14	701.70	590.61	16.851	.172	.6602	.552	2.0992
15	700.53	590.61	16.963	.170	.6574	.241	2.0935
16	714.65	590.61	15.706	.194	.6891	.465	2.0163
17	712.68	590.61	15.868	.191	.6850	.536	2.0415
18	708.99	590.61	16.185	.184	.6770	.472	2.0462
19	703.62	590.61	16.670	.175	.6647	.478	2.0724
20	704.09	590.61	16.626	.176	.6659	.477	2.0706
21	706.69	590.61	16.389	.180	.6719	.238	2.0614
22	711.02	590.61	16.010	.188	.6814	.469	2.0335
23	710.93	590.61	16.017	.188	.6812	.538	2.0487
24	709.17	590.61	16.169	.185	.6774	.471	2.0423
25	706.44	590.61	16.412	.180	.6713	.474	2.0571
26	706.45	590.61	16.410	.180	.6713	.545	2.0744
27	707.80	590.61	16.289	.182	.6744	.545	2.0729
28	708.58	590.61	16.220	.184	.6761	.272	2.0735
29	705.36	590.61	16.509	.178	.6688	7.125	2.0825
30	647.46	590.61	24.730	.076	.4613	4544.684	2.5658

Figure 2-31 : MDNBR Vs. Elevation - Case 4

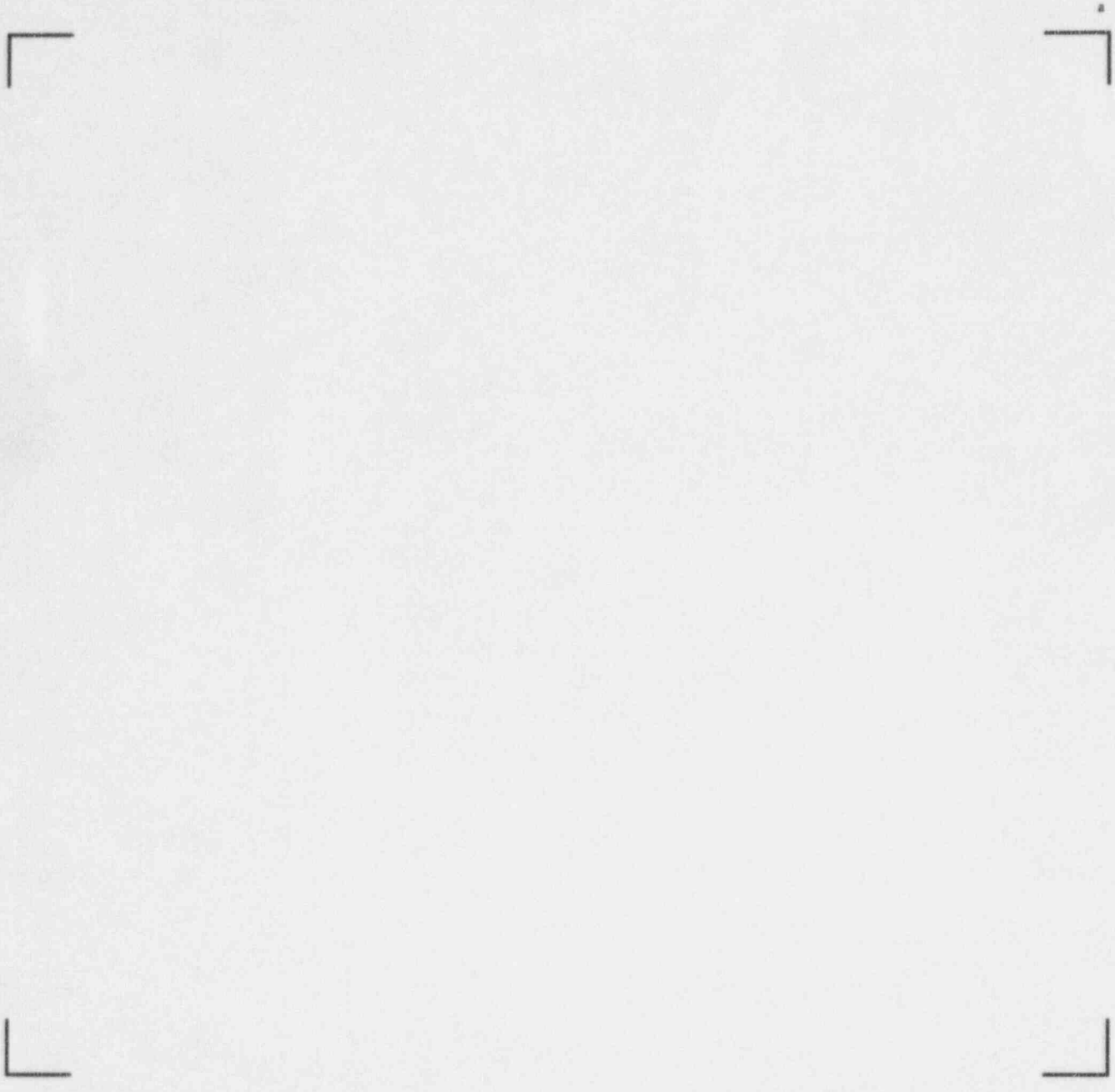

Figure 2-22 : Local Mass Flux Vs. Elevation - Channels 4 & 5 : Case 4

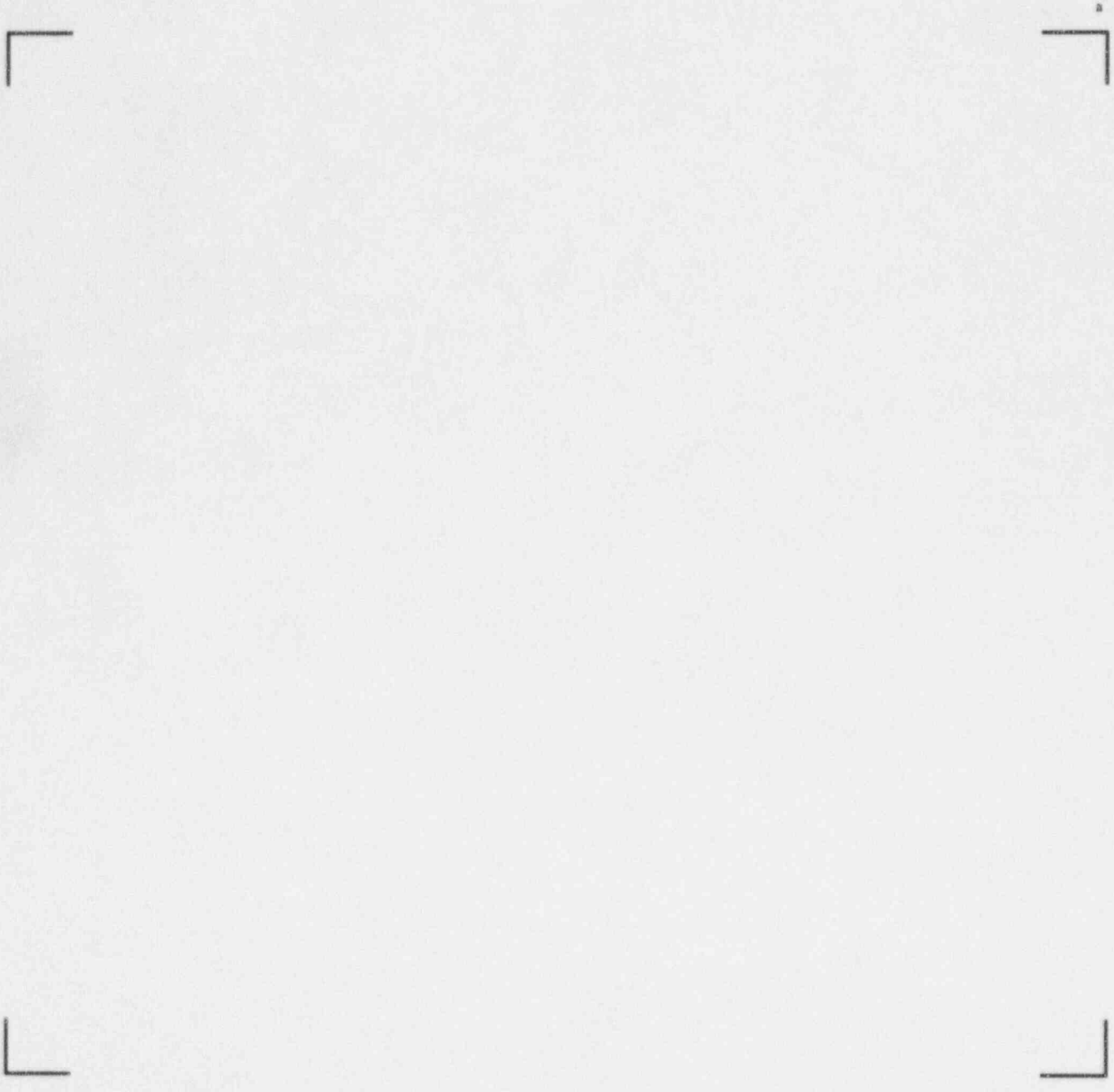

2.2.1.2.6 Base Model Performance : Case 5

Table 2-7 indicates that the predicted minimum DNBR for the low pressure, intermediate flow case run of the base model was 1.449. The limiting channel was channel 14. Channel 14 is a unit cell channel between the highest power rods in the reference radial power distribution. The axial position of minimum DNBR for the low pressure case was 110.1 inches. This places MDNBR just prior to the 5th mixing vane grid.

A summary of channel exit conditions for case 5 is shown in Table 2-12. This table indicates that channel 20 has the highest exit enthalpy, 823.42 BTU/lb_m. The limiting channel for DNB, channel 14, has an exit enthalpy of 820.53 BTU/lb_m with the adjacent guide tube channel, channel 15, having an exit enthalpy of 822.80 BTU/lb_m. While bundle exit flow is generally distributed in a manner similar to the base case, with channel exit mass flux [ ]^a in channels closer to the center of the core, the low flow used in this case results is a slightly different crossflow distribution pattern as compared to the base case. Specifically, channel exit enthalpies are highest in those channels surrounding [ ]^a as opposed to the base case where the highest exit enthalpies occurs in [ ]^a As indicated in the table, the low pressure, intermediate flow case results in significant voiding in the hot assembly with exit conditions in all hot assembly channels at saturation temperature.

The predicted DNBR in the limiting channel, channel 14, and the adjacent unit cell, channel 15, is plotted as a function of axial height in Figure 2-33. Again, the dependence of the predicted DNBR on the [ ]^a is apparent. While channel 14 is the limiting channel for DNB, there is very little difference between predicted DNBRs for channel 14 and channel 15.

The local mass flux in channels 14 and 15 are plotted as functions of axial elevation in Figure 2-34. As was seen in previous cases, the mass flux in the guide tube channel is less than that in the adjacent unit cell. Again, this behavior is attributed to the larger form loss at the spacer grids and the increased axial drag. However, comparison of the results from case 5, Figure 2-34, with those from case 1, Figure 2-24, indicates that the difference between unit cell and guide tube cell mass flux is smaller for the high power case. This is attributed to the larger influence of the [ ]^a on axial drag at the high quality conditions associated with case 5. Since the unit cell has a higher linear heat rate, and consequently higher void fraction, the [ ]^a serves to equalize the form loss between the unit and guide tube cells. This behavior is consistent with previous model performance.

Table 2-12 : Channel Exit Summary - Case 5

Channel	Enthalpy (BTU/lb_m)	Temp. (°F)	Density (lb_m/ft^3)	Quality	Void Fraction	Flow (lb_m/sec)	Mass Flux ($MLb_m/hr\text{-}ft^2$)
1	791.95	628.42	15.460	.271	.6930	.140	1.2123
2	791.05	628.42	15.519	.269	.6913	.322	1.2244
3	789.57	628.42	15.619	.266	.6884	.162	1.2311
4	792.41	628.42	15.429	.272	.6939	.279	1.2107
5	791.63	628.42	15.480	.271	.6925	.321	1.2226
6	794.42	628.42	15.296	.276	.6978	.139	1.2051
7	804.42	628.42	14.667	.297	.7160	.272	1.1796
8	803.43	628.42	14.726	.295	.7143	.313	1.1917
9	807.74	628.42	14.470	.304	.7217	.270	1.1710
10	816.50	628.42	13.972	.322	.7361	.133	1.1490
11	812.67	628.42	14.185	.314	.7300	.307	1.1694
12	813.21	628.42	14.154	.315	.7308	.308	1.1708
13	816.05	628.42	13.996	.321	.7354	.305	1.1606
14	820.53	628.42	13.753	.330	.7424	.301	1.1475
15	822.80	628.42	13.635	.335	.7459	.131	1.1340
16	816.53	628.42	13.970	.322	.7362	.265	1.1505
17	817.60	628.42	13.911	.324	.7379	.304	1.1576
18	819.11	628.42	13.830	.327	.7402	.264	1.1438
19	822.20	628.42	13.666	.334	.7450	.261	1.1338
20	823.42	628.42	13.602	.336	.7468	.261	1.1318
21	823.40	628.42	13.602	.336	.7468	.131	1.1355
22	814.84	628.42	14.064	.318	.7335	.266	1.1537
23	816.61	628.42	13.965	.322	.7363	.305	1.1591
24	817.71	628.42	13.906	.324	.7380	.264	1.1459
25	820.28	628.42	13.768	.330	.7420	.263	1.1394
26	822.03	628.42	13.674	.333	.7447	.301	1.1467
27	822.32	628.42	13.658	.334	.7452	.302	1.1497
28	821.43	628.42	13.704	.332	.7439	.152	1.1547
29	806.91	628.42	14.517	.302	.7203	4.055	1.1853
30	705.83	628.42	25.084	.094	.4145	2763.416	1.5602

Figure 2-33 : MDNBR Vs. Elevation - Case 5

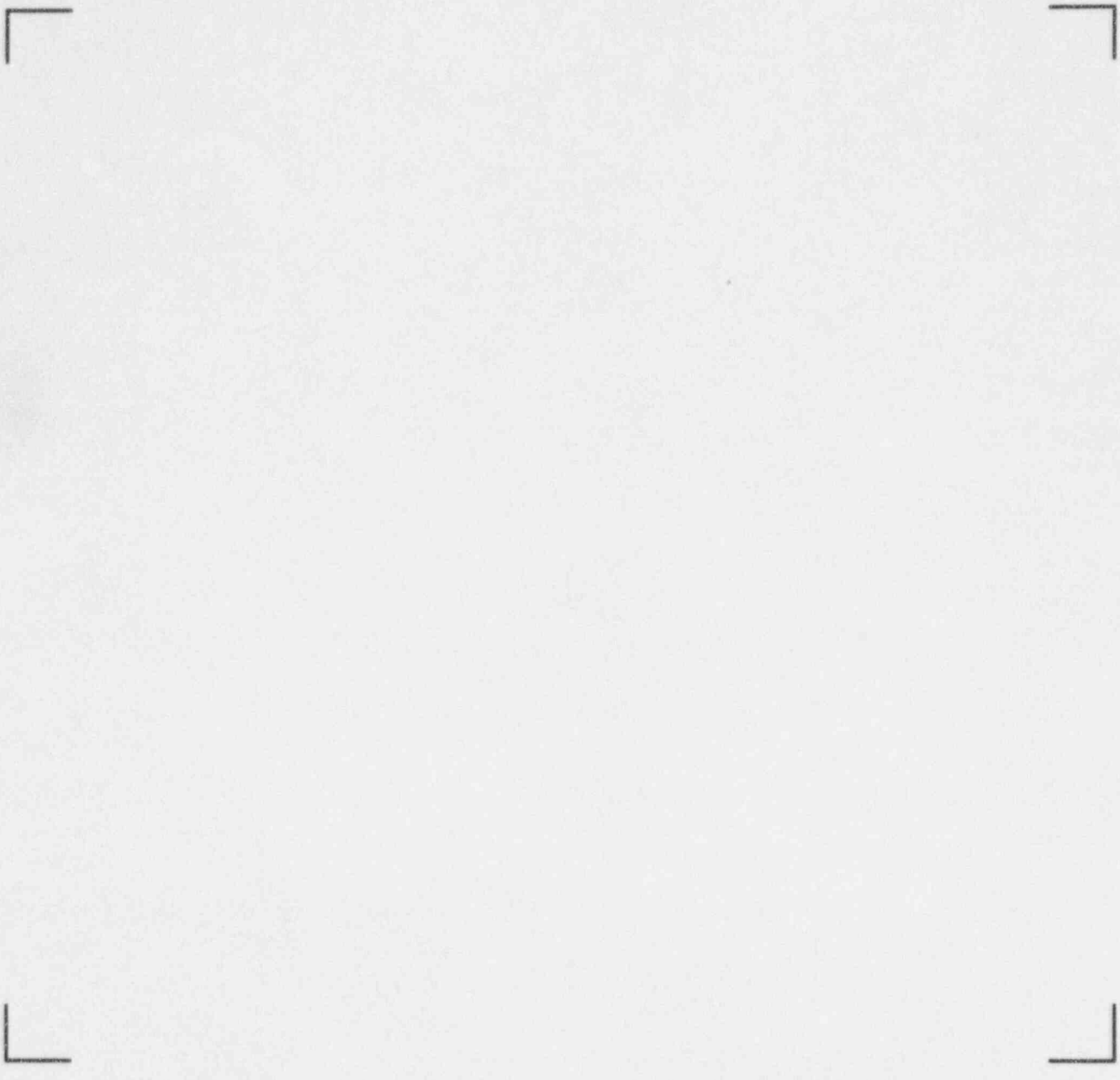

Figure 2-34 : Local Mass Flux Vs. Elevation - Channels 14 & 15 : Case 5

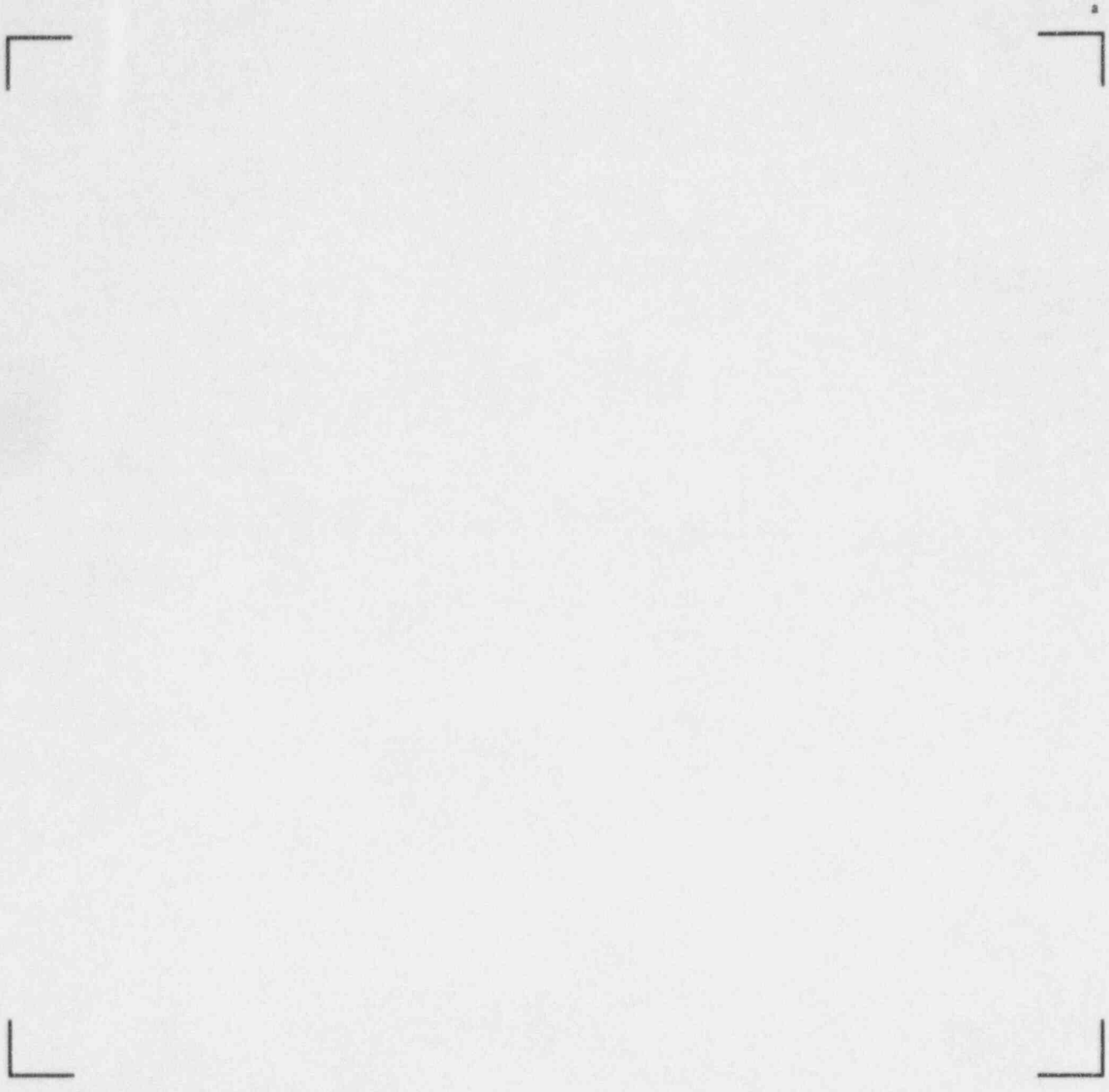

2.2.1.2.7 Base Model Performance : Case 6

Table 2-7 indicates that the predicted minimum DNBR for the low pressure, low flow, and intermediate power case run of the base model was 1.565. The limiting channel was channel 2. Channel 2 is a unit cell located adjacent to the center instrument tube channel. The axial position of minimum DNBR for the low pressure case was 119.8 inches. This places MDNBR just prior to the 3rd intermediate flow mixer grid.

A summary of channel exit conditions for case 6 is shown in Table 2-13. This table indicates that channel 1 has the highest exit enthalpy, 903.52 BTU/lb_m. The limiting channel for DNB, channel 2, has an exit enthalpy of 902.19 BTU/lb_m. Bundle exit flow is generally distributed in a manner similar to the base case that is, channel exit mass flux [ ]^a in channels closer to the center of the core. As indicated in the table, the low pressure, low flow, intermediate power case results in significant voiding in the hot assembly with exit conditions in all hot channels at saturation temperature.

The predicted DNBR in the limiting channel, channel 2, and the adjacent unit cell, channel 1, is plotted as a function of axial height in Figure 2-35. Again, the dependence of the predicted DNBR on the [ ]^a is apparent. While channel 2 is the limiting channel for DNB, there is very little difference between predicted DNBRs for channel 2 and channel 1.

The local mass flux in channels 1 and 2 are plotted as functions of axial elevation in Figure 2-36. As was seen in previous cases, the mass flux in the guide tube channel is less than that in the adjacent unit cell. Again, this behavior is attributed to the larger form loss at the spacer grids and the increased axial drag. However, comparison of the results from case 6, Figure 2-36, with those from case 1, Figure 2-24, indicates that the difference between unit cell and guide tube cell mass flux is smaller for the high power case. This is attributed to the larger influence of the [ ]^a on axial drag at the high quality conditions associated with case 6. Since the unit cell has a higher linear heat rate, and consequently higher void fraction, the [ ]^a serves to equalize the form loss between the unit and guide tube cells. This behavior is consistent with previous model performance.

Table 2-13 : Channel Exit Summary - Case 6

Channel	Enthalpy (BTU/lb_m)	Temp. (°F)	Density (lb_m/ft^3)	Quality	Void Fraction	Flow (lb_m/sec)	Mass Flux ($MLb_m/hr\text{-}ft^2$)
1	903.52	628.42	10.365	.501	.8405	.082	.7129
2	902.19	628.42	10.407	.498	.8393	.190	.7222
3	899.92	628.42	10.482	.494	.8371	.095	.7270
4	898.59	628.42	10.529	.491	.8358	.166	.7188
5	895.09	628.42	10.645	.484	.8324	.192	.7306
6	889.28	628.42	10.848	.472	.8265	.084	.7300
7	891.94	628.42	10.755	.477	.8292	.168	.7267
8	887.67	628.42	10.903	.468	.8249	.194	.7396
9	877.08	628.42	11.290	.447	.8137	.172	.7449
10	859.70	628.42	11.972	.411	.7940	.088	.7669
11	888.16	628.42	10.886	.470	.8254	.194	.7391
12	882.44	628.42	11.090	.458	.8195	.197	.7482
13	870.67	628.42	11.532	.433	.8067	.200	.7606
14	856.00	628.42	12.125	.403	.7896	.204	.7783
15	853.17	628.42	12.247	.397	.7860	.089	.7757
16	884.14	628.42	11.031	.461	.8212	.170	.7365
17	879.72	628.42	11.190	.452	.8166	.197	.7495
18	871.64	628.42	11.496	.435	.8078	.173	.7518
19	859.62	628.42	11.976	.411	.7939	.177	.7657
20	860.27	628.42	11.949	.412	.7946	.176	.7652
21	865.59	628.42	11.734	.423	.8009	.088	.7606
22	876.43	628.42	11.314	.445	.8130	.172	.7457
23	875.97	628.42	11.330	.444	.8126	.198	.7538
24	871.92	628.42	11.486	.436	.8081	.173	.7506
25	865.53	628.42	11.736	.423	.8008	.175	.7585
26	865.25	628.42	11.745	.422	.8005	.202	.7675
27	868.01	628.42	11.636	.428	.8037	.201	.7665
28	869.74	628.42	11.568	.432	.8057	.101	.7665
29	866.34	628.42	11.702	.425	.8018	2.632	.7691
30	743.25	628.42	19.708	.171	.5701	1773.552	1.0013

Figure 2-35 : MDNBR Vs. Elevation - Case 6

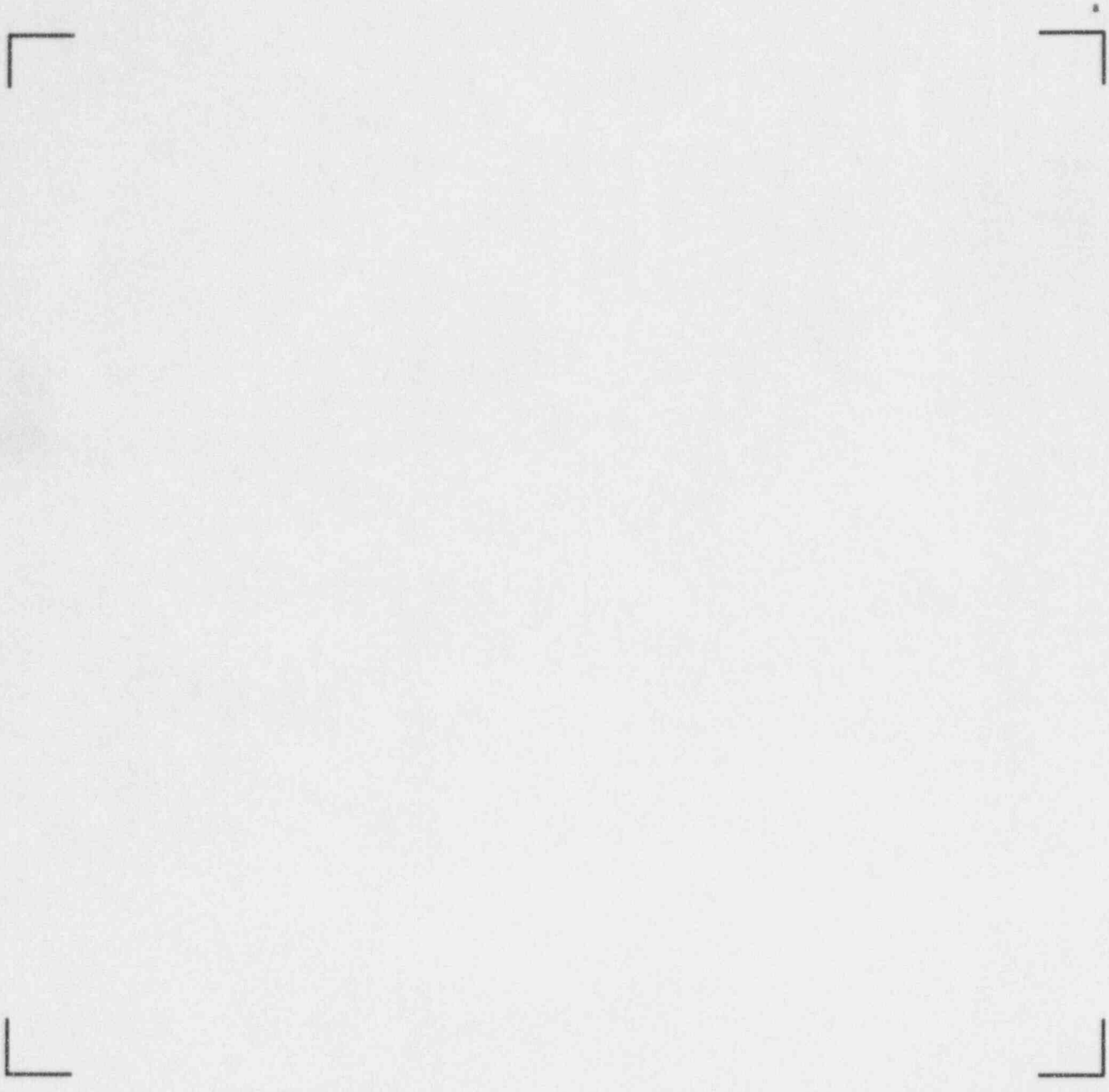

Figure 2-36 : Local Mass Flux Vs. Elevation - Channels 1& 2 : Case 6

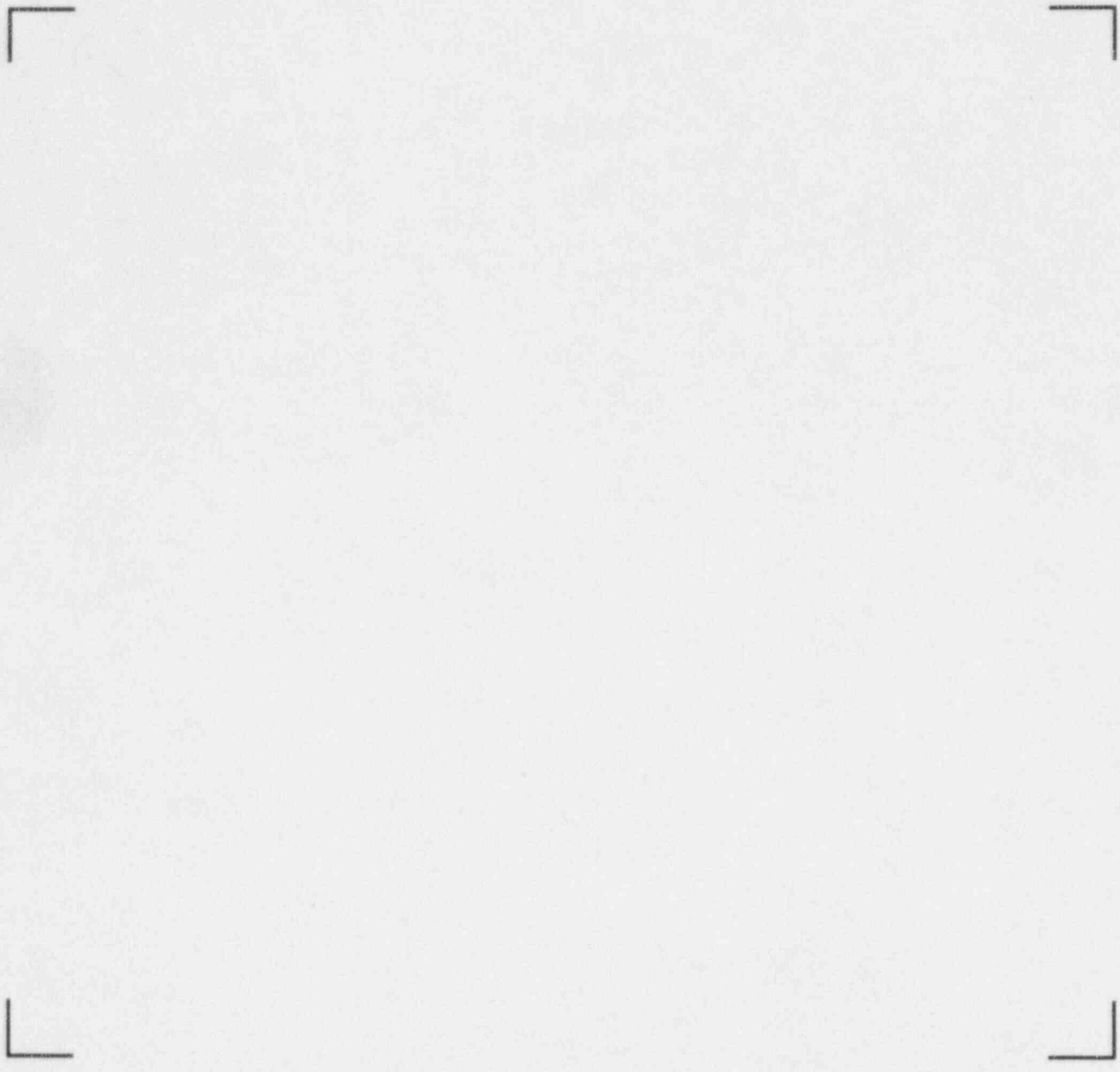

2.2.1.2.8 Base Model Performance : Case 7

Table 2-7 indicates that the predicted minimum DNBR for the high inlet temperature case run of the base model was 1.575. The limiting channel was channel 14. Channel 14 is a unit cell located between the highest power rods in the reference radial power distribution. The axial position of minimum DNBR for the low pressure case was 110.1 inches. This places MDNBR just prior to the 5th mixing vane grid.

A summary of channel exit conditions for case 7 is shown in Table 2-14. This table indicates that channel 15 has the highest exit enthalpy, 798.20 BTU/lb_m. The limiting channel for DNB, channel 14, has an exit enthalpy of 797.62 BTU/lb_m. Bundle exit flow is generally distributed in a manner similar to the base case that is, channel exit mass flux [ ]^a in channels closer to the center of the core. As indicated in the table, the low pressure, low flow, intermediate power case results in significant voiding in the hot assembly with exit conditions in all hot channels at saturation temperature.

The predicted DNBR in the limiting channel, channel 14, and the adjacent guide tube channel, channel 15, is plotted as a function of axial height in Figure 2-37. Again, the dependence of the predicted DNBR on the [ ]^a is apparent. While channel 14 is the limiting channel for DNB, there is very little difference between predicted DNBRs for channel 14 and channel 15.

The local mass flux in channels 14 and 15 are plotted as functions of axial elevation in Figure 2-38. As was seen in previous cases, the mass flux in the guide tube channel is less than that in the adjacent unit cell. Again, this behavior is attributed to the larger form loss at the spacer grids and the increased axial drag. However, comparison of the results from case 7, Figure 2-38, with those from case 1, Figure 2-24, indicates that the difference between unit cell and guide tube cell mass flux is smaller for the high power case. This is attributed to the larger influence of the [ ]^a on axial drag at the high quality conditions associated with case 7. Since the unit cell has a higher linear heat rate, and consequently higher void fraction, the [ ]^a serves to equalize the form loss between the unit and guide tube cells. This behavior is consistent with previous model performance.

Table 2-14 : Channel Exit Summary - Case 7

Channel	Enthalpy (BTU/lb_m)	Temp. (°F)	Density (lb_m/ft^3)	Quality	Void Fraction	Flow (lb_m/sec)	Mass Flux ($MLb_m/hr\text{-}ft^2$)
1	756.07	653.94	23.814	.127	.4204	.247	2.1395
2	760.76	653.94	23.124	.139	.4432	.558	2.1221
3	767.10	653.94	22.258	.154	.4720	.274	2.0869
4	771.00	653.94	21.762	.163	.4885	.472	2.0476
5	776.76	653.94	21.069	.177	.5115	.533	2.0282
6	782.33	653.94	20.443	.191	.5322	.229	1.9862
7	786.08	653.94	20.044	.200	.5455	.453	1.9673
8	787.54	653.94	19.893	.204	.5505	.518	1.9726
9	791.41	653.94	19.505	.213	.5634	.447	1.9408
10	796.10	653.94	19.057	.224	.5783	.221	1.9168
11	792.56	653.94	19.392	.216	.5671	.512	1.9483
12	793.69	653.94	19.283	.218	.5707	.511	1.9468
13	795.64	653.94	19.099	.223	.5769	.508	1.9326
14	797.62	653.94	18.915	.228	.5830	.504	1.9193
15	798.20	653.94	18.863	.229	.5847	.220	1.9061
16	794.70	653.94	19.188	.221	.5739	.444	1.9253
17	795.53	653.94	19.110	.223	.5765	.508	1.9337
18	796.46	653.94	19.023	.225	.5794	.442	1.9160
19	797.51	653.94	18.926	.228	.5826	.440	1.9069
20	797.43	653.94	18.933	.228	.5824	.440	1.9080
21	796.69	653.94	19.001	.226	.5801	.221	1.9164
22	792.89	653.94	19.361	.216	.5682	.445	1.9308
23	794.08	653.94	19.246	.219	.5720	.509	1.9377
24	794.58	653.94	19.200	.221	.5735	.443	1.9216
25	795.54	653.94	19.110	.223	.5765	.442	1.9165
26	796.16	653.94	19.051	.224	.5785	.507	1.9285
27	795.92	653.94	19.073	.224	.5777	.508	1.9351
28	795.26	653.94	19.134	.222	.5757	.255	1.9425
29	787.16	653.94	19.932	.203	.5492	6.746	1.9717
30	728.82	653.94	28.883	.061	.2521	4203.311	2.3731

Figure 2-37 : MDNBR Vs. Elevation - Case 7

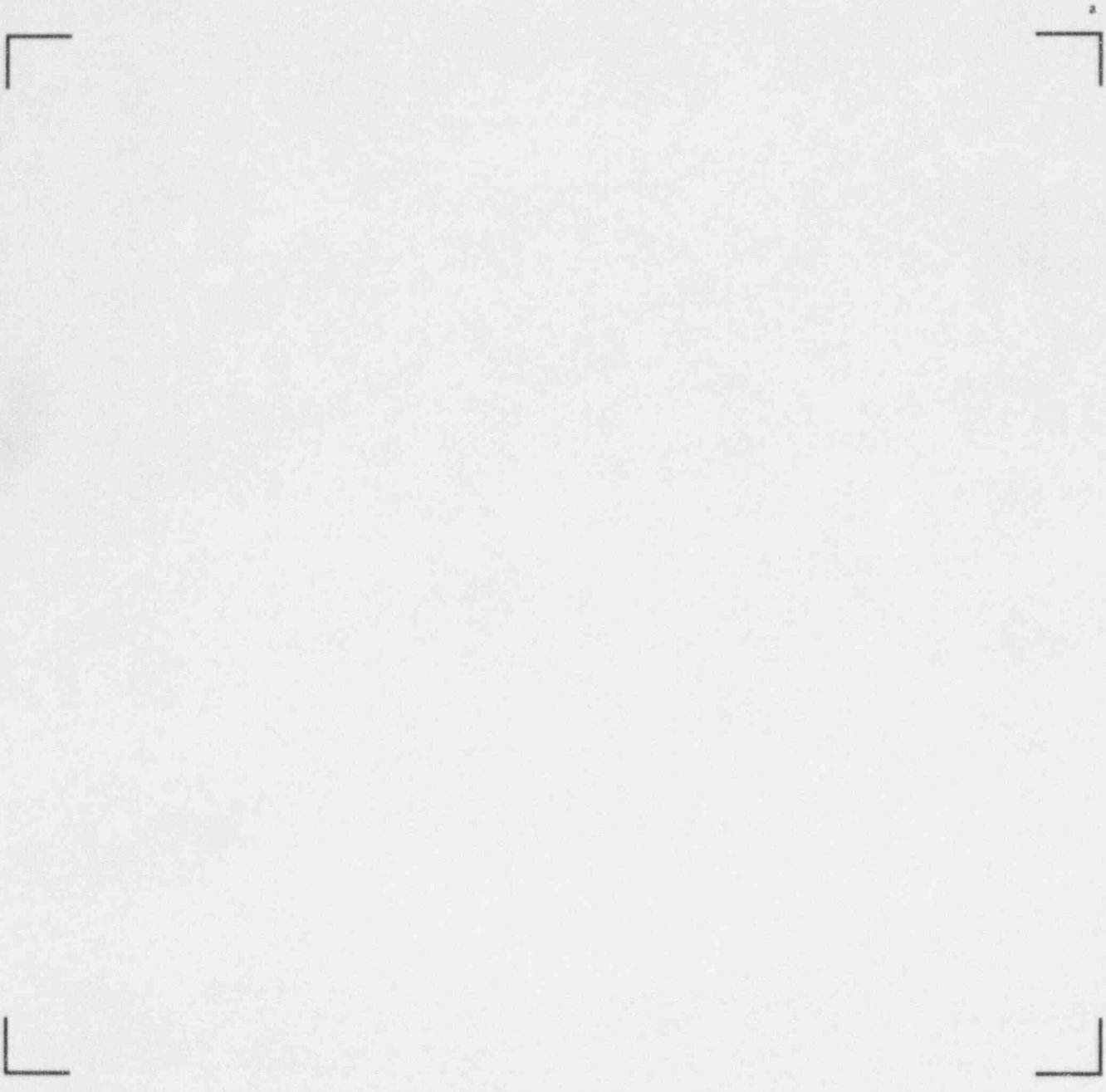

Figure 2-38 : Local Mass Flux Vs. Elevation - Channels 14 & 15 : Case 7

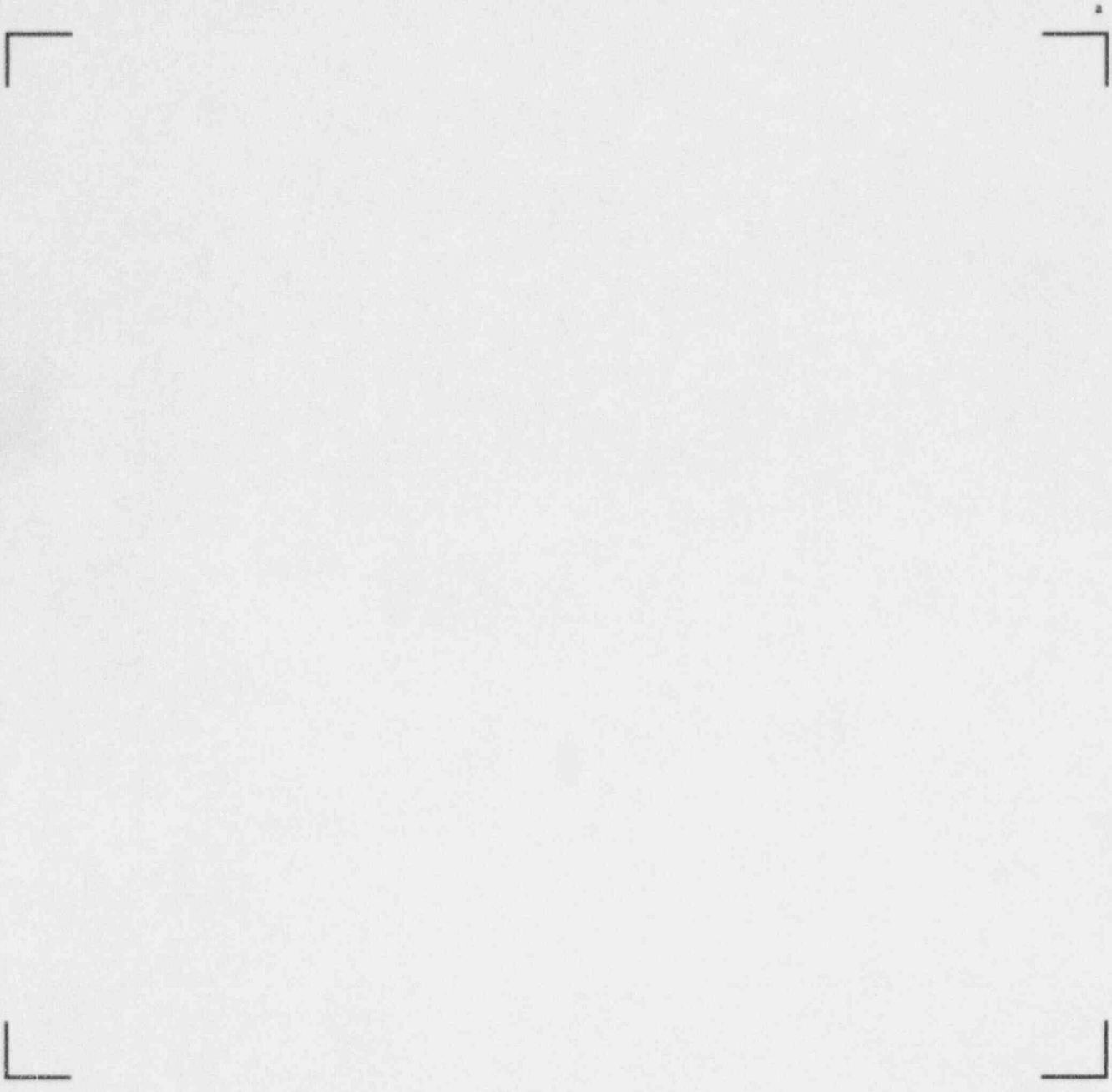

2.2.1.2.9 Additional Base Model Performance Studies

This section describes additional studies made with the base thermal-hydraulic model which were designed to provide further understanding of the effect of local quality on the location of the limiting channel with respect to DNBR. Specifically, a study was made in which the core average power was increased in small increments (1%) from the nominal power of 5.8429 kW/ft to 7.0114 kW/ft. This represents a change from the nominal rated power of 3565 MW_{th} to 140% of nominal. All other core state variables were held constant at their nominal conditions values. A second study was then made in which the inlet mass flux was decreased in increments of 2% from the nominal value to a value representing 60% of nominal flow.

Results from the increasing power study are summarized in Table 2-15. The predicted minimum DNBR is plotted as a function of the fraction of rated thermal power in Figure 2-39. As indicated in the figure, the prediction for MDNBR approximates an [ ]^a relationship with power over the range from full rated thermal power to 140% of rated thermal power.

Examination of the results shown in Table 2-15 indicate that at low quality conditions, a [ ]^a will typically be limiting with respect to DNBR. As power increases and consequently, the local quality increases, a point is reached where [ ]^a become the limiting channel. For the power ramp study, this switch took place at 133% rated thermal power (i.e., case 14). The mechanism for this behavior can be understood by examination of the normalized mass flux in each cell type at difference conditions. Figure 2-40 provides the normalized mass flux in channel 5, a unit cell, as a function of elevation for both the nominal power case and the 133% power case. Note that for the nominal conditions case, the normalized mass flux [ ]^a at all axial elevations. Thus, the mass flux in the unit channel [ ]^a from the inlet value. At the high power conditions, the profile of the normalized mass flux in the unit cell tracks the nominal power profile in the lower regions of the core (i.e., below 52.0 inches). However, in the upper regions of the core, the high power normalized mass flux in the unit cell [ ]^a in local mass flux.

Behavior in the unit cell should be contrasted with the response of the local mass flux in the guide tube channel (see Figure 2-41). At nominal conditions, the response of the local mass flux in the guide tube channel approximates a [ ]^a up the channel. It can thus be inferred that under nominal conditions, the [ ]^a in the guide tube channel has a greater influence on crossflow distribution than the [ ]^a effect. The result is an [ ]^a in flow in the unit cell at the expense of flow in the guide tube channels. As long as the [ ]^a is dominate, it can be expected that the limiting channel for DNBR will be [ ]^a

Consideration of the ratio of normalized mass flux in a unit channel with the normalized mass flux in a guide tube channel provides further understanding of the effect of quality on the limiting channel for DNBR (see Figure 2-42). As indicated, at nominal conditions, the ratio of normalized mass flux is [ ]^a at all axial elevation; indicating [ ]^a mass flow in the unit cell channel. At the high power conditions, the ratio [ ]^a, from the nominal power case as the flow proceeds up the channel. This indicates [ ]^a flow in the unit channel.

The results of the decreasing flow study, summarized in Table 2-16, indicate that the switch in the limiting channel type occurs at approximately 72% of nominal flow. The relationship between inlet mass flux and predicted minimum DNBR, shown in Figure 2-43, exhibits the same [ ]^{a} relationship found in the power study.

The relationship between local thermodynamic quality and crossflow in the flow study is similar to that observed in the power study (see Figure 2-44 through Figure 2-46). However, the lower mass flow rates dampens the effect to some extent.

Table 2-15 : Effect of Quality on Limiting Channel - Power Study

a

```
WLF999 02153 power.inp KENNAMORE 01/31/95 08:51:55 WCNOC mangler
AN 95-004 Rev 0 / Base Deck 30 Channel / Power Ramp/ DUMMY ROD MODEL
1
    *********** OPERATING CONDITIONS ***********     *CRITICAL LOCATION*** HOT CHANNEL CONDITIONS **** PREDICTED **
    * SYSTEM   INLET      INLET      AVERAGE   *     *              AXIAL*MASS FLUX         HEAT FLUX*   CRITICAL  *
    *PRESSURE ENTHALPY  MASS FLUX   HEAT RATE  *     *  HOT    HOT LEVEL*(MLBM/HR-  EQUIL.  (MBTU/HR-*  HEAT FLUX  *CORR* TIME  *
CASE* (PSIA)  (BTU/LBM)(MLBM/HR-FT2)(BTU/SEC-FT)*MDNBR*CHANNEL ROD (IN.)*   FT2)   QUALITY    FT2)  *(MBTU/HR-FT2)*FLAG* (SEC) *
*-*-*-*-*-*-*-*-*-*-*-*-*-*-*-*-*-*-*-*-*-*-*-*-*-*-*-*-*-*-*-*-*-*-*-*-*-*-*-*-*-*-*-*-*-*-*-*-*-*-*-*-*-*-*-*-*-*-*-*-*-*-
```

```
WLF999 02173 power2.inp KENNAMORE 01/31/95 13:25:48 WCNOC mangler
AN 95-004 Rev 0 / Base Deck 30 Channel / Power Ramp 2/ DUMMY ROD MODEL
1
    *********** OPERATING CONDITIONS ***********     *CRITICAL LOCATION*** HOT CHANNEL CONDITIONS **** PREDICTED **
    * SYSTEM   INLET      INLET      AVERAGE   *     *              AXIAL*MASS FLUX         HEAT FLUX*   CRITICAL  *
    *PRESSURE ENTHALPY  MASS FLUX   HEAT RATE  *     *  HOT    HOT LEVEL*(MLBM/HR-  EQUIL.  (MBTU/HR-*  HEAT FLUX  *CORR* TIME  *
CASE* (PSIA)  (BTU/LBM)(MLBM/HR-FT2)(BTU/SEC-FT)*MDNBR*CHANNEL ROD (IN.)*   FT2)   QUALITY    FT2)  *(MBTU/HR-FT2)*FLAG* (SEC) *
*-*-*-*-*-*-*-*-*-*-*-*-*-*-*-*-*-*-*-*-*-*-*-*-*-*-*-*-*-*-*-*-*-*-*-*-*-*-*-*-*-*-*-*-*-*-*-*-*-*-*-*-*-*-*-*-*-*-*-*-*-*-
```

Table 2-16 : Effect of Quality on Limiting Channel - Flow Study

a

WLF999 02154 flow.inp KENNAMORE 01/31/95 08:52:31 WCNOC mangler
AN 95-004 Rev 0 / Base Deck 30 Channel / Flow Ramp/ DUMMY ROD MODEL
1

CASE	SYSTEM PRESSURE (PSIA)	INLET ENTHALPY (BTU/LBM)	INLET MASS FLUX (MLBM/HR-FT2)	AVERAGE HEAT RATE (BTU/SEC-FT)	MDNBR	CRITICAL LOCATION HOT CHANNEL	CRITICAL LOCATION HOT ROD	CRITICAL LOCATION AXIAL LEVEL (IN.)	HOT CHANNEL CONDITIONS MASS FLUX (MLBM/HR-FT2)	HOT CHANNEL CONDITIONS EQUIL. QUALITY	HOT CHANNEL CONDITIONS FT2	PREDICTED CRITICAL HEAT FLUX (MBTU/HR-FT2)	PREDICTED CRITICAL HEAT FLUX FLAG	PREDICTED CRITICAL HEAT FLUX TIME (SEC)

Figure 2-39 : MDNBR Vs. Power

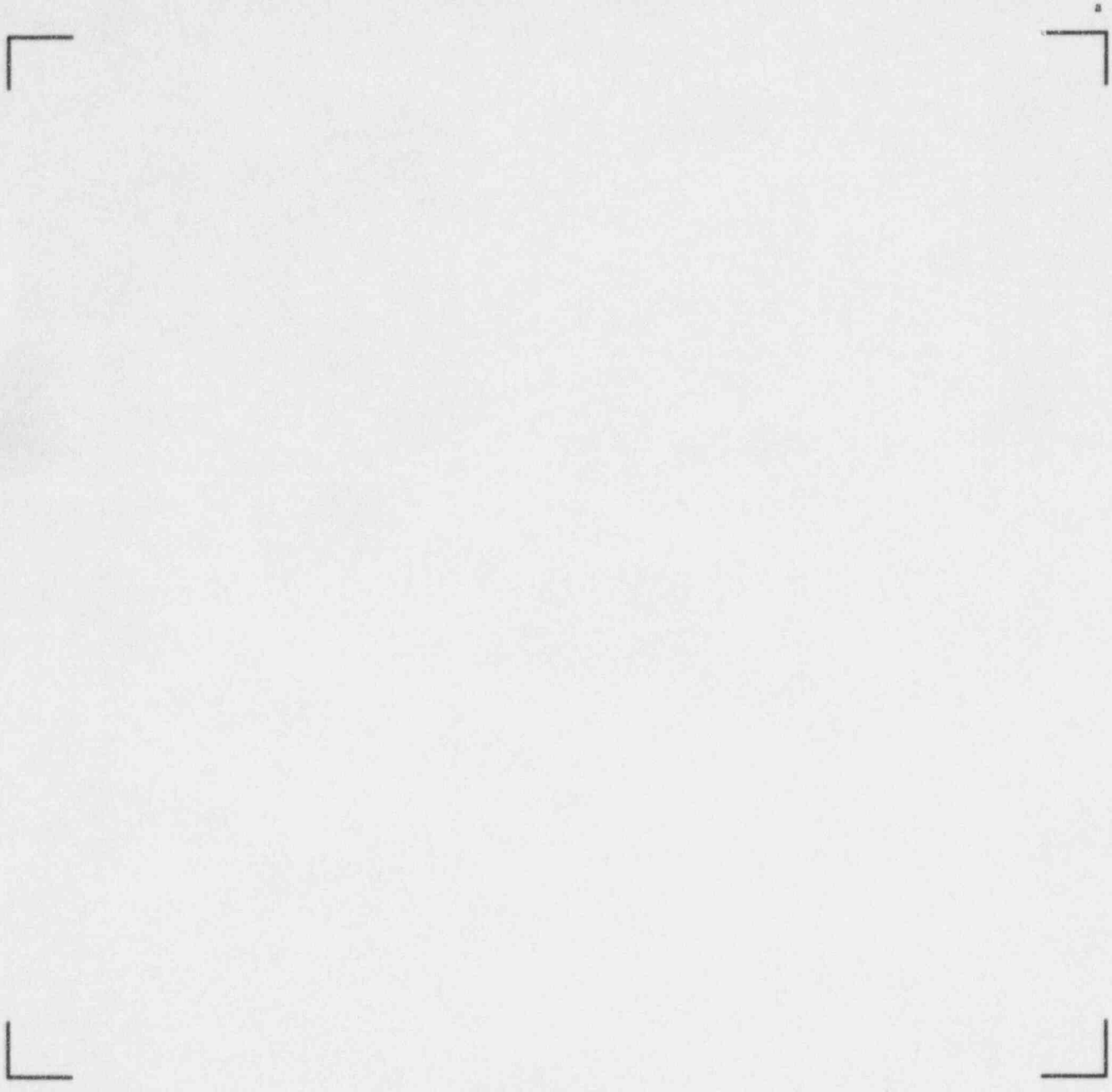

Figure 2-40: Normalized Mass Flux Vs. Elevation - Power Study : Channel 5

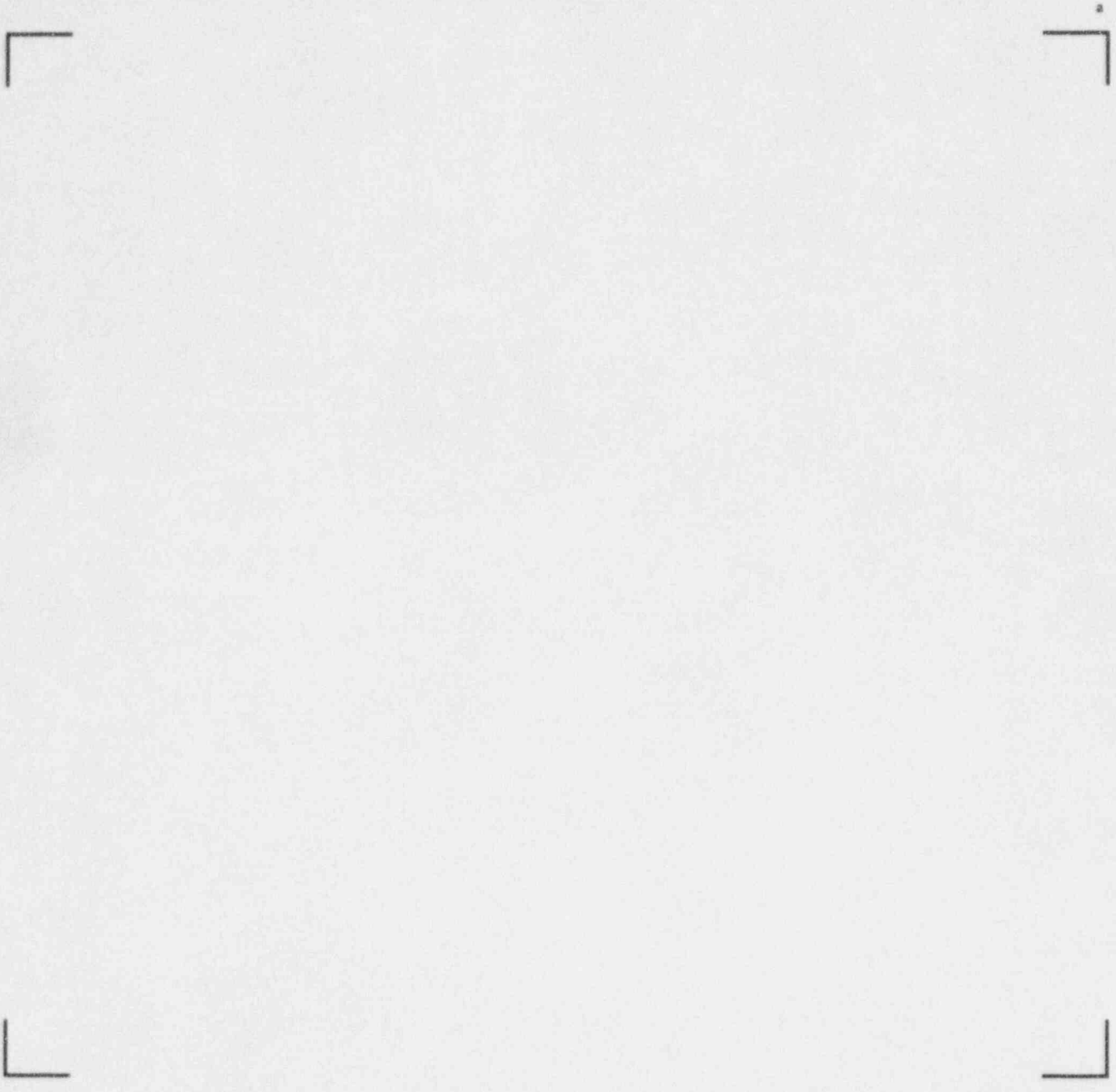

Figure 2-41: Normalized Mass Flux Vs. Elevation - Power Study : Channel 15

Figure 2-42: Ratio of Normalized Mass Flux - Power Study : Channel 5 Vs. Channel 15

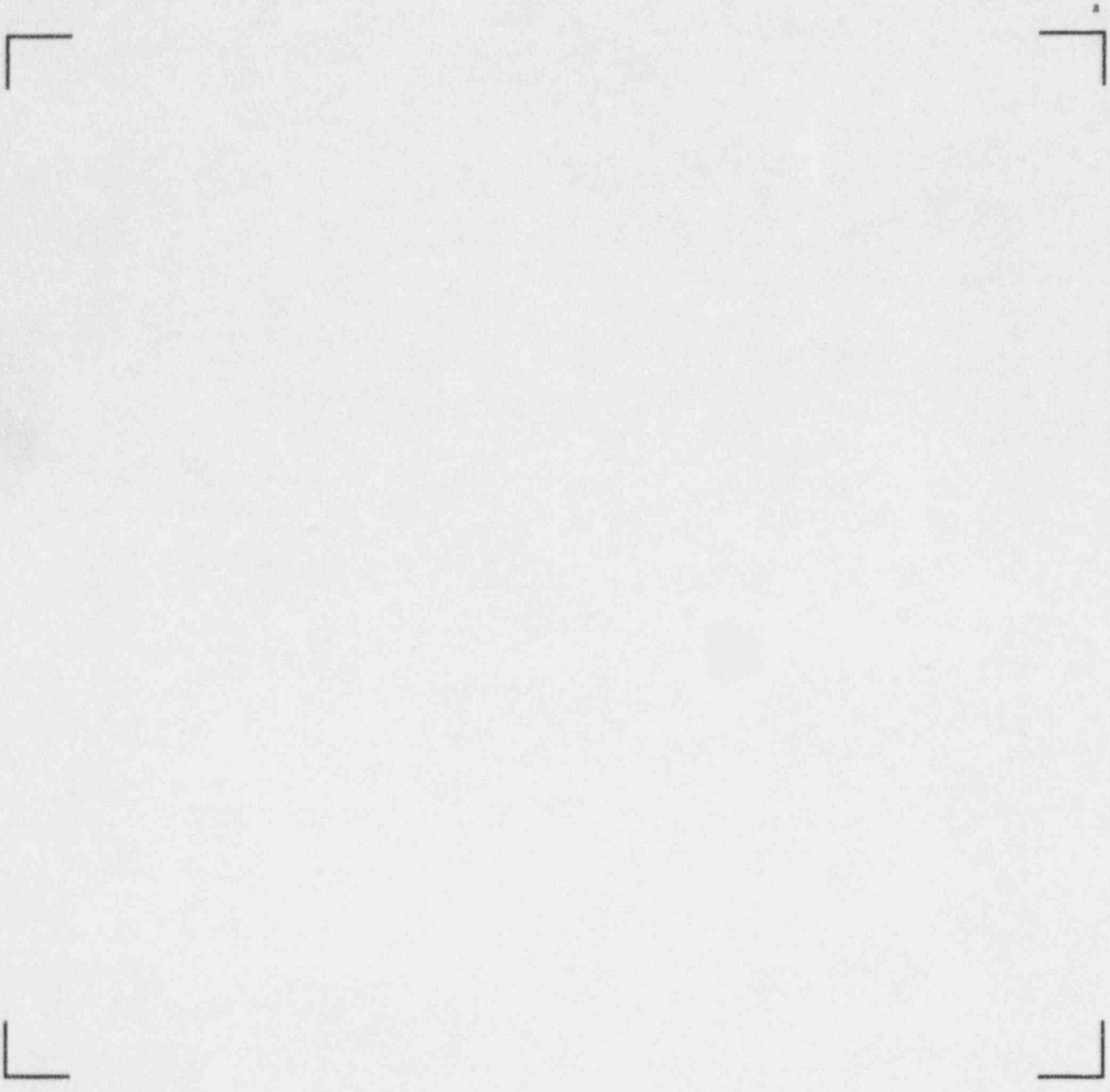

Figure 2-43 : MDNBR Vs. Fraction of Nominal Flow

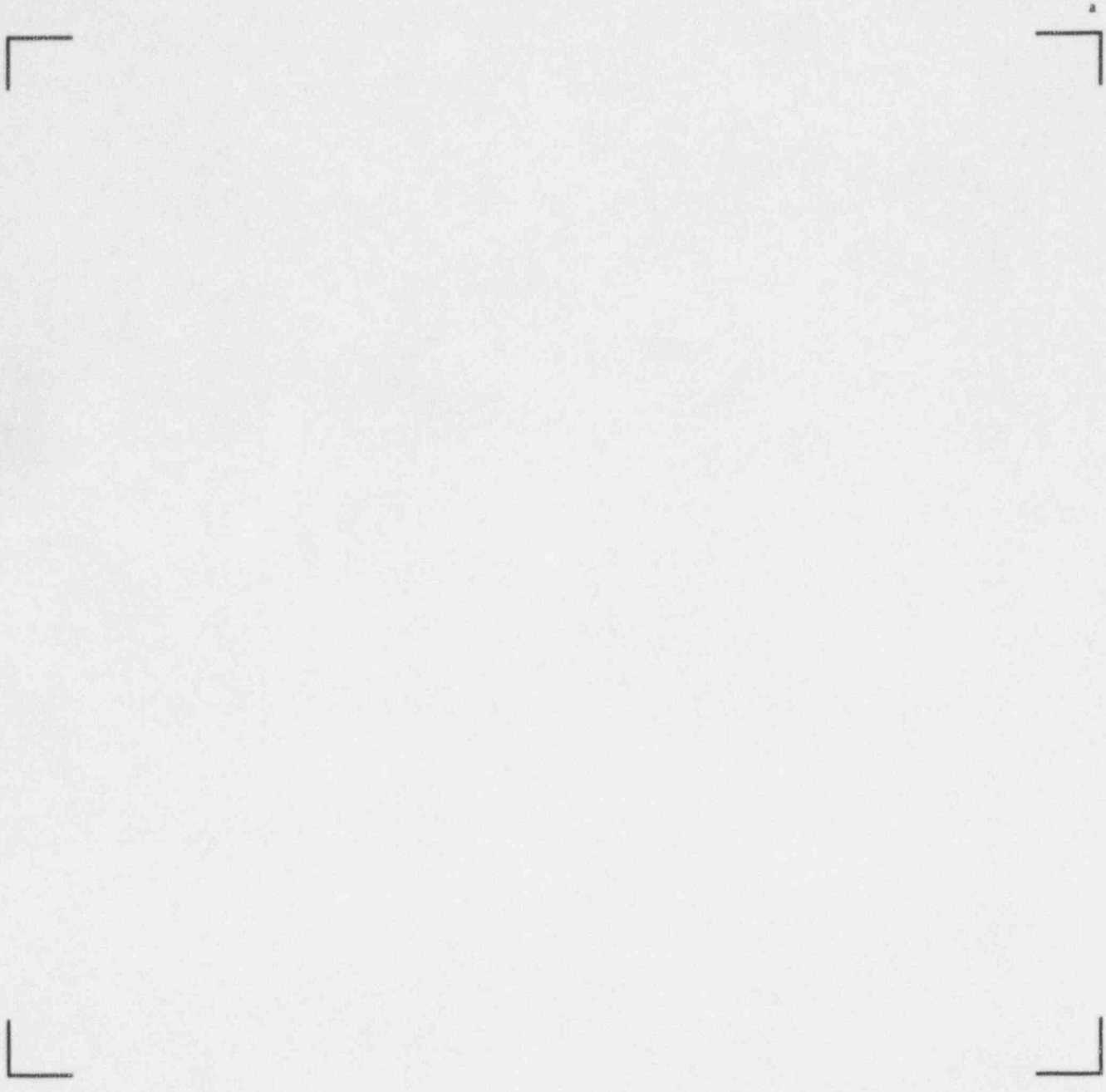

Figure 2-44: Normalized Mass Flux Vs. Elevation - Channel 14, Flow Study

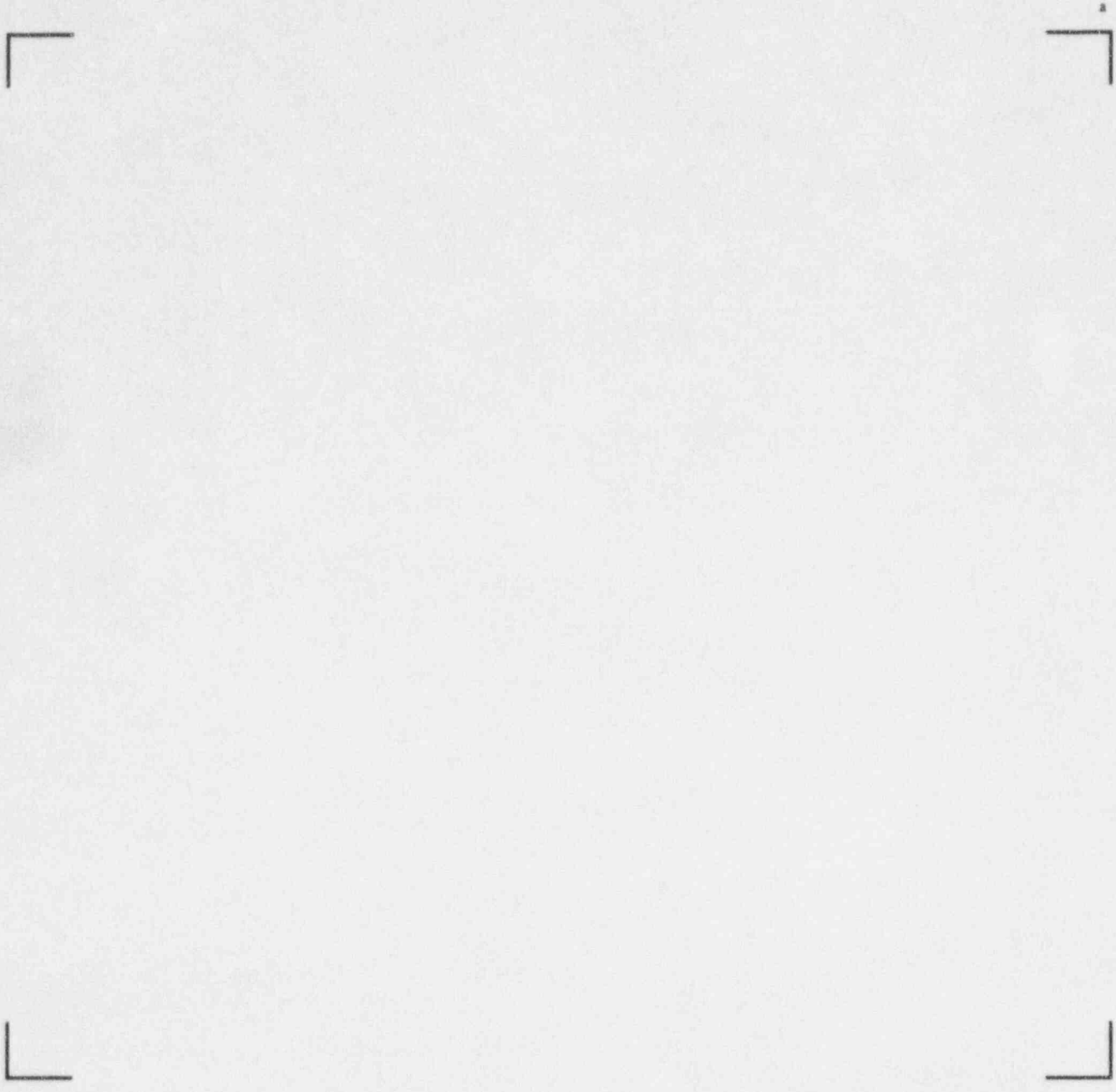

Figure 2-45: Normalized Mass Flux Vs. Elevation - Channel 15 : Flow Study

Figure 2-46: Ratio of Normalized Mass Flux - Flow Study : Channel 14 Vs. Channel 15

2.2.1.3 Summary of Base Model Performance

The importance of the [ ]^{b} on DNB calculations made using the WRB-2 critical heat flux correlation was demonstrated in each of the sensitivity cases examined with the revised base thermal-hydraulic model. In each case, the predicted DNBR was observed to reach a local minimum value just prior to each of the mixing vane or intermediate flow mixer grids. The DNBR then rises sharply just after each grid. This phenomena has been confirmed in critical heat flux testing, where the point of critical heat flux is usually observed at an axial location just upstream to a mixing grid. The DNBR increases downstream from the grids because of the increased turbulence and consequently, the increased subchannel crossflow, that occurs when the coolant flow encounters the grid.

The flow distribution in the base thermal-hydraulic model remained consistent in each of the sensitivity cases examined. Generally, the flow distribution was observed to be [ ]^{a} to the distance from the center of the core. That is, flow is [ ]^{a} near the center of the core (i.e., the hot assembly) with [ ]^{a} mass flow occurring in the channels representing the exterior of the core. This behavior is the result of two mechanisms. First, a [ ]^{a} was applied to the hot assembly in all sensitivity runs. Turbulent crossflow was observed to redistribute the inlet flow so that much of the [ ]^{a} is eradicated in the lower region of the core. However, some of the reduction of flow in the hot assembly must be attributed to the flow penalty. The second mechanism causing the mass flow reduction in the hot assembly is the increased flow resistance due to the presence of [ ]^{a} conditions associated with the high power in the hot assembly. Voiding results in an increase in axial drag through the [ ]^{a} This phenomena was magnified in the sensitivity cases which featured large void fractions.

Crossflow patterns between subchannels in the base thermal-hydraulic model maintained the same general pattern for each case examined. Generally, large crossflows which [ ]^{a} of the guide tube channels [ ]^{a} unit cells were observed at axial elevations corresponding to the locations of the spacer grids. This behavior is attributed to the [ ]^{a} for the guide tube channels at the grids. Crossflow in the unit channels was [ ]^{a} at the axial elevations of the grids. However, crossflow in the unit channels was generally [ ]^{a} in the regions between the grids. This effect was more pronounced in the middle and upper regions of the core. The underlying mechanism for this behavior is the higher linear heat rate and consequently, higher thermodynamic quality, in the unit channels. Higher quality results in [ ]^{a}. This effect was more significant when conditions resulted in higher void fractions.

It was determined that the limiting channel type for DNB in the base thermal-hydraulic model is largely dependent on the local quality. Conditions in which the coolant flow remains largely subcooled, such as those associated with nominal conditions, will be DNB limited in a [ ]^{a}. However, conditions which result in higher quality tend to be DNB limited in [ ]^{a}. This occurs because of the increased flow resistance associated with [ ]^{a} flow conditions, which tends to [ ]^{a} of the unit cells in the regions between the spacer grids. As the local thermodynamic quality increases further, the [ ]^{a} of the unit cell channels reaches a point where the effects of the flow resistance in the guide tube channels, due to

larger wetted perimeter and higher grid form loss, is offset. This causes the limiting channel for DNB to [ ]^{a}.

Results from the sensitivity runs on the base thermal-hydraulic model suggest that the quality in the unit channels is typically higher than in the adjacent guide tube channels. This is expected behavior due to the higher linear heat rate in the unit cell channels. Therefore, when a high power rod is bounded on one side by a unit channel and on the other side by a guide tube channel (see rod 11, Figure 2-20), the higher quality in the unit channel tends to [ ]^{a}.

Under normal conditions, the greater subcooled axial drag and higher grid form loss causes [ ]^{a} in the guide tube channel. This offsets the quality effect in the unit cell and, consequently, the [ ]^{a} for DNB. However, as the quality increases in the unit channel (i.e., accident conditions), increasing flow resistance in the unit channel due to [ ]^{a} conditions tends to reduce the difference in the unit cell channel and guide tube channel mass flow. This allows the quality effect on predicted DNB to become dominate in the unit cell channel.

The changes made to the base thermal-hydraulic model affect only the radial detail of the model (i.e., number of channels and rod models). Axial features of the model, such as the elevation of grids, are unchanged from the previously licensed model. Further, modeling philosophies adopted during the development and licensing of the WCNOC thermal-hydraulic analysis methodology were observed in the development of the Cycle 9 VIPRE-01 model.

Sensitivity studies performed on the model performance demonstrate that the revised base thermal-hydraulic model is adequate for calculation of accurate and conservative thermal-hydraulic conditions within the hot assembly.

2.2.2 Revised Thermal Design Procedure (RTDP)

Energy produced in the fuel of a nuclear reactor is removed from the surface of the fuel cladding by the coolant flow. Under normal conditions, the heat transfer mechanism is highly efficient nucleate boiling. Heat transfer coefficients under these conditions are typically around 50,000 Btu/Hr-ft^2-°F.

Conditions adverse to heat transfer from the cladding (i.e., increased heat flux, pressure decrease, flow reduction, etc.) degrade the ability of the coolant to accept heat from the clad surface. Eventually, the coolant flow past the fuel may reach conditions which result in the formation of a continuous layer of steam around the fuel rod. The phenomena is accompanied by a dramatic reduction in the heat transfer coefficient to around 500 Btu/Hr-ft^2-°F. The heat transfer coefficient falls because under these conditions, heat transfer is principally accomplished by conduction through the insulating layer of steam. This phenomena is defined as film boiling heat transfer. Figure 2-47 illustrates the various modes of heat transfer which can occur in a reactor core. As indicated, transition to the film boiling region of heat transfer must be accompanied by a dramatic increase in the clad temperature to maintain the heat transfer rate. This temperature increase can be so severe as to cause fuel damage.

Figure 2-47 : Definition of the Boiling Curve

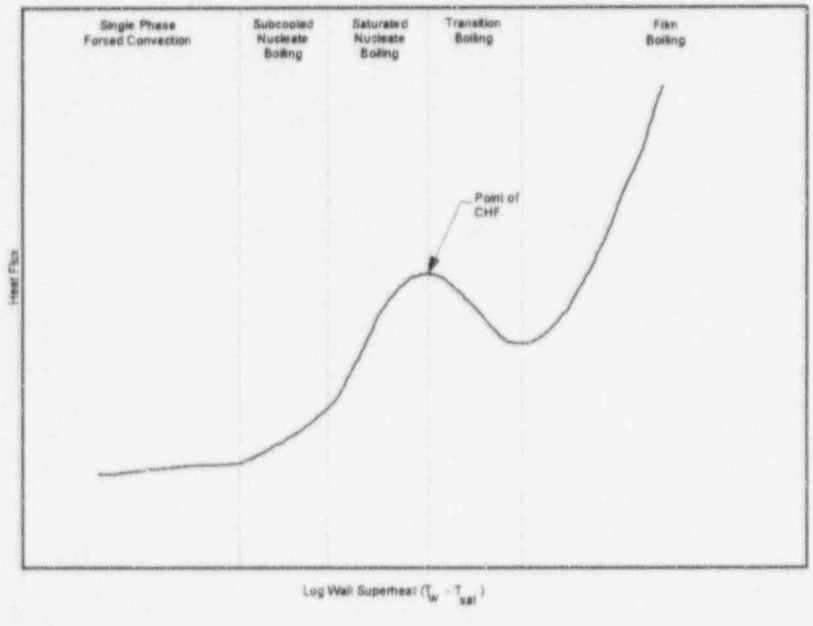

The heat flux at which the steam film starts to form around the fuel rod is known as the critical heat flux (CHF) or the point of DNB. The DNBR, which is defined as the ratio of the predicted critical heat flux to the actual heat flux, provides a measure of the thermal margin to film boiling in the core. The greater the DNB ratio is above 1.0, the greater the thermal margin.

Due to the complexity of heat transfer conditions within a fuel bundle and due to the complexity of the physical phenomena associated with the transition from nucleate boiling to film boiling, the critical heat flux must be predicted from an empirical correlation. The critical heat flux correlation relates the critical heat flux as a function of the local thermodynamic conditions and the bundle

geometry. Critical heat flux correlations are developed from experimental data obtained with electrically heated test sections which incorporate geometries and conditions typical of those found in a reactor core. Thus, application of a critical heat flux correlation is limited by both the range of thermal-hydraulic conditions and the test bundle geometries used to develop the correlation.

A critical heat flux correlation is essentially a least squares fit to the experimental data obtained in the critical heat flux tests. As such, each correlation has an associated uncertainty. The correlation uncertainty is quantified for use in design analyses by defining a correlation design limit. This design limit is defined as the DNBR at which there remains at least a 95% probability at the 95% confidence level that DNB will not occur on a specific fuel pin[32].

Core DNBR calculations are typically performed utilizing thermal-hydraulic analysis codes such as COBRA[33] and VIPRE[34]. These codes predict DNBR in the core for a given set of core state variables (i.e., power, flow, pressure, etc.). The DNB analysis performed with the thermal-hydraulic code is complicated by both the uncertainty associated with the critical heat flux correlation and by the uncertainties on the values of the core state variables.

The traditional design philosophy for protection from DNB in nuclear reactor cores has followed an extremely conservative approach. Essentially, core thermal-hydraulic design analyses were performed with all core statepoint variables (i.e., power, flow, pressure, inlet temperature, radial peaking factors, axial peaking factors, axial peak elevation, etc.) assumed to be at their most adverse values with respect to DNB. Thus, design analyses were performed with the core power assumed to be at the upper bound of the associated uncertainty, the flow was assumed to be at the lower bound of the measurement uncertainty, and pressure is assumed to be at the lower bound of the measurement uncertainty. This philosophy was applied to each of the core state variables and the resulting DNB ratio was then compared to the 95/95 design limit for the critical heat flux correlation.

The compounding of uncertainties on the critical heat flux correlation and the core state variables is unnecessarily restrictive. The simultaneous occurrence of all core state variables at their most detrimental limit is not realistic. A more realistic approach can be developed in which the distribution of the core state variables about their "reference" values is considered. Westinghouse has accomplished this using a statistical method termed "Revised Thermal Design Procedure" or RTDP[35].

In the RTDP methodology, the important variables, their uncertainties, and their distributions are identified and considered statistically to obtain a DNB uncertainty factor. The uncertainty on the DNBR is used to establish a design limit DNBR which replaces the original critical heat flux correlation 95/95 design limit. The design limit DNBR is by definition higher than the critical heat flux correlation design limit since it includes uncertainties on the correlation as well as the uncertainties on the core state parameters treated. The benefit of this approach is that the thermal-hydraulic analyses are then performed using the nominal values for the core state variables treated in the development of the design limit DNBR. Results from these nominal

condition analyses are then compared to the design limit DNBR, rather than the correlation design limit, to determine the thermal margin for a given core state.

2.2.2.1 Introduction to RTDP

In a Standard Thermal Design Procedure (STDP), all core state parameters (i.e., power, T_{in}, and pressure) are treated in a conservative way from a DNBR standpoint; that is, uncertainties are added to all parameters to give the lowest minimum DNBR. Historically, most plants using the STDP were designed to a minimum DNBR greater than or equal to 1.30 based on the W-3, L-grid, or R-grid DNB correlation.

In the Revised Thermal Design Procedure (RTDP), the following uncertainties are statistically combined with the DNBR correlation uncertainties to obtain the overall DNBR uncertainty factor used to define the design limit DNBR;

- Plant operating parameters (vessel coolant flow, core power, coolant temperature, system pressure, effective core flow fraction).
- Nuclear and thermal parameters ($F_{\Delta H}^{N}$).
- Fuel fabrication parameters ($F_{\Delta H,1}^{E}$).
- Thermal-Hydraulic and transient codes.

The uncertainty factor obtained is used to define the design limit DNBR which satisfies the DNB design criterion. The DNB design criterion is that the probability that DNB will not occur on the most limiting fuel rod is at least 95 % at a 95 % confidence level during normal operation and operational transients (Condition I events) and during transient conditions arising from faults of moderate frequency (Condition II events).

To produce margin to offset penalties such as those due to rod bow, lower plenum flow anomaly, and transition cores, and for core design flexibility, the design limit DNBR values are increased to values designated as the Safety Analysis Limit DNB's. The Safety Analysis Limit DNB's are used when performing the thermal-hydraulic analysis with RTDP.

Improved Thermal Design Procedure (ITDP) and Mini-RTDP are two other improved methodologies that can be applied to DNB analyses. A comparison of the STDP, ITDP, RTDP, and Mini-RTDP methodologies is provided in Figure 2-48. The 95 % line in this figure corresponds to the DNB design basis. That is, there is at least a 95 % probability at a 95 % confidence level that DNB will not occur on the limiting fuel rod for any Condition I or II event. For STDP, all uncertainties are added and thus the probability of DNB not occurring is much greater than 95 %. For ITDP, a portion of the conservatism is removed by statistically combining peaking factor and plant and computer code uncertainties, and adding to the correlation uncertainty. For RTDP, all the ITDP uncertainties are statistically combined with the correlation uncertainties. As indicated in the figure, there is still margin remaining with RTDP due to such things as the conservatism in transient methodology and axial power shapes. Figure 2-48 is

intended to indicate the relative DNB margin between each thermal design procedure and not to quantitatively define available DNB margins.

Figure 2-48 : Comparison of Westinghouse Thermal-Hydraulic Design Methodologies

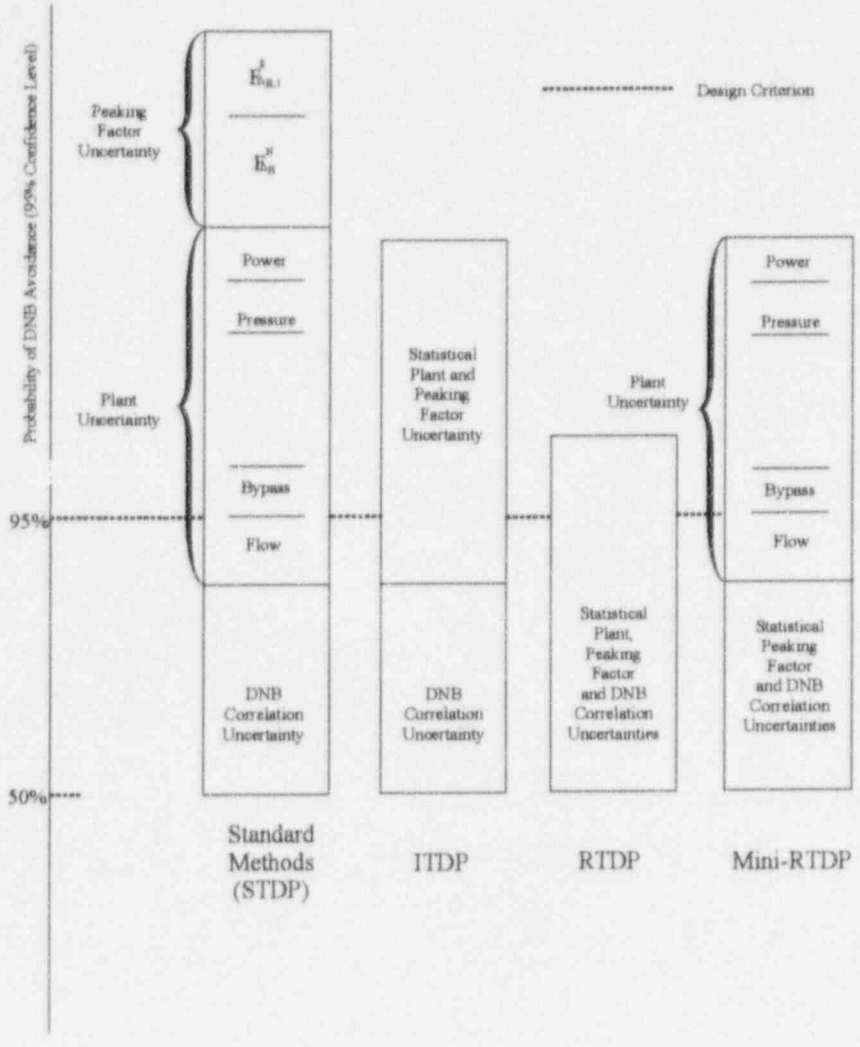

2.2.2.2 Design Input Data

This section provides the design data used in the development and application of RTDP for the WCGS. Included are definitions of the core statepoint nominal values, identified uncertainties, and trip setpoints.

Plant Parameters	
Parameter	**Design Value**
Power (MW_{th})	3565.0
Flow (GPM/Loop)	93,600.0
Pressure (psia)	2250.0
Inlet Temperature (°F)	554.8
Design Radial Peaking Factor, $F_{\Delta H}$	1.65
Design Axial Peaking Factor	1.55
Design Normalized Axial Peak Height	0.5
Design Bypass Flow (% of Total RCS Flow)	8.4
Best Estimate Bypass Flow (% of total RCS Flow)	6.61
Pressurizer Pressure High Analysis Trip Setpoint (psia)	2400.0
Pressurizer Pressure Low Analysis Trip Setpoint (psia)	1900.0
High Power Trip Setpoint (% of Rated Thermal Power)	112.3

Identified Uncertainties	
Parameter	**Design Value**
Core Power (% of Nominal)	±2.0
Core Flow (% of Nominal)	2.5
Pressure (psi)	30.0
Inlet Temperature (°F)	4.85
Core Bypass Flow	1.79
Radial Peaking Manufacturing Uncertainty (i.e. Hot Channel Factor) (%)	3.0
Radial Peaking Initial Rod Bow & Bundle Spacing Uncertainty (%)	1.3
Engineering Hot Channel Factor for Heat Flux, F_Q	1.033
Engineering Hot Channel Factor for Enthalpy Rise $F_{\Delta H,3}$	1.021

2.2.2.3 Theory

This section presents a brief derivation of the statistical theory employed in the RTDP. The RTDP is essentially an extension of the ITDP and thus, the mathematical relationships used in the ITDP are derived in the first part of this section. The second part of this section shows the extension of these relationships to the RTDP.

2.2.2.3.1 ITDP Methodology[36]

To relate the variations in design parameters to DNBR variations, an uncertainty factor, defined by the following equation is used;

[ ]^b

Equation 2.4

The value of DNBR (nominal) is determined by considering the values of all the design parameters to be at their nominal or best estimate values. The value of DNBR (variable) is based on values of the design parameters including their uncertainties and deviations from nominal values.

The DNBR uncertainty factor is considered to be affected by changes in the values of the design parameters according to a relation of the form;

[ ]^b

Equation 2.5

Where,

x_i = Value of the i^{th} design parameter.

∂x_i = Differential change in the value of x_i.

∂y = Differential change in y resulting from the differential changes ∂x_i.

The factor s_i represents the sensitivity factor associated with the i^{th} parameter. If all the parameters in Equation 2.5 are held constant except for one, and the x_i values are independent;

[ ]^b

Equation 2.6

Thus the value of s_i can be interpreted as representing the percentage change in DNBR resulting from a one (1) percent change in x_i, all other parameters being held constant.

Integrating Equation 2.5, considering the s_i values fixed, and taking antilogarithms, yields the following expression;

[ ]^b

Equation 2.7

where C is obtained from the constant of integration.

To evaluate the uncertainty factor y to be used in the design value of the DNBR, it is necessary to obtain a relationship between it and the uncertainties in the design parameters used to determine DNBR. Consider each of the independent design parameters x_i as being distributed about a mean value μ_i, the following expression is obtained;

[ ]^b

Equation 2.8

The partial derivatives in Equation 2.8 are evaluated at the point where all the x_i are at their mean values μ_i. The value of y at this point is represented by μ_y.

From Equation 2.7;

[ ]^b

Equation 2.9

If the perturbations from the mean values are small, the higher order terms in Equation 2.8 will be considerably smaller in magnitude than the first order terms and as a result can be ignored. The variance of y determined using Equation 2.8 results in the following expression;

[ ]^b

Equation 2.10

Using Equation 2.7 and Equation 2.9 in Equation 2.10 leads to the following;

[ ]b

Equation 2.11

Thus, if the sensitivity factors defined by Equation 2.6 as well as the mean and standard deviation of the probability distribution, are known for each of the design parameters, x_i, the value of σ/μ for the DNBR uncertainty factor can be determined.

The ratio σ/μ is called the coefficient of variation. Equation 2.11 enables the coefficient of variation of the DNBR uncertainty factor y to be determined in terms of the sensitivity factors s_i and coefficients of variation σ_i/μ_i of th design parameters x_i used in evaluating DNBR.

To satisfy the DNB thermal design criterion, an ITDP design limit value DL_I is determined such that the probability that CL, the Correlation Limit DNBR, is exceeded is 95 % with 95 % confidence. The governing variables are considered to be at such levels that with each at its mean value, the DNBR value on the peak power rod is DL_I. This results in the following relation for the design limit DNBR;

[ ]b

Equation 2.12

where 1 and 1.645 represent the mean value of y and the standardized normal variable corresponding to a 95 % probability, respectively.

2.2.2.3.2 RTDP Methodology[37]

The RTDP used the DNB correlation statistical characteristics $m_{M/P}$ and $s_{M/P}$, and the uncertainty factor statistical parameters μ_y and σ_y, calculated in the same manner as in the ITDP.

The statistically combined system and correlation design limit DNBR for the RTDP (DL_R) is selected such that for a statepoint with mean DNBR at the DL_R, there is a 95 % probability that the DNBR (variable) for the limiting fuel rod exceeds the correlation *P/M* (variable) with 95 % confidence. DNB will not occur if;

$$\text{DNBR (variable)} \geq P/M \text{ (variable)}$$

Equation 2.13

Using Equation 2.4;

[ ]^b

Equation 2.14

Rearranging Equation 2.14 results in;

[ ]^b

Equation 2.15

RTDP uses a parameter *z* defined by;

[ ]^b

Equation 2.16

the analysis of *z* in the RTDP is comparable to the analysis of y in the ITDP.

The equation for the coefficient of variation of *z* is as follows;

[ ]^b

Equation 2.17

Where;

[ ]^{b} is the ITDP design parameter coefficient of variation (Equation 2.11).

Once the coefficient of variation of z has been obtained, the RTDP Design Limit (DL_R) can be calculated from the expression;

[ ]^{b}

Equation 2.18

2.2.2.4 Calculation of Design Limit DNBR

This section documents application of the RTDP methodology, described in section 2.2.2.3, to arrive at the design limit DNBR for use in thermal-hydraulic design analyses for Cycle 9 operation of the WCGS. Included herein are the definition of the nominal values for each of the core state parameters, calculation of the parameter sensitivities, assignment of parameter standard deviations based on uncertainty distribution, and calculation of the Cycle 9 design limit DNBR.

2.2.2.4.1 Determination of Nominal Parameters

This section defines the nominal values for each of the core state parameters. The nominal statepoint provides the reference DNBR for use in the calculation of parameter sensitivities.

Pressure

The nominal operating pressure for the WCGS is 2250 psia (measured at the pressurizer). DNB analyses should take credit for the elevation head between the pressurizer and the core. Under full flow conditions, this elevation head is typically 30 psi. However, because the flow rates for complete loss of flow and locked rotor are based on a fraction of minimum measured flow, use of 30 psi may not always be conservative. Therefore, an elevation head of 20 psi will be assumed for RTDP analyses of the WCGS. The nominal DNB pressure is then 2270 psia.

Flow Rate

The flow rate for RTDP analyses is the minimum measured flow. Minimum measured flow is related to thermal design flow according to the expression;

$$\text{Minimum Measure Flow} = \frac{\text{Thermal Design Flow}}{1 - \text{Measurement Uncertainty}}$$

Referring to section 2.2.2.2, the minimum measured flow for the WCGS is;

$$\text{Minimum Measure Flow} = \frac{374{,}400\ \text{GPM}}{1 - 0.025}$$

$$\text{Minimum Measure Flow} = 384{,}000\ \text{GPM}$$

Bypass Flow

Best estimate bypass flow should be used in RTDP analyses. The best estimate bypass flow is 6.61%. The effective flow is then;

$$\text{Effective Flow} = (1 - 0.0661)\text{Minimum Measured Flow}$$

$$\text{Effective Flow} = (1 - 0.0661)384{,}000\ \text{GPM}$$

$$\text{Effective Flow} = 358{,}618\ \text{GPM}$$

Power

The rated thermal power, 3565 MW_{th} should be used in RTDP analyses. Conversion to units of kW/ft yields;

$$RTP = 3565MW * \frac{1000kW}{MW} * \frac{1}{193assy * 264\frac{rod}{assy} * \left(\frac{143.7}{144}\right)\left(12\frac{ft}{rod}\right)}$$

$$RTP = 5.8428\,kW/ft$$

Temperature

Nominal inlet temperature for the WCGS at rated thermal power is 554.8 °F. Allowing for 1.65 °F due to steam generator fouling, the inlet temperature is 556.5 °F.

$F^N_{\Delta H}$

The nominal value of $F^N_{\Delta H}$ is determined by taking the nuclear engineering design value and dividing by the measurement uncertainty. For the WCGS this yields;

$$F^N_{\Delta H} = \frac{1.65}{1.04} = 1.587$$

$F^E_{\Delta H,1}$

The nominal value of $F^E_{\Delta H,1}$ for RTDP analyses is 1.0.

F_Q

The nominal value of F_Q for RTDP analyses is 1.0.

2.2.2.4.2 Determination of Parameter Sensitivities

The sensitivity of each core state parameter with respect to DNBR is calculated by running VIPRE-01 with all parameters except one held constant over the range of parameters expected in the DNBR analysis of the core. This includes core limits, loss of flow, locked rotor, and rod misalignment events at power. In this section, a set of [ ]^b core states will be defined at which parameter sensitivities will be calculated. Documentation of the calculation of the parameter sensitivities follows.

2.2.2.4.3 Conditions Used in Sensitivity Analysis

A set of [ ]^b core states are used to calculate the σ_y/μ_y values in the RTDP analyses. These are;

b

These cases were identified according to the following table.

Case	Description

A second set of reference statepoints was then developed which featured a minimum DNBR close to the expected WRB-2 design limit. These statepoints were derived by taking the original [ ]^{b} statepoints above and adjusted one core state parameter until the predicted MDNBR was approximately 1.40. For the statepoints based on the Cycle 8 core limits, the inlet temperature was increased to attain the target MDNBR. For the loss of flow and locked rotor statepoints, the inlet mass flux was adjusted to yield the target MDNBR. Finally, the power in the rod withdrawal at power statepoint was adjusted to yield the 1.40 MDNBR. The adjustment to the core state parameters was made using the automatic iteration to a specified MDNBR option in VIPRE-01.

2.2.2.4.4 Calculation of Sensitivities

For each of the [ ]^{b} of conditions described above, the sensitivity of each parameter with respect to DNBR is calculated. Variations made on each core state parameter are selected such that the VIPRE-01 results give DNBRs close to the expected design limit DNBR. The sensitivity is calculated using the modified form of Equation 2.6;

$$\left[\qquad\qquad\right]^{b}$$

Equation 2.19

The range of core state parameters used to establish the various sensitivities must be broad enough to bound conditions at which DNBR calculations will be made. This includes both steady state core limit analyses and transient accident condition analyses. Based on this guideline, the following ranges of the core state parameters were selected for use in the sensitivity study;

- Pressure - From 1775 to 2420 psia.
- Flow Rate - From 60 % to 102 % of nominal.
- Core Power - From 80 % to 120 %.
- Core Inlet Temperature - From nominal T_{in}-30 °F to 610 °F.
- $F^{N}_{\Delta H}$ - From 1.49 to 1.8.
- $F^{E}_{\Delta H,1}$ - From 1.0 to 1.021.

After reviewing the sensitivity study results and selecting the maximum valid sensitivity for each core state parameter, the following sensitivities were established for the WRB-2 critical heat flux correlation used in conjunction with the base thermal-hydraulic model.

Table 2-17 : WCNOC WRB-2 Sensitivities

Parameter	WRB-2 Sensitivity
Power	
Temperature	
Pressure	
Flow	
Bypass Flow	
$F^N_{\Delta H}$	
$F^E_{\Delta H,1}$	

Comparison of the WCNOC sensitivities with the sensitivities reported by Westinghouse for WRB-2 with Vantage 5 fuel and the THINC thermal-hydraulic analysis code show excellent agreement. The sensitivities shown in Table 2-17 are only applicable over the range of core state parameters examined and when used in conjunction with the WCNOC base thermal-hydraulic model. Extension of these sensitivities to conditions outside the range of those used in their development or changes to the base thermal-hydraulic model will require further confirmatory analysis.

2.2.2.5 Determination of Standard Deviations

The standard deviation of each core state parameter is calculated by dividing the uncertainty of 2, 1.645 or $\sqrt{3}$ depending on whether the uncertainty can be described with a two-sided normal distribution, a one-sided normal distribution, or a uniform distribution.

Plant specific values for instrumentation uncertainty on pressure, temperature, power, and flow are used in the calculation of parameter standard deviations. Originally, the treatment of these instrumentation uncertainties was based on the conservative assumption that the uncertainties could be described with [ ]^b. Current Westinghouse technology is based on the more realistic assumption that the uncertainties can be described with random, [ ]^b.

The uncertainties may also include instrumentation biases. If these biases are in the direction of decreased DNBR, the effect of the bias should either be accounted for in the analysis by assigning DNB margin, or used directly in the analysis. If information on the bias is not obtained until after the DNBR design limit has been determined, the bias may be accounted for by assigning DNB margin.

Special attention must be paid to the calculation of the standard deviation (σ) of effective flow fraction (i.e., bypass flow). Effective flow fraction is defined as;

$$\mu = (1.0 - \text{best estimate bypass flow})$$

Equation 2.20

The associated uncertainty is equal to design bypass minus best estimate bypass. Effective flow fraction is treated with a uniform distribution.

$F_{\Delta H}^{N}$ and $F_{\Delta H,1}^{E}$ are one-sided normal distributions. The uncertainty is $F_{\Delta H}^{N}$ is four (4) percent and the nominal design value for $F_{\Delta H}^{N}$ is 1.587 (see section 2.2.2.2). Thus, the standard deviation of $F_{\Delta H}^{N}$ is;

$$\sigma_{F_{\Delta H}^{N}} = \frac{0.04 * 1.587}{1.645} = 0.0386$$

Equation 2.21

The uncertainty on $F_{\Delta H,1}^{E}$ is three (3) percent and thus;

$$\sigma_{F_{\Delta H,1}^{E}} = \frac{0.03}{1.645} = 0.0182$$

Equation 2.22

Westinghouse reports a standard deviation of [ ]^{b} for the THINC IV code and [ ]^{b} for the transient analysis codes. WCNOC will the same [ ]^{a} standard deviation for VIPRE-01 and will also adopt the [ ]^{a} for the transient analysis codes.

2.2.2.6 Design Limit DNBR

The DNBR design limit for thermal-hydraulic design analyses for Cycle 9 operation of the WCGS is calculated as follows. First, the values of σ_y/μ_y are obtained using Equation 2.11 for the set of conditions that gives the highest value. Next the parameter σ_{MP}/μ_{MP} is calculated for use with Equation 2.17. This parameter is based on the WRB-2 correlation statistics, and is the standard deviation and the mean, at a 95 % confidence level, of the data used to develop the WRB-2 critical heat flux correlation. The term σ_{MP} is given by;

$$\left[\quad\right]^{b}$$

Equation 2.23

Where, $s_{M/P}$ = Sample standard deviation associated with the WRB-2 data set.
k = Owen's factor[41].

The mean associated with the WRB-2 correlation data set, $\mu_{M/P}$, is taken as the equal to the mean of the data set $M_{M/P}$, since k included the effects of the uncertainties in both $s_{M/P}$ and $M_{M/P}$. For the WRB-2 correlation, the relevant statistical data is[42];

Table 2-18 : WRB-2 Statistical Data

[a]

Correlation	# Data Points	$M_{M/P}$	$S_{M/P}$	K Factor
WRB-2				

The calculation of the design limit DNBR, shown in Table 2-19, yields a 95/95 design limit of 1.23 for use in thermal-hydraulic design analyses.

Table 2-19 : Calculation of Design Limit DNBR

a,b

Parameter	μ	σ	σ/μ	s	$s^2(\sigma/\mu)^2$

2.2.2.7 Safety Analysis Limit DNBR

The Safety Analysis Limit DNBR is defined as;

$$\text{Safety Analysis Limit DNBR} = \frac{\text{Design Limit DNBR}}{1 - \text{Margin}}$$

Equation 2.24

The margin in Equation 2.24 is the plant specific DNBR margin that is retained for the purpose of offsetting DNBR penalties such as rod bow, transition core effects, and the lower plenum flow anomaly; as well as to increase the flexibility in design and operation of the plant.

There are two opposing goals is the selection of the Safety Analysis Limit DNBR or margin. One goal is to maximize the value of the available margin to provide increased flexibility in design which can be used for flexibility in loading pattern selection, increased peaking factors, and longer cycle lengths. However, increasing the retained DNB margin can only be done at the expense of thermal operating space. If the Safety Analysis Limit DNBR is set too high, unacceptable reactor trip setpoints (i.e., OTΔT and OPΔT) will result.

In previous cycles, the Safety Analysis Limit DNBR of 1.80 has been used. However, Cycle 9 will be the first reload design performed exclusively with Westinghouse methodologies, and it is unclear if the same Safety Analysis Limit DNBR will be acceptable. Thus, the Cycle 9 Safety Analysis Limit DNBR was set high enough to cover all known DNBR penalties, plus nine (9) percent retained margin for flexibility. The known DNBR penalties for cycle 9 are;

Table 2-20 : Cycle 9 DNBR Penalties & Margins

[b]

Penalty	Value (% DNBR Margin)

Inclusion of the desired 9 percent retained margin means that at least [ ][b] percent margin must be included in the calculation of the Safety Analysis Limit DNBR. Thus;

$$\text{SafetyAnalysis Limit DNBR} = \left[\quad\right]^{b}$$

2.2.2.8 Exit Quality Limit

In the RTDP, thermal-hydraulic calculations use nominal parameters and DNBR uncertainties are included in the Design Limit DNBR. For consistency with this approach, the DNB correlation exit quality limit is reduced to account for the uncertainty in exit quality.

The sensitivity (s_i) of exit quality (X_{out}) to plant parameter i (y_i) is defined by[43];

[ ]^b

Equation 2.25

The exit quality sensitivities are obtained from the same runs used in the DNBR sensitivity study. The sensitivities which are highest in magnitude in the range of interest are used. Studies to date have shown reductions of up to six (6) percent in exit quality limit.

2.2.3 Core Limit Generation and Protection

The purpose of this section is to establish the core thermal limit design methodology for the WCGS. The core thermal limits are used to define a region of allowable operation for which the core is protected should a Condition I or II event occur. This allowable region of operation is demarcated by the OPΔT and OTΔT trip functions. These trip functions provide primary protection against DNB and fuel centerline melting during normal operational transients and postulated faults of moderate frequency.

The principle objective of the thermal-hydraulic design of the reactor core is to insure that adequate heat transfer exists between the surface of the fuel rods and the coolant at all times to guarantee that safety criteria are met. Specifically, adequate heat transfer is achieved by preventing a DNB in the core. The thermal-hydraulic design basis is to protect against DNB such that there is at least a 95% probability at the 95% confidence level that a DNB will not occur during normal operation, operational transients, or as a result of conditions arising from any fault of moderate frequency (i.e. Condition I and II events).

The DNB design criteria is conservatively met by limiting the MDNBR in the core to the safety analysis limit. The safety analysis limit is the design DNBR for which 95/95 protection is guaranteed plus retained margin. To ensure that the MDNBR is always greater than the thermal design limit, a set of core DNB limits which define the allowable range of core operating

conditions are calculated or confirmed for each operating cycle. These core DNB limits represent the allowable combinations of power, pressure, and inlet temperature for which;

1. The MDNBR is greater than the thermal design limit.
2. The maximum exit quality from the hot channel is less than the upper limit of the range of applicability for the critical heat flux correlation utilized in the thermal-hydraulic design.
3. The vessel exit enthalpy is less than the saturation enthalpy at all system pressures.

The core thermal limits are the primary bases for generation of the OPΔT and OTΔT trip functions. These trip functions, defined in terms of vessel ΔT, pressure, and axial offset, cause a reactor trip if core conditions are such that a violation of the core thermal limit design criteria could occur. The design basis for the OPΔT and OTΔT trip functions is threefold; to prevent fuel centerline melting, to prevent a DNB, and to prevent vessel exit boiling[44].

The fuel centerline melting design basis is that during a Condition I or II event, the UO_2 melting temperature shall not be exceeded for at least 95% of the fuel at a 95% confidence level. The fuel centerline melting design basis has historically been met by limiting the reactor power to 118% of rated thermal power (RTP).

The DNB design basis is met by insuring that the OPΔT and OTΔT trip functions will produce a reactor trip before conditions arise which could lead to a violation of the core DNB limits.

The vessel exit boiling design criteria is met by insuring that the OPΔT and OTΔT trip functions will produce a reactor trip before conditions arise which could lead to the vessel exit enthalpy reaching the saturation enthalpy at the applicable system pressure. While vessel exit boiling is not strictly required for core protection, the exit boiling design criteria is imposed because the core protection system is based upon the assumption that the vessel ΔT is proportional to the core power. This is a valid assumption as long as the coolant remains subcooled.

2.2.3.1 Vessel Exit Boiling Limits

The vessel exit boiling limit lines are a family of curves which represent the locus of points at which the vessel exit enthalpy is equal to the saturation enthalpy at the applicable system pressure. While the vessel exit boiling limits do not serve a direct function in core protection, it is necessary to limit the vessel exit enthalpy to a subcooled state, since many of the reactor protection system functions use vessel ΔT as indicator of core power. The inherent assumption in these protection system functions is that vessel ΔT is proportional to core power; a valid assumption as long as the coolant remains subcooled. Thus, to guarantee that vessel ΔT remains proportional to power, the core exit enthalpy is restricted such that exit boiling will not occur.

The non-statistical expression for calculation of vessel exit enthalpy is simply;

$$H_{ex} = H_{in} + \Delta H$$

$$H_{ex} = H_{in} + \frac{Q}{W}$$

Equation 2.26

Where,
H_{ex} = Vessel exit enthalpy (Btu/lb_m).
H_{in} = Inlet enthalpy (Btu/lb_m).
ΔH = Vessel enthalpy rise (Btu/lb_m).
Q = Total power (Btu/hr).
W = Vessel flow rate (lb_m/hr).

To determine the vessel exit boiling limits for each power and pressure combination, a search is made to inlet temperature. This results in an exit enthalpy, H_{ex}, equal to the saturation enthalpy.

For applications utilizing the RTDP, the vessel exit enthalpy should be performed on a basis consistent with the DNB design philosophy. Specifically, the vessel exit boiling limits must be determined such that there is a least a 95% probability at the 95% confidence level that vessel exit boiling will not occur. To accomplish this, a statistical treatment of the associated uncertainties in the vessel exit boiling limit calculation is required. Specifically, the statistical exit enthalpy is given by;

$$\left[\qquad\qquad\right]^{b}$$

Equation 2.27

Where,
H_{ex}^{max} = Statistical Exit Enthalpy (Btu/lb_m)
H_f = Saturated liquid enthalpy (Btu/lb_m)
σ_H = Standard deviation of exit enthalpy distribution considering uncertainty in all parameters (Btu/lb_m).

Following the same rationale applied to the statistical treatment of uncertainties in the development of a critical heat flux correlation statistical design limit[45], the overall coefficient of variation for the statistical exit enthalpy is;

[ ]b

Equation 2.28

Where, [ ]b = Overall coefficient of variation of vessel exit enthalpy

[ ]b = Coefficient of variation of parameter i where σ is the upper 95% confidence level value for the standard deviation of parameter i.

S_i = Sensitivity of vessel exit enthalpy to parameter i.

For vessel exit boiling calculations, the pertinent parameters to be considered in Equation 2.28 are the core power, vessel flow, vessel inlet enthalpy (or temperature), and system pressure. Core parameters such as radial peaking, axial peaking, and elevation of maximum heat flux need not be considered in a statistical treatment of vessel exit boiling since these are bundle phenomena and have no influence on a vessel energy balance.

The sensitivity of vessel exit enthalpy to any single parameter i may be expressed as;

[ ]b

Equation 2.29

The coefficients of variation are the same as those used in the DNB analysis. Only those parameters which affect the exit enthalpy are considered. Extension of Equation 2.29 to the individual sensitivities of vessel exit enthalpy to power, flow, inlet temperature, and system pressure yields the following expressions for sensitivity;

Power (Q)

[ ]b

Equation 2.30

Flow (W)

[ ]b

Equation 2.31

Pressure (P)

[ ]b

Equation 2.32

Inlet Temperature (T_{in})

[ ]b

Equation 2.33

The method for determination of the parameter coefficients of variation is identical to that used to determine the coefficient of variation for DNB sensitivity. Specifically, the standard deviation for each parameter is calculated by dividing the associated uncertainty by the appropriate, distribution dependent factor. For parameters with a one-sided, normally distributed uncertainty function, the uncertainty is divided by 1.645. Two-sided, normal distributions are divided by 2 and uniform distributions are divided by $\sqrt{3}$. To maintain consistency with the RTDP

methodology, the power, pressure, and flow are treated with uncertainties which are assumed to be [ ][b]. Thus, the coefficients of variations for use in the statistical calculation of vessel exit boiling limits are;

$$\left(\frac{\sigma}{\mu}\right)_Q = [\quad]^{a,b}$$

$$\left(\frac{\sigma}{\mu}\right)_W = [\quad]^{a,b}$$

$$\left(\frac{\sigma}{\mu}\right)_P = [\quad]^{a,b}$$

$$\left(\frac{\sigma}{\mu}\right)_T = [\quad]^{a,b}$$

2.2.3.2 Core DNB Limits

This section defines the basis for and method used for the generation of the core departure from nucleate boiling limits for use in establishing the core thermal limits. The core DNB limits are used to insure that adequate heat transfer between the fuel rods and the coolant is maintained for all Condition I and Condition II events. The DNB design basis requires that there is at least a 95% probability at the 95% confidence level that a DNB will not occur during normal operation, operational transients, or as a result of conditions arising from any fault of moderate frequency.

The methodology required to generate the core DNB limits is straightforward. Generally, at each combination of pressure and power, an iteration on inlet temperature is made to determine the inlet temperature which yields the applicable cycle critical heat flux thermal design limit.

The core DNB limits will be generated at the same pressures examined in the vessel exit boiling limit analysis. At a minimum, the range of pressures examined must cover the span from the pressurizer low pressure trip to the pressurizer high pressure trip. A typical set of pressures for the WCGS would include core DNB limit calculation for 1900, 2000, 2250, and 2400 psi.

Core DNB limits are generated over a range of reactor powers such that the intersection of the DNB limits and the vessel exit boiling limits can be clearly resolved. Typically, core DNB limits are generated from 80% of rated thermal power to 120% rated thermal power. For power level

below nominal full power, the radial peaking factor is assumed to increase with decreasing power according to the expression;

$$F_{\Delta H}^{N} = F_{\Delta H,\,\text{design}}^{N} * \left[1.0 + K(1.0 - P)\right]$$

Equation 2.34

Where, $F_{\Delta H}^{N}$ = Maximum radial peaking factor at relative power P.

$F_{\Delta H,\,\text{design}}^{N}$ = Hot full power maximum radial peaking factor (1.587 for WCGS).

P = Fraction of nominal rated core thermal power.

K = Part power multiplier.

The design axial power distribution is a chopped cosine with a peak-to-average value of 1.55 (see Figure 2-49).

Figure 2-49 : Design Axial Power Shape - Core DNB Limits

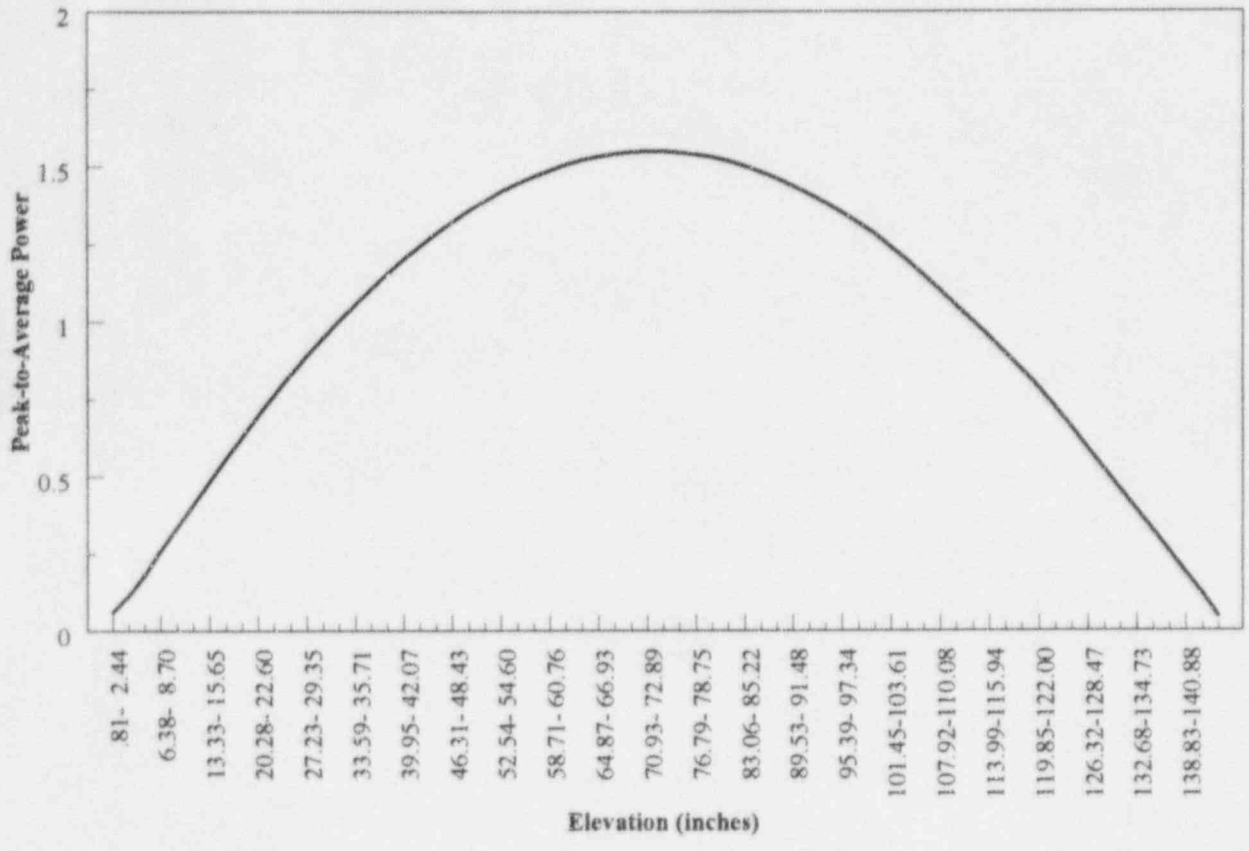

2.2.3.3 Core Thermal Limits

This section presents the method used to transpose the vessel exit boiling limits, core DNB limits, and core exit quality limits into the core thermal limits as defined in the USAR. Specifically, the vessel exit boiling limits and core DNB limits are transposed from functions of inlet temperature versus fraction of rated thermal power into a combined function of vessel ΔT versus T_{avg}. The transposition is made utilizing expressions involving the first law of thermodynamics and the log mean temperature difference equation. The purpose of this section is to define the methodology WCNOC intends to apply in the generation of core thermal limits. The data presented herein is intended solely for illustrative purposes and does not represent design data for Cycle 9.

The discussion of the transposition will be enhanced by first presenting a combined plot of the vessel exit boiling limits and the core DNB limits. This plot, shown in Figure 2-50, shows the relationship between the vessel exit boiling limits and the core DNB limits. As the figure indicates, the core is vessel exit boiling limited over much of the power range shown. Further, Figure 2-50 indicates that lower pressures trend to a vessel exit boiling limited condition at higher powers than do the higher pressures.

Using linear interpolation, the intersection of the vessel exit boiling limit lines and the core DNB limit lines are determined for each of the system pressures examined and the results are combined into a set of four curves which define the core thermal limits over the entire range of operating pressures and power levels. This set of curves, shown in Figure 2-51, represent the core thermal limits for use in establishing the core protection trip functions.

The thermal limits shown in Figure 2-51 provide the combinations of thermal power and core inlet temperature, as a function of system pressure, for which the core thermal design limits are met. However, the OPΔT and OTΔT trip functions utilize the measurement of vessel ΔT and T_{avg} to generate trip signals to protect the core. Thus, it is useful to convert the limits to define the core thermal limits in units of vessel ΔT as a function of core average temperature, T_{avg}.

In performing the conversion of the core thermal limits to functions of vessel ΔT versus T_{avg}, it is also useful to consider the limitations on reactor power and temperature imposed by the action of the steam generator safety valves. As primary side temperature increases, heat transfer across the steam generator tubes will eventually result in secondary side conditions which lift the steam generator safety valves. Thus, the maximum secondary side temperature is approximately constant at the saturation temperature corresponding to the lift pressure for the safety valves. The primary side temperature cannot exceed this secondary side saturation pressure plus the temperature drop across the steam generator tubes. Realizing that the temperature drop across the steam generator is proportional to the power transferred, the saturation temperature corresponding to the lift pressure for the steam generator safety valves places a direct physical limitation on reactor power and temperature. This temperature will serve to define one of the boundaries on reactor power and temperature in the definition of the core thermal limits[46]. The locus of points, in terms of ΔT and T_{avg}, at which the steam generator safety valves open is called the steam generator safety valve line, and this line will be included in the converted core thermal limits discussed below.

To change the core thermal limits from units of inlet temperature as a function of power to units of vessel ΔT as a function of core T_{avg}, the following procedure is used;

1. For each point on the thermal limit lines the following is known;
   a) Power (MWth)
   b) System pressure (psia)
   c) Minimum measured flow (gpm)
   d) Core inlet temperature (°F)

2. Using this information, the core inlet enthalpy is known and the vessel average enthalpy rise can be calculated. Using the exit enthalpy, the exit temperature (T_{out}) is also known. Thus, ΔT and T_{avg} for each point are computed using the expressions;

$$\Delta T = T_{out} - T_{in}$$

Equation 2.35

$$T_{avg} = \frac{T_{out} + T_{in}}{2}$$

Equation 2.36

3. For points corresponding to the vessel exit boiling limits, ΔT and T_{avg} are computed from the saturation temperature corresponding to the reference system pressure according to the relation;

$$T_{sat} = \frac{\Delta T}{2} + T_{avg}$$

Equation 2.37

4. The steam generator safety valve line is computed from the log mean temperature difference equation for heat transfer across a shell and tube heat exchanger. Specifically;

$$Q = UA * \frac{T_{out} - T_{in}}{\ln\left[\frac{T_{out} - T_{sv}}{T_{in} - T_{sv}}\right]}$$

Equation 2.38

Where, Q = Power (MW).

UA	=	Overall heat transfer coefficient based on performance of the steam generators at nominal conditions (MW/°F).
T_{out}	=	Vessel outlet temperature (°F).
T_{in}	=	Vessel inlet temperature (°F).
T_{sv}	=	Saturation temperature corresponding to 103% of the steam generator shell design pressure (i.e. safety valve set pressure plus 3 % accumulation).

The intersections of the core thermal limit lines and the steam generator safety valve line are determined by testing points on the thermal core limit line for each pressure until Equation 2.38 is satisfied.

The converted core thermal limits are shown in Figure 2-52. As indicated, the DNB limited regions occur at high vessel ΔT, which corresponds to the DNB limited regions at high thermal power from Figure 2-51. Further, Figure 2-52 indicates that the steam generator safety valve line intersects the low pressure limit line (i.e., 1900 psia) well down on the vessel exit boiling portion of the limit line while the steam generator safety valve line intersects the high pressure limit line (i.e., 2400 psia) on the DNB limit line.

The limits shown represent the thermal limits which define the allowable operating region for the WCGS, Cycle 7. These limits are protected, in part, by the action of the OPΔT and OTΔT trip function. Derivation of the OPΔT and OTΔT trip functions and their relationship with the core thermal limits shown is provided in section 2.2.3.4 below.

Figure 2-50 : Vessel Exit Boiling & Core DNB Limit Lines

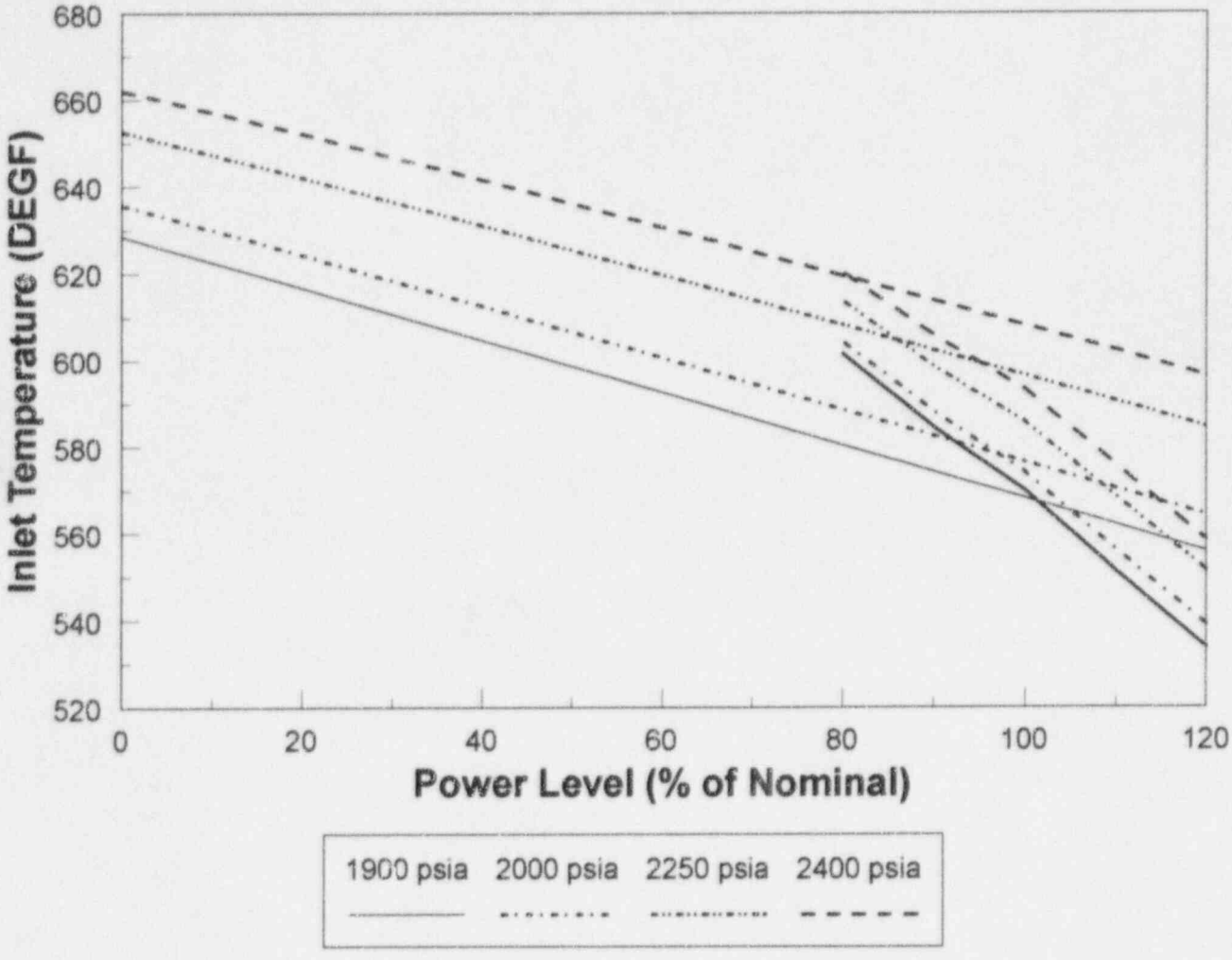

Figure 2-51 : Core Thermal Limits

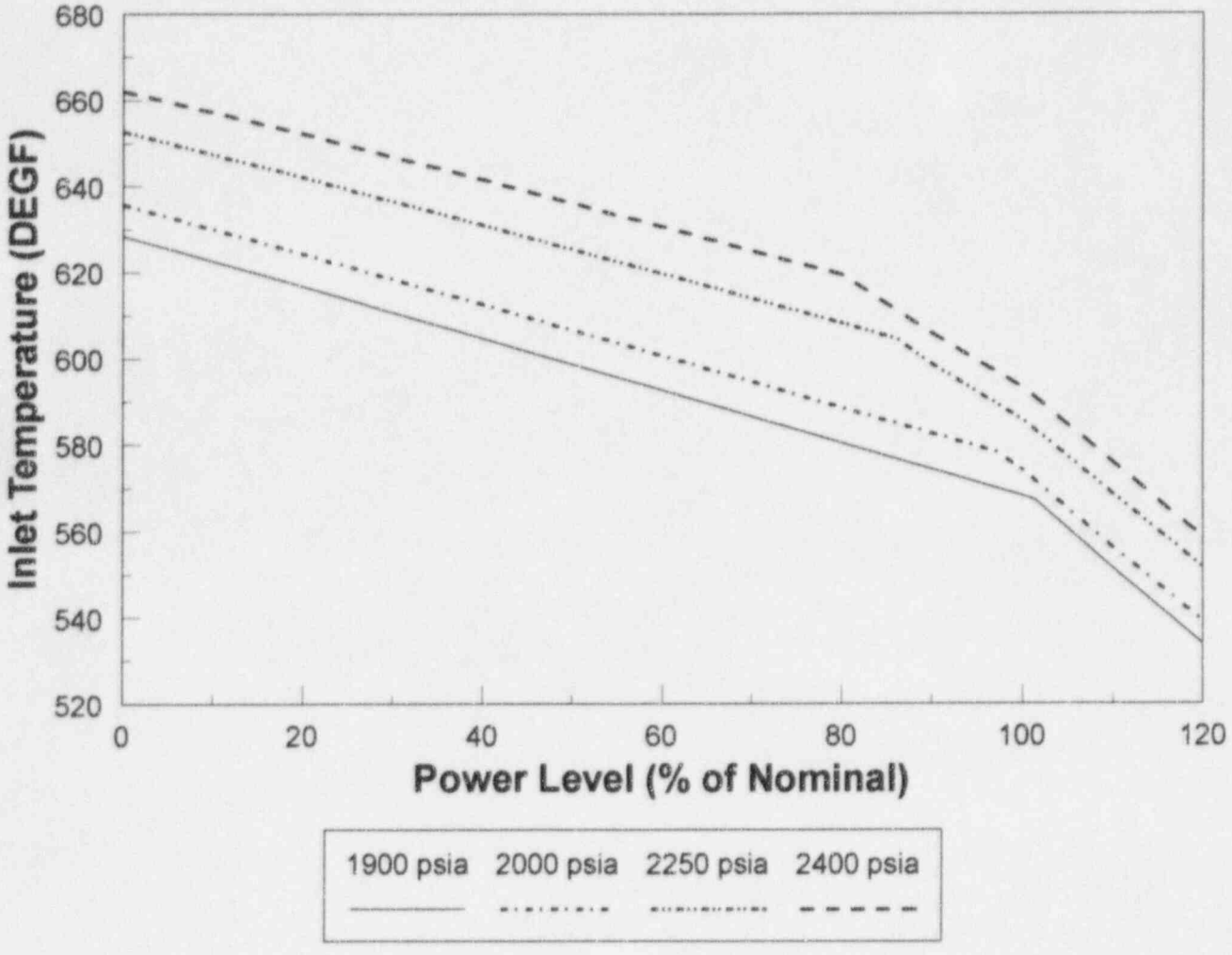

Figure 2-52 : Core Thermal Limits - Vessel ΔT Vs. T_{avg}

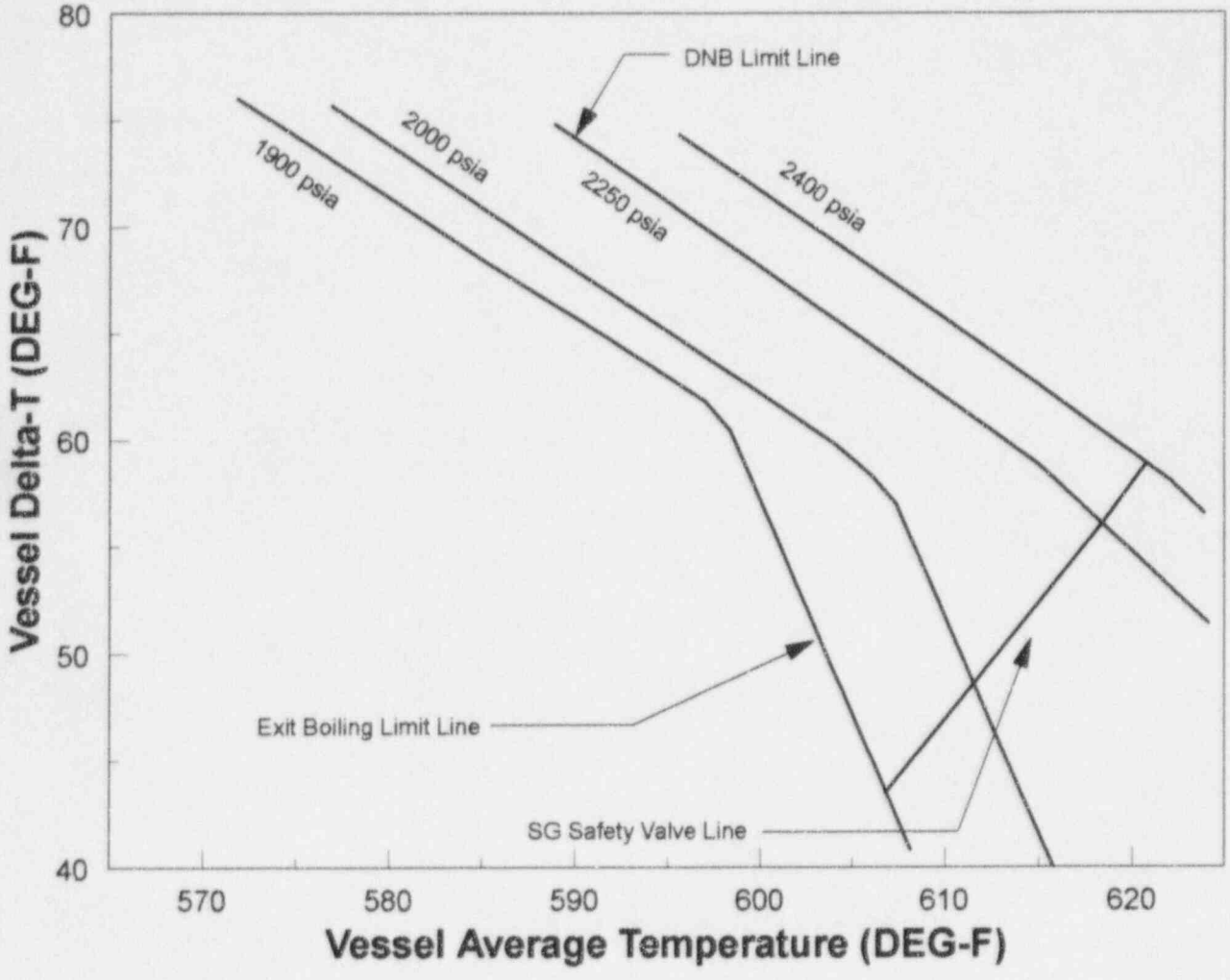

2.2.3.4 Overpower and Overtemperature ΔT Protection

As discussed previously, the design basis for the OPΔT and OTΔT trip functions consists of three components; prevention of fuel centerline melting, prevention of a departure from nucleate boiling, and prevention of vessel exit boiling[47]. This section will first describe each of the three components of the OPΔT, OTΔT design basis. Second, functional descriptions for the OPΔT and OTΔT trip functions will be provided. Included in these discussions are the calculational methods for establishing the coefficients of the OPΔT and OTΔT trip equations. Finally, a discussion of the compensation for core power distribution effects on the OPΔT and OTΔT trip functions is provided.

2.2.3.4.1 OPΔT and OTΔT Design Basis

The design basis for the OPΔT and OTΔT trip functions are intended to insure fuel integrity during Condition I and II events. Specific Condition II events which are protected by the OPΔT and OTΔT trip functions include;

- Rod withdrawal at power.
- Boron dilution/addition events.
- Excessive cooldown due to feedwater system malfunction.
- Excessive cooldown due to turbine throttle valve malfunction.
- Excessive steam load increase.

As previously discussed, the OPΔT and OTΔT trip functions insure fuel integrity by preventing fuel centerline melting, preventing an occurrence of a DNB, and by preventing vessel exit boiling.

The fuel centerline melt design basis is intended to limit the UO_2 temperature such that a fuel melt will not occur. This protection is provided at the 95/95 confidence level. Preventing fuel centerline melt insures that fuel geometry will be preserved during Condition I and II events and precludes molten fuel/clad interactions. Currently, fuel melt is precluded by limiting the peak kW/ft in the fuel rods such that the calculated fuel centerline temperature does not exceed 4,700 °F. This conservative limit includes a reduction in the theoretical UO_2 melting temperature to account for irradiation effects.

Preventing a DNB insures that adequate heat transfer from the fuel rods to the coolant is maintained during Condition I and II events. The protection criteria requires that DNB is prevented in 95% of the fuel rods at the 95% confidence level. The design basis is met by insuring that the minimum DNB ratio is greater than the critical heat flux correlation safety analysis limit.

The limit on the vessel exit temperature to less than the saturation temperature at the applicable system pressure is not directly derived from a core protection limit. Rather, it is based upon the fact that the core protection system uses core ΔT as an indicator of reactor power. As long as the exit enthalpy remains less than the saturation enthalpy, this is a valid inference. Thus, the

protection system is designed to preclude vessel exit boiling to assure that ΔT is proportional to core power.

2.2.3.4.2 Functional Description - OPΔT

This section provides the functional description of the thermal OPΔT trip function. Calculational methods used to establish values of the trip function coefficients are also provided. First, a general discussion of how the measurable process variables in the reactor coolant system are used to protect the core thermal limits is provided. This discussion is followed by a presentation of the thermal OPΔT trip function and definition of terms. Finally, the method for establishing values for the coefficients in the OPΔT trip function by utilizing the core thermal limits is given.

The core thermal limits provide limits on design variables which result from the implementation of the core protection design basis. The purpose of the OPΔT and OTΔT trip functions is to relate these limits on core design parameters to measurable process variables in the plant. Specifically, the OPΔT and OTΔT trip functions relate vessel ΔT, core average temperature (T_{avg}), system pressure, and core axial flux difference (ΔI), at a given volumetric flow rate, to the limits defined by the core thermal limits. Protection is provided in the form of a reactor trip should any unacceptable combination of process variables occur which could lead to a violation of the core thermal limits.

The OPΔT trip is specifically intended to prevent centerline fuel melt. Westinghouse has shown that the fuel temperature design basis can be met by limiting reactor power to 118% of the nominal rated thermal power[48]. The OPΔT trip function relates the difference between the hot leg and cold leg temperatures (i.e., vessel ΔT) to core power. The OPΔT trip function also includes terms to account for changes in coolant density and heat capacity as the average core temperature is varied from nominal. Further, compensation for skewed axial power distributions is made through the inclusion of the F(ΔI) term.

The OPΔT trip function is designed to provide a reactor trip whenever the measured temperature difference between the hot legs and cold legs exceeds the trip setpoint. The trip setpoint is generated according to the expression;

$$\Delta T_{setpoint} = K_4 - K_5 \frac{\tau_3 S}{1+\tau_3 S} T_{avg} - K_6\left(T_{avg} - T'_{avg}\right) - F(\Delta I)$$

Equation 2.39

Where, $\Delta T_{setpoint}$ = OPΔT setpoint, in % of full power ΔT.

K_4 = A preset, manually adjustable bias, in % of full power ΔT.

K_5 = Compensation term to account for piping and thermal delays, in % of full power ΔT/°F.

K_6 = Compensation term to account for the changes in coolant density and coolant heat capacity, in % of full power ΔT/°F.

T'_{avg} = Indicated core average temperature at full power, in °F.

T_{avg} = Measured core average temperature, in °F.

τ_3 = Time constant, in seconds.

S = Laplace transform operator, in seconds^{-1}.

F(ΔI) = A function of the axial flux imbalance between the upper and lower halves of the core.

Determination of the coefficients in the Equation 2.39 is based upon the intersection of the overpower limit (i.e., 118% nominal power) and the core thermal limit lines. The locus of conditions at which the ΔT corresponds to 118% rated thermal power are determined for a variety of system pressures spanning the range between the high and low pressurizer pressure trip settings. At each system pressure examined, the core average temperature is varied to establish the relationship between vessel ΔT and T_{avg} at 118% of rated thermal power. For a given system pressure, the vessel ΔT corresponding to 118% thermal power decreases as T_{avg} is increased. Figure 2-53 provides a plot of the locus of points corresponding to the overpower condition as a function of system pressure as well as the intersection of these overpower points with the core thermal limit lines. Examination of these intersection points reveal a slight dependence of the overpower/core thermal limit intersection on the system pressure.

The overpower/core thermal limit pressure dependence is included in the OPΔT trip function by using a two equation approach. At core average temperatures equal to or less than the nominal T_{avg}, a constant ΔT setpoint is used to protect the overpower condition. Above the nominal T_{avg}, the overpower setpoint is a diminishing ΔT. This approach is illustrated in Figure 2-54. The solid line connecting points A and B represent the locus of points at 118% power at which the DNBR is equal to the thermal design limit. Point A is the intersection point, at the nominal vessel average temperature, of the vessel ΔT corresponding to 118% power at the low pressurizer pressure trip setpoint and the DNBR limit line. Point B is the intersection of the points corresponding to the vessel ΔT at 118% power at the high pressurizer pressure trip setpoint and the DNBR limit line.

The OPΔT trip function is then defined with two equations. At or below the nominal T_{avg}, the OP ΔT trip function is;

$$\Delta T_{sp} = \Delta T_0 * K_4$$

Equation 2.40

While above the nominal T_{avg} the trip function is given by;

$$\Delta T_{sp} = \Delta T_0 * \left[K_4 - K_6 \left(T_{avg} - T_{avg,nom} \right) \right]$$

Equation 2.41

Where, ΔT_{sp} = Trip setpoint of ΔT, in °F.
ΔT_0 = Indicated ΔT at nominal plant conditions, in °F.
T_{avg} = Measured average temperature, in °F.
$T_{avg,nom}$ = Nominal average temperature at rated power, in °F.
K_4 = Preset, manually adjustable bias.
K_6 = A constant term which compensates for the change in density, flow, and heat capacity of water with change in temperature.

Referring to Figure 2-54, the ΔT at point A (ΔT_A) is then the constant overpower ΔT protection limit (ΔT_{pl}) for T_{avg} less than nominal. This can be written in terms of indicated ΔT at nominal plant conditions (ΔT_0) according to the expression;

$$\Delta T_{pl} = \frac{\Delta T_A}{\Delta T_0} * \Delta T_0$$

Equation 2.42

Obviously, Equation 2.42 can be reduced to yield Equation 2.40. The manually adjusted bias term, K_4, is then defined as;

$$K_4 = \frac{\Delta T_A}{\Delta T_0}$$

Equation 2.43

For a vessel average temperature greater than the nominal T_{avg}, the overpower ΔT protection limit is represented by an equation which defines the line connecting points A and B as shown in Figure 2-54. The slope of this line is;

$$\text{slope} = \frac{\Delta T_A - \Delta T_B}{T_{avg\text{-}A} - T_{avg\text{-}B}}$$

Equation 2.44

Obviously, the slope of the line defined by Equation 2.44 is always negative. Thus, a negative sign is preserved in the trip equation and the slope is expressed in absolute units. In terms of the

ΔT at nominal plant conditions (ΔT_0), the OPΔT equation for vessel average temperatures above nominal is given by;

$$\Delta T_{pl} = \Delta T_0 * \left[\frac{\Delta T_A}{\Delta T_0} - \frac{\Delta T_A - \Delta T_B}{T_{avg\text{-}A} - T_{avg\text{-}B}} * \frac{1}{\Delta T_0} \left(T_{avg\text{-}B} - T_{avg\text{-}A} \right) \right]$$

Equation 2.45

The compensation term (K_6) is therefore defined as;

$$K_6 = \frac{\Delta T_A - \Delta T_B}{T_{avg\text{-}A} - T_{avg\text{-}B}} * \frac{1}{\Delta T_0}$$

Equation 2.46

If Equation 2.46 is substituted in Equation 2.45, the result is the simplified expression for the OPΔT trip function for T_{avg} above nominal (i.e., Equation 2.41). When computing coefficients for the OPΔT trip function, checks are made to guarantee that all points on the overpower locus between points A and B, Figure 2-54, are indeed protected. Should a point be found which is not protected, the slope defined by Equation 2.44 is adjusted until the protection criteria is satisfied.

2.2.3.4.3 Functional Description - OTΔT

This section provides the functional description of the thermal OTΔT trip function. Calculational methods used to determine values of the trip function coefficients are also provided. The thermal OTΔT trip function provides protection for the DNB limit lines and the vessel exit boiling limits. The trip function is correlated with vessel ΔT, the system pressure, and the vessel average temperature. As was done for the OPΔT trip function, a compensation term to account for the effects of skewed power distributions is also incorporated in the OTΔT trip equation. Specifically, the OTΔT trip equation is given by;

$$\Delta T_{setpoint} = K_1 - K_2 \frac{1 + \tau_1 s}{1 + \tau_2 s} \left(T_{avg} - T_{avg}^{nom} \right) + K_3 \left(P - P^{nom} \right) - F(\Delta I)$$

Equation 2.47

Where,

$\Delta T_{setpoint}$ = Overtemperature ΔT setpoint, in percent of full power ΔT.

K_1 = Preset, manually adjustable bias, in percent of full power ΔT.

K_2 = Constant compensation term to account for the effect of temperature on the design limits, in percent of full power ΔT/°F.

K_3 = Constant compensation term to account for the effect of pressure on the design limits, in percent of full power ΔT/psi.

T_{avg} = Measured average reactor coolant temperature, in °F.

T_{avg}^{nom} = Nominal average reactor coolant temperature at full power, in °F.
P = Indicated pressurizer pressure, in psig.
P^{nom} = Nominal reactor coolant pressure, in psig.
τ_1, τ_2 = Time constants, in seconds.
s = Laplace transform operator, in seconds^{-1}.
$F(\Delta I)$ = Function of the neutron flux difference between the upper and lower long ion chambers, in percent of full power ΔT.

Ideally, the OTΔT trip equation would, after allowing for measurement and instrument uncertainties, exactly match the core thermal limits. However, the form shown in Equation 2.47 was adopted to simplify the protection system.

Determination of the coefficients and constants in the OTΔT trip function is based upon the intersection of the core thermal limits and the locus of conditions where ΔT corresponds to 118% of rated thermal power as well as the intersection of the core thermal limits and the steam generator safety valve line.

As previously discussed, the core thermal limits are converted into a ΔT versus T_{avg} coordinate system. The region which must be protected by the OTΔT trip function is then bounded by;

- OPΔT trip function as defined in section 2.2.3.4.2.
- Steam generator safety valve line as defined by Equation 2.38.
- The core thermal limit lines corresponding to the high and low pressurizer pressure trip setpoints.

Figure 2-55 is a representation of the intersection points used to establish the coefficients in the OTΔT trip function. Referring to this figure, the intersection points shown are;

Point A : Intersection of the 118% overpower line and the core thermal limit line at the pressure corresponding to the high pressurizer pressure trip setpoint.
Point B : Intersection of the 118% overpower line and the core thermal limit line at the pressure corresponding to the low pressurizer pressure trip setpoint.
Point C : Intersection of the core thermal limit line and the steam generator safety valve line at the pressure corresponding to the high pressurizer pressure trip setpoint.
Point D : Intersection of the core thermal limit line and the steam generator safety valve line at the pressure corresponding to the low pressurizer pressure trip setpoint.

The slopes and constants for four different OTΔT equations can be defined based upon the four intersection points above (i.e., points A, B, C, & D). These equations are;

- A line parallel to AC which intersects B.
- A line parallel to AC which intersects D.
- A line parallel to BD which intersects A.
- A line parallel to DB which intersects C.

The constants K_1, K_2, and K_3 can be determined by solving simultaneous equations based upon the lines described above. Figure 2-56 provides a graphical representation of this procedure. In this figure, a line segment BD has been constructed and transposed to intersect point A. As the figure indicates, an OTΔT trip function based upon this line would, in fact, provide the required protection against DNB and violation of the vessel exit boiling limits at both the high and low pressurizer pressure setpoints.

An example of a potential OTΔT trip function which *fails* to protect the limits at all allowable system pressures is shown in Figure 2-57. In this figure, a line segment AC has been constructed and transposed to intersect point B. As the figure indicates, an OTΔT trip function based upon this line would protect the core limits at the high pressurizer pressure trip setpoint, but fails to provide complete protection for the vessel exit boiling limits along the low pressurizer pressure line.

Figure 2-58 provides a representation of a potential OTΔT function which satisfies all protection criteria but results in an unacceptable loss of operating space along the low pressure limits as compared to the trip function shown in Figure 2-56. Thus, selection of the final OTΔT trip function must satisfy two criteria. First, the selected function must protect all portions of the core thermal limits previously described (i.e., DNB limits, vessel exit boiling limits, steam generator safety valve line, and overpower limit) and secondly, the selected OTΔT function must maximize the available operating region.

In the final equation selected, the values of K_1, K_2, and K_3 are determined by dividing by indicated ΔT at nominal plant conditions and the resulting overtemperature ΔT protection equation is then;

$$\Delta T_{pl} = \Delta T_0 * \left[K_1 - K_2 \left(T_{avg} - T_{avg}^{nom} \right) + K_3 \left(P - P^{nom} \right) \right]$$

Equation 2.48

Where,

ΔT_{pl}	=	The overtemperature ΔT protection limit, in °F.
ΔT_0	=	Indicated ΔT at nominal plant conditions, in °F.
T_{avg}	=	Measured average vessel temperature, in °F.
T_{avg}^{nom}	=	Nominal T_{avg} at rated thermal power, in °F.
K_1	=	Preset, manually adjustable bias.
K_2, K_3	=	Preset, manually adjustable gains.
P	=	Measured pressurizer pressure, psig.
P^{nom}	=	Nominal pressurizer pressure, psig.

The function shown in Equation 2.48 represents the maximum allowable ΔT, during operation, which falls within the core limits. The final values of the trip function coefficients (i.e., K_1, K_2, and K_3) must be adjusted to account for the appropriate uncertainties and instrument errors. Further, the trip function coefficients must be adjusted such that limiting Condition II event, which is terminated by the OTΔT trip function, exhibits acceptable DNB performance.

Finally, the final setpoint value for ΔT_0 in Equation 2.48 is based upon actual plant startup test measurements on a cycle specific basis. The variables T_{avg}^{nom} and P^{nom} are fixed reference points.

Figure 2-53 : Overpower ΔT Protection - Intersection of Core Limits & 118% Power Conditions

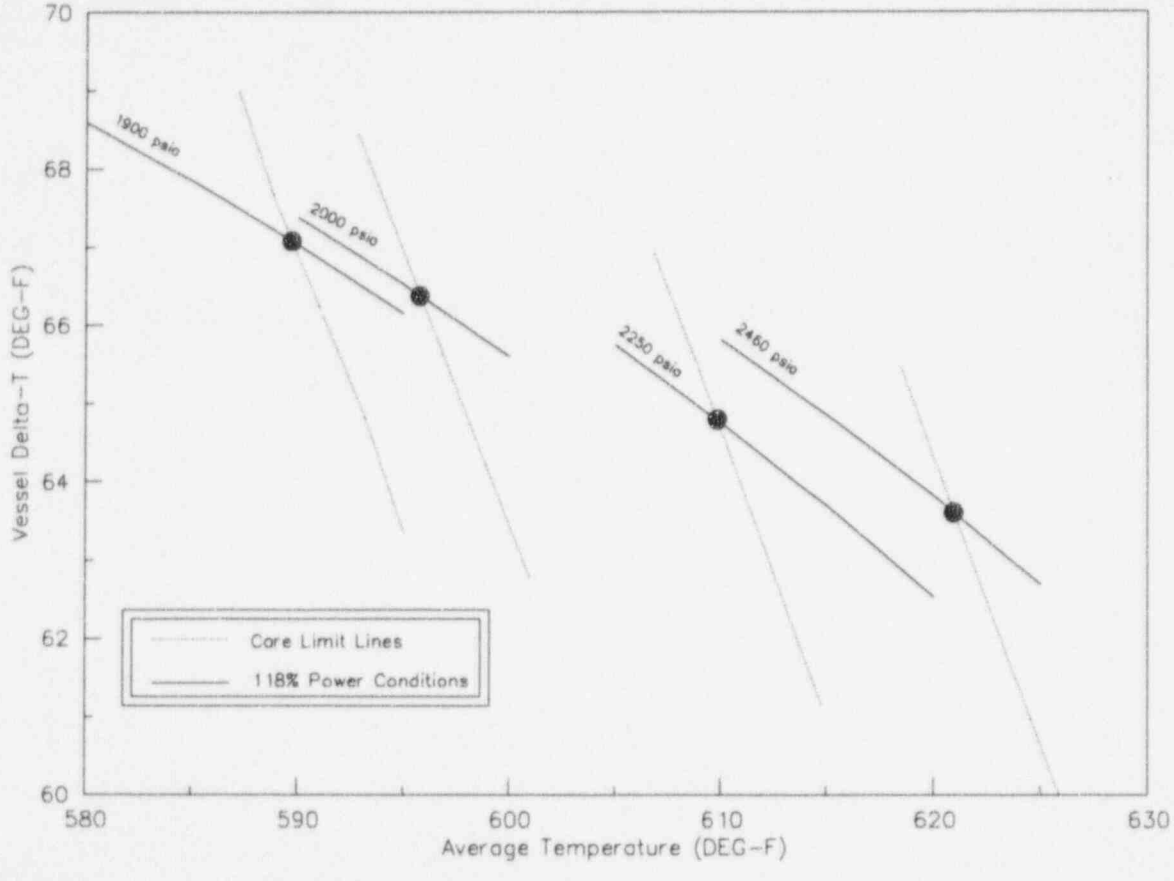

Figure 2-54 : Overpower Protection

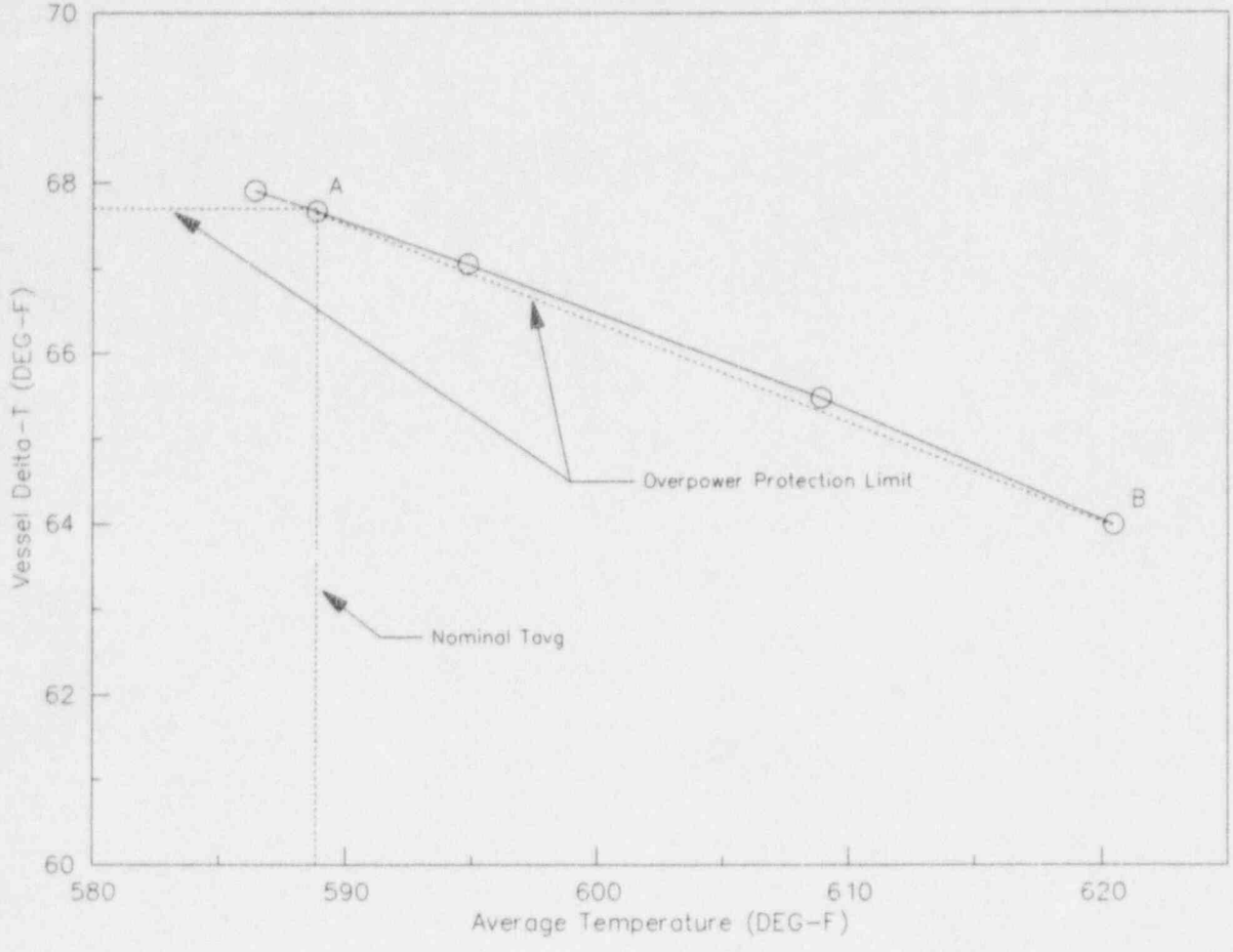

Figure 2-55 : Overtemperature ΔT Protection - Points used to Establish OTΔT Protection

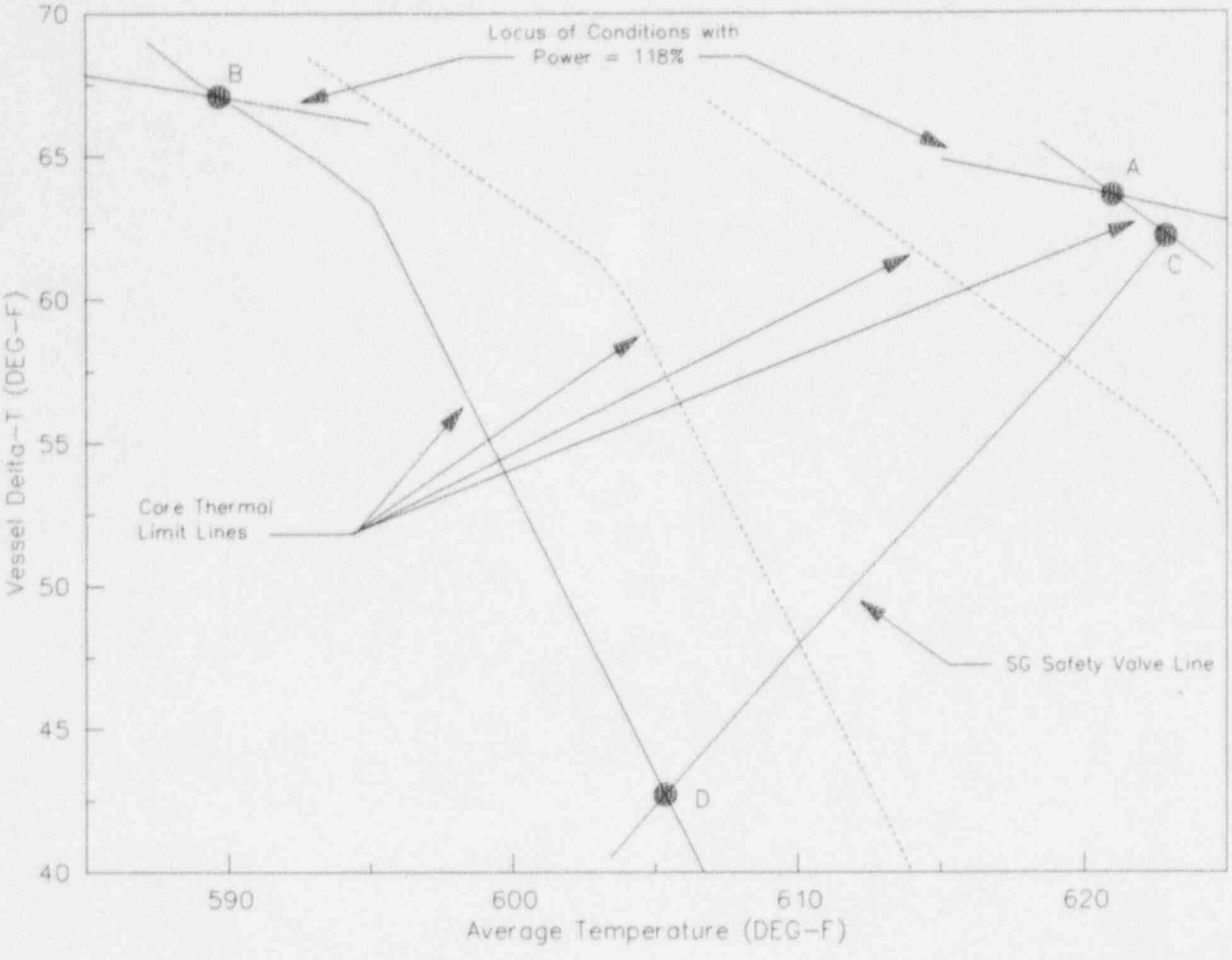

Figure 2-56 : Overtemperature ΔT Protection - Establishing OTΔT Coefficients

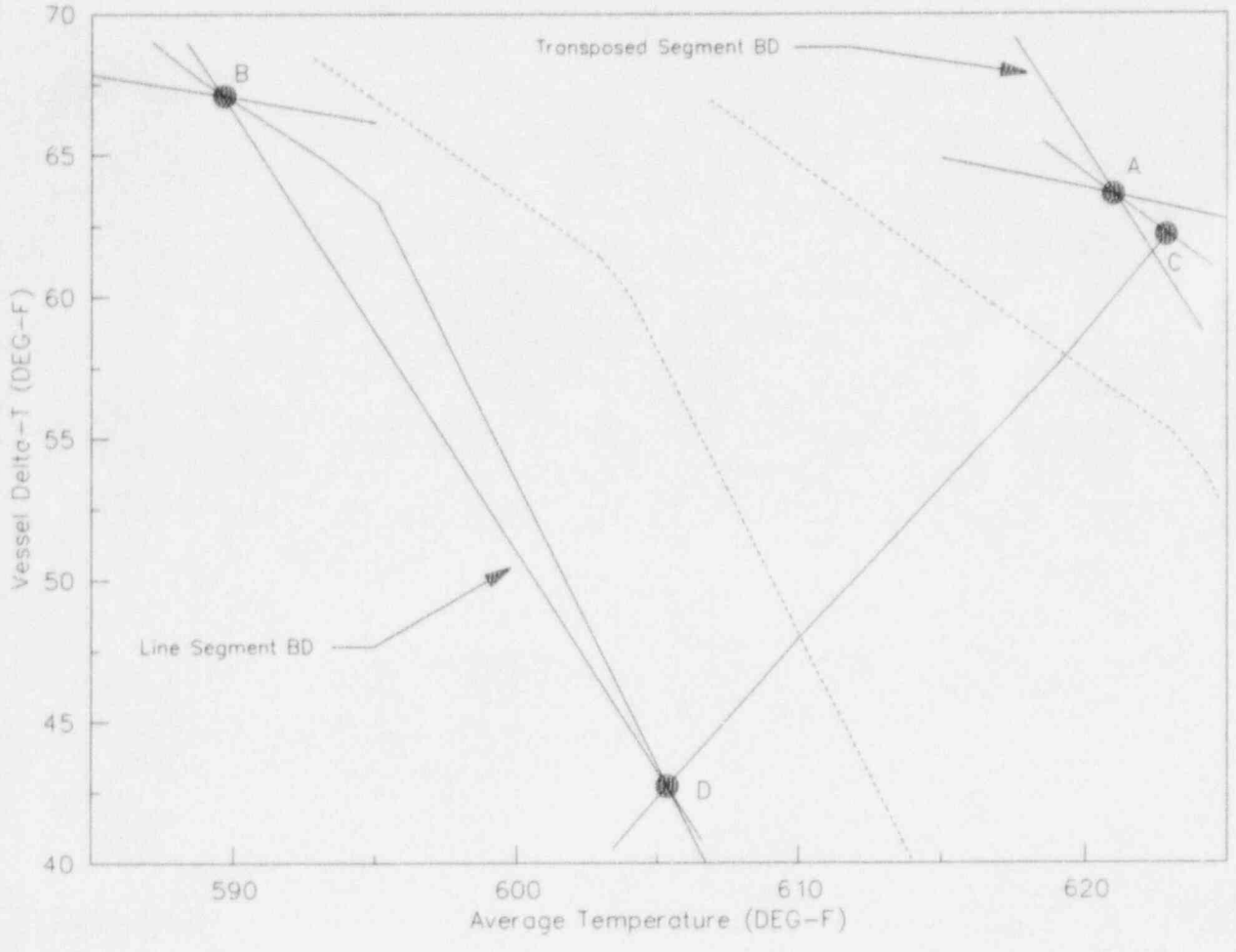

Figure 2-57 : Establishing OTΔT Coefficients - Failed Protection Function

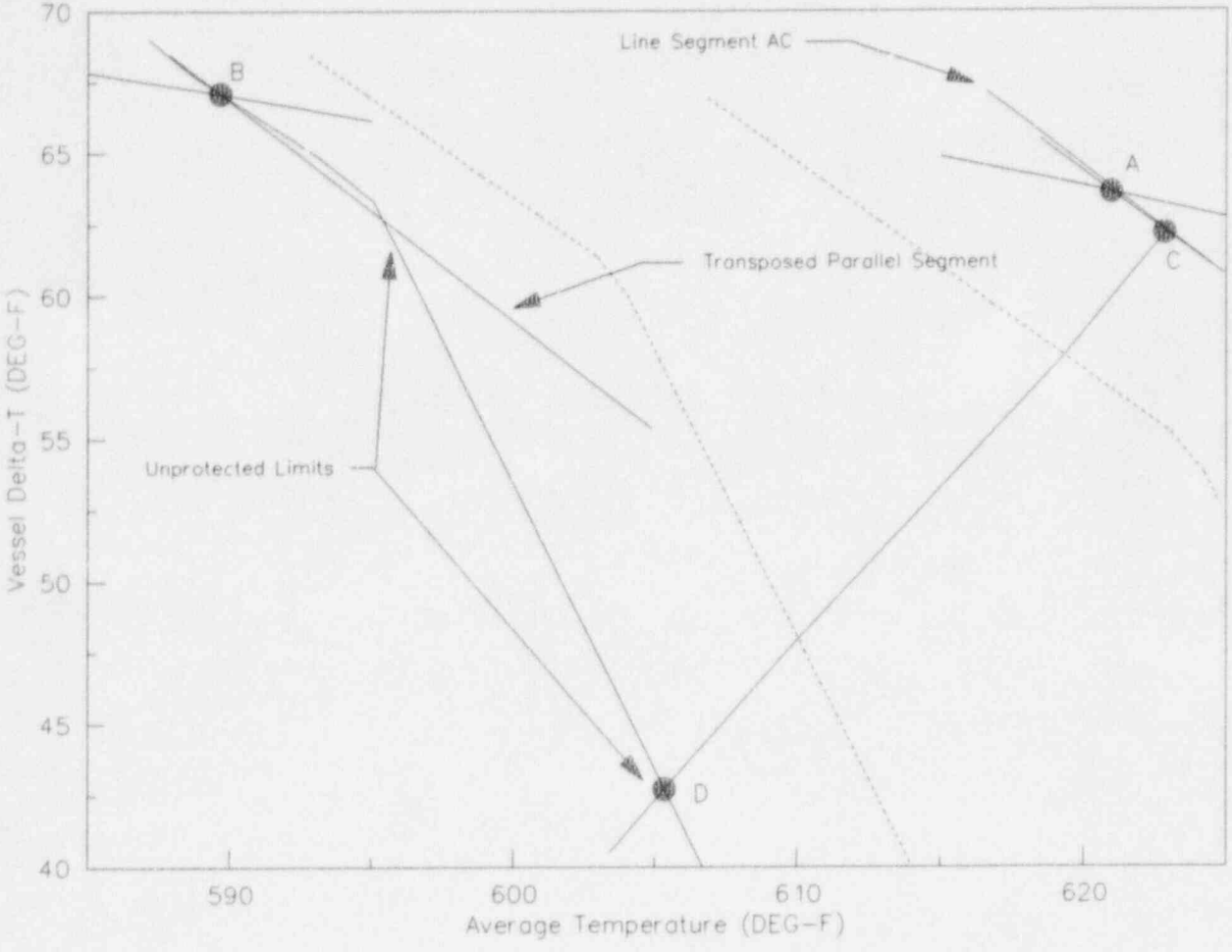

Figure 2-58 : Establishing OTΔT Coefficients - Restrictive Protection Function

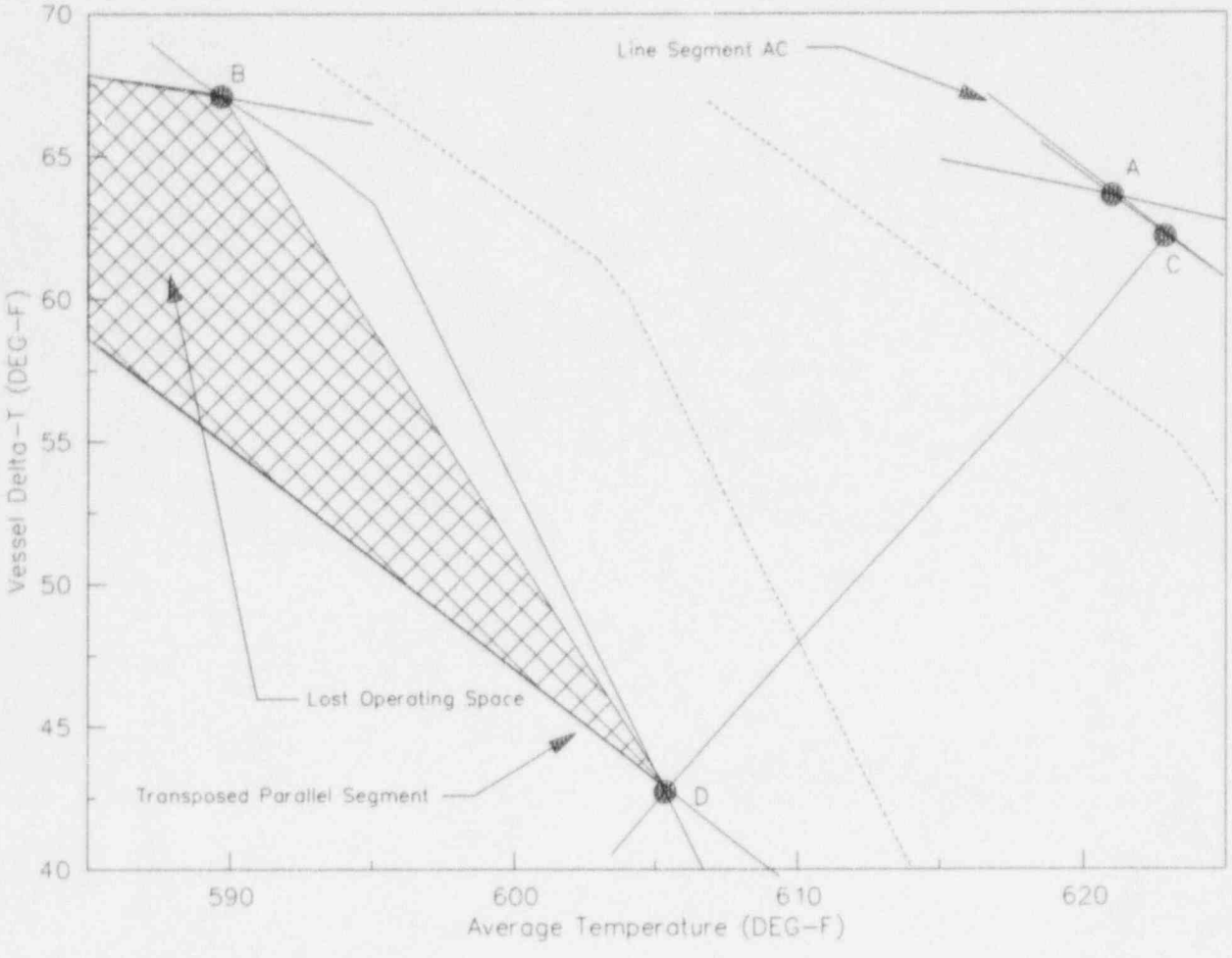

2.2.3.4.4 Compensation for Power Distributions

The core limits, generated with the 1.55 symmetric chopped cosine axial power distribution, form the basis from which the OPΔT and OTΔT trip functions are derived. Since both normal operations and anticipated transient events can result in power distributions which are not represented by the design distribution, compensation for potential off normal power distributions is built into the OPΔT and OTΔT trip functions. These power distribution compensation terms are referred to as the $f(\Delta I)$ functions.

It can be shown that two categories of accident or abnormal events are potentially limiting during an overpower event. These are transients related to control bank malfunctions and boration/dilution system malfunctions[49]. Utilizing static, one-dimensional core models, the response of the axial power profile during these limiting events for a large number of initial conditions and xenon distributions has been calculated. For each case examined, the nuclear peaking factor is determined according to the expression;

$$F_Q = \max\left[P_z(Z) * F_{XY}(Z) * S(Z)\right] * F_U^N * F_Q^E$$

Equation 2.49

Where, $P_Z(Z)$ = Core average axial power distribution.
$F_{XY}(Z)$ = Ratio of the peak power density to the average power density at elevation Z.
$S(Z)$ = Fuel densification spike factor.
F_U^N = Nuclear uncertainty factor.
F_Q^E = Engineering heat flux hot channel factor.

For each set of conditions examined, the maximum power density during the transient is defined as;

Maximum Power (kW/ft) = Average Power Density (kW/ft) * F_Q * Power

A typical representation of the results for the control bank malfunction analysis is shown in Figure 2-59. Typical results from the boration/dilution event analysis is provided in Figure 2-60.

After extensive analysis of these type of events, it was determined that;

1. The 118% overpower limit used to establish the OPΔT setpoint is sufficient to prevent centerline fuel melt.
2. The $f_2(\Delta I)$ function in the OPΔT equation is not required. Even without the $f_2(\Delta I)$ compensation term, the maximum linear heat rate is significant less than the 22.5 kW/ft melt limit. This assumption is confirmed on a cycle specific basis during the RAOC analysis.

Effects of variations in the axial power distribution on protection of the DNB portions of the core thermal limits are compensated for by the $f_1(\Delta I)$ function applied to the OTΔT trip equation.

The design criteria for the $f_1(\Delta I)$ function is identical to that given for protection of the DNB limit lines. That is, the $f_1(\Delta I)$ function must adjust the OTΔT trip setpoint so that no axial power distribution can result in a DNB ratio which is less than the safety analysis limit.

To generate the $f_1(\Delta I)$ function, a set of reference axial power distributions are used. It is assumed, and later confirmed, that these reference distributions still bound any actual axial power distribution which may exist at the core limits during cycle operation. These reference axial power shapes, shown in Figure 2-61 through Figure 2-65, represent a bounding envelope of axial offsets which historically have provided a limiting relationship between axial offset and allowable power. The validity of this assumption is confirmed on a cycle specific basis by a DNB power shape verification analysis. This verification analysis is discussed in section 2.2.4 later in this evaluation. The core designer is not restricted to using only the reference power shapes. Any set of shapes may be used to establish the DNB axial offset limits as long as the resulting limits are confirmed as part of the DNB power shape verification.

b

Figure 2-59 : OPΔT - Linear Heat Rates Vs. ΔI for Typical Control Bank Malfunctions

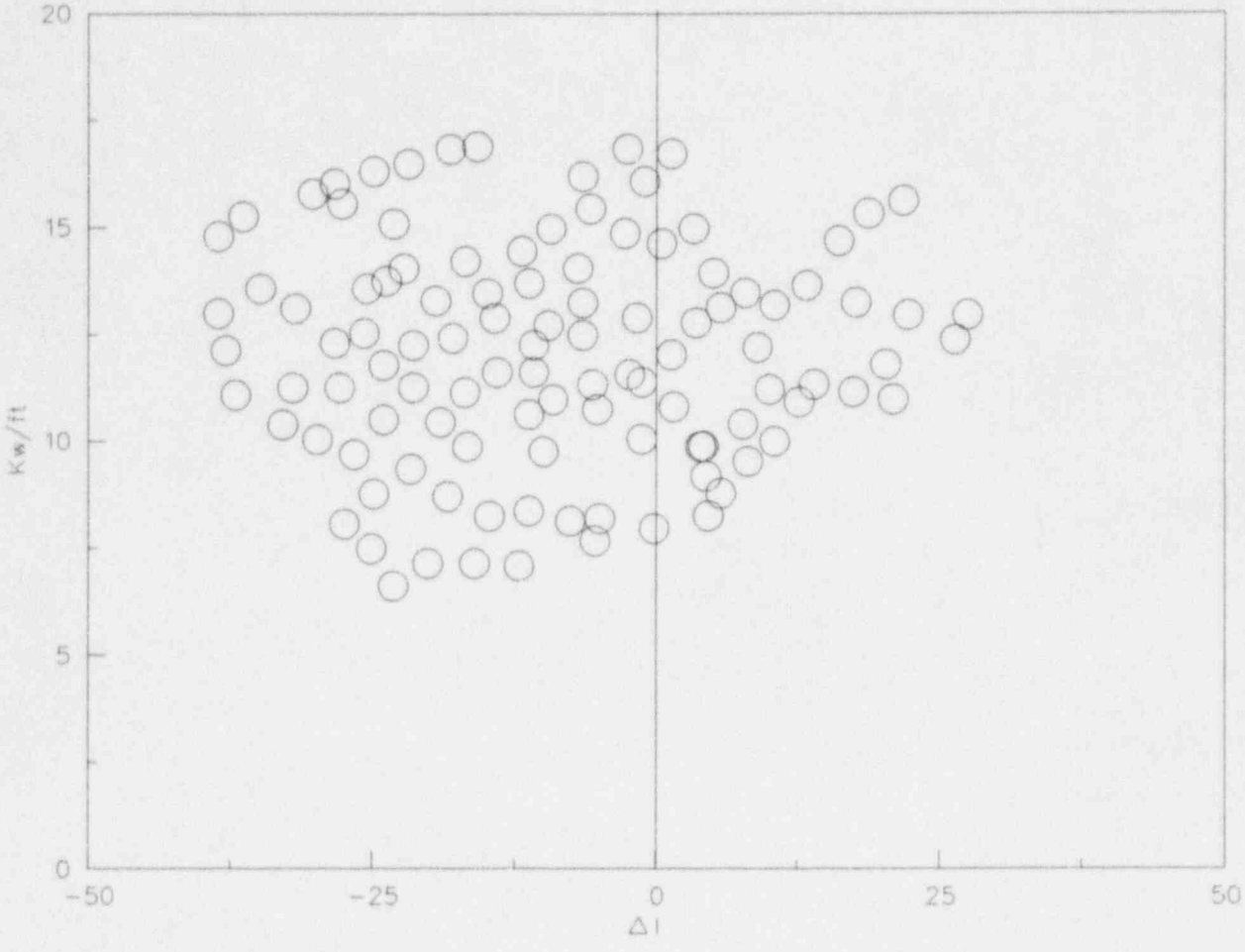

Figure 2-60 : OPΔT - Linear Heat Rate Vs. ΔI for Boration/Dilution Events

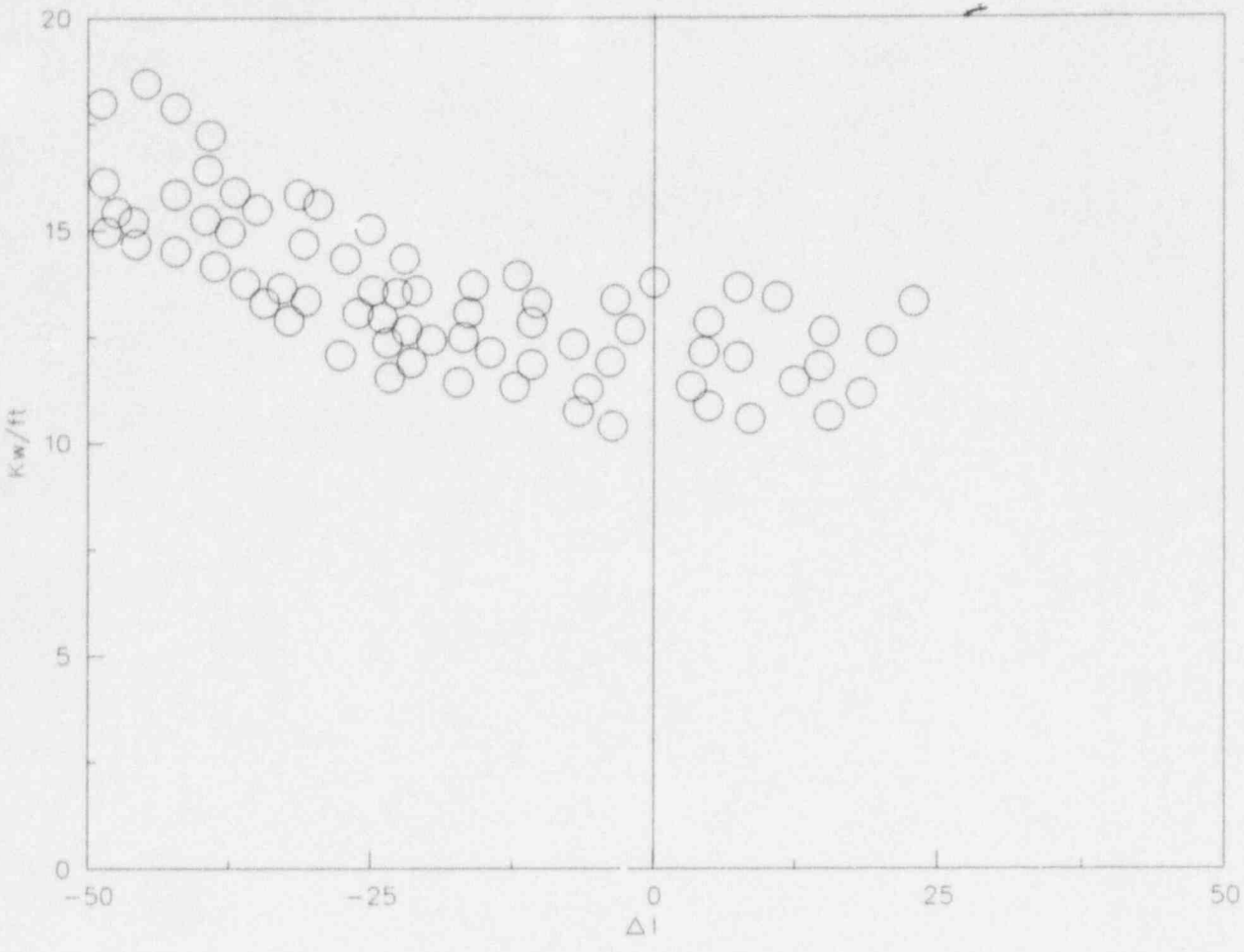

Figure 2-61 : Shape 1803 (Core Axial Offset = -27.9%)

b

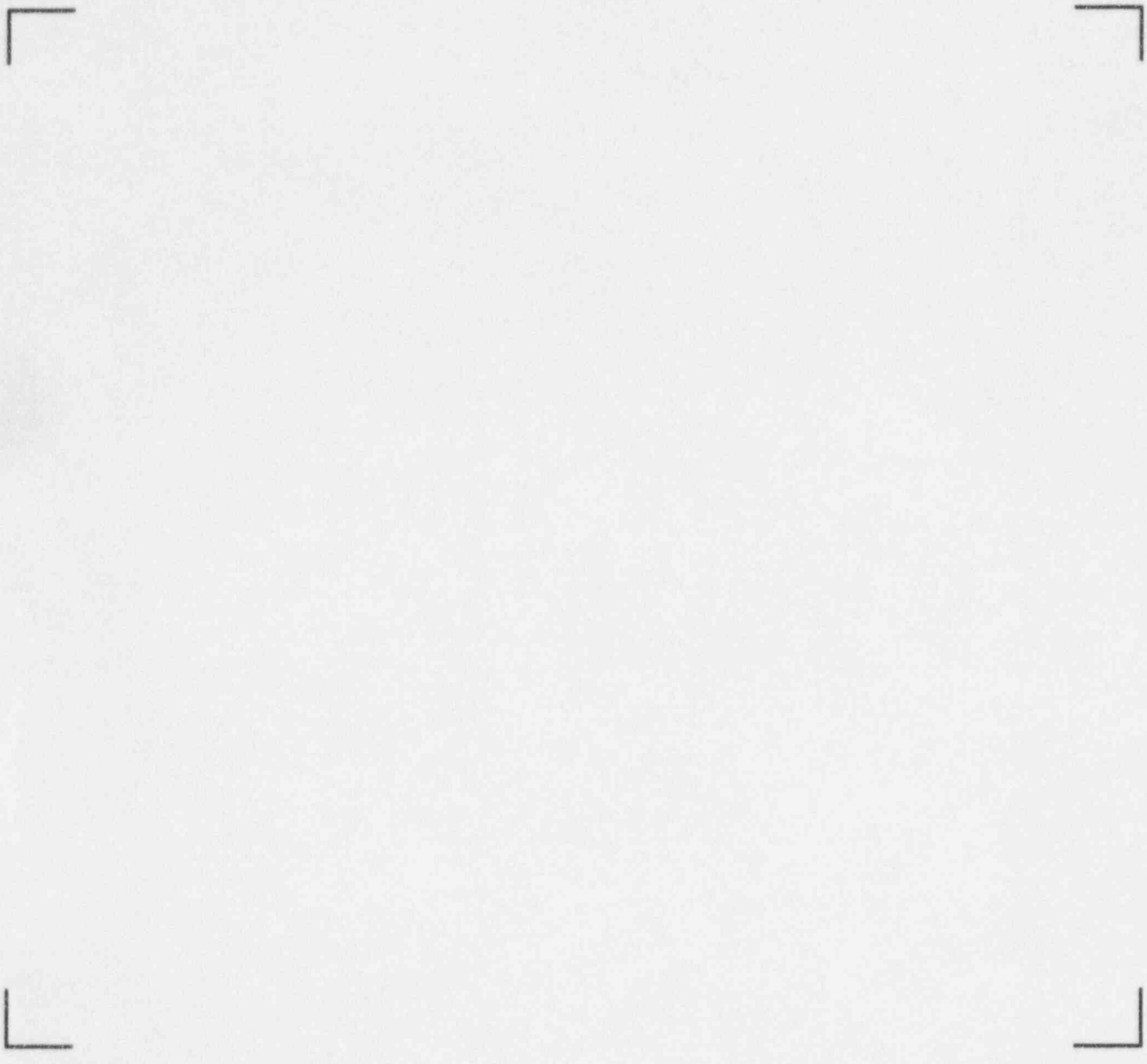

Figure 2-62 : Shape 1803A (Core Axial Offset = -22.5%)

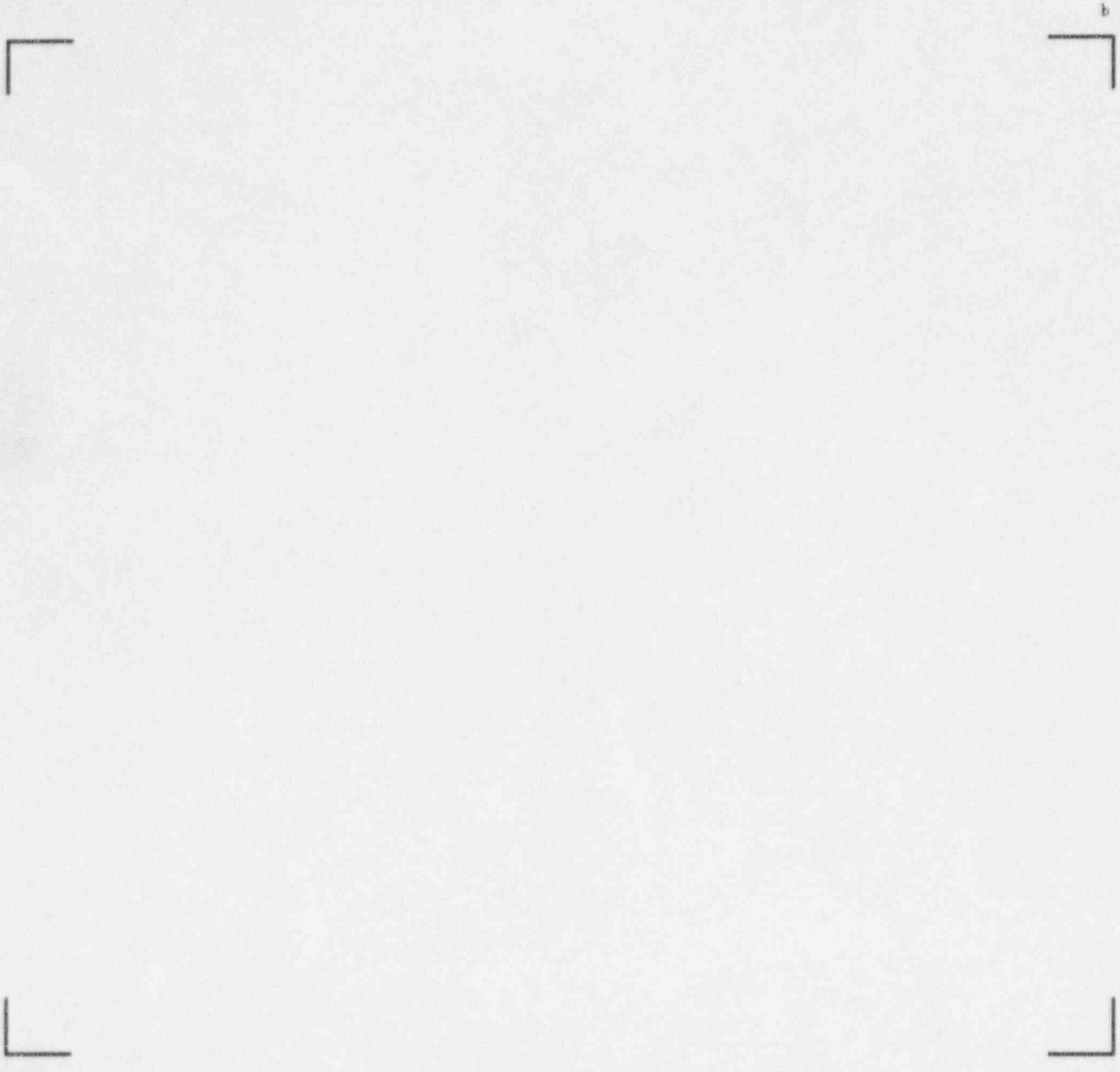

Figure 2-63 : Shape 1959 (Core Axial Offset = -2.4%)

b

Figure 2-64 : Shape MB (Core Axial Offset = -2.71%)

b

Figure 2-65 : Shape EA (Core Axial Offset = +25.2%)

b

Figure 2-66 : Typical DNB Axial Offset Limits

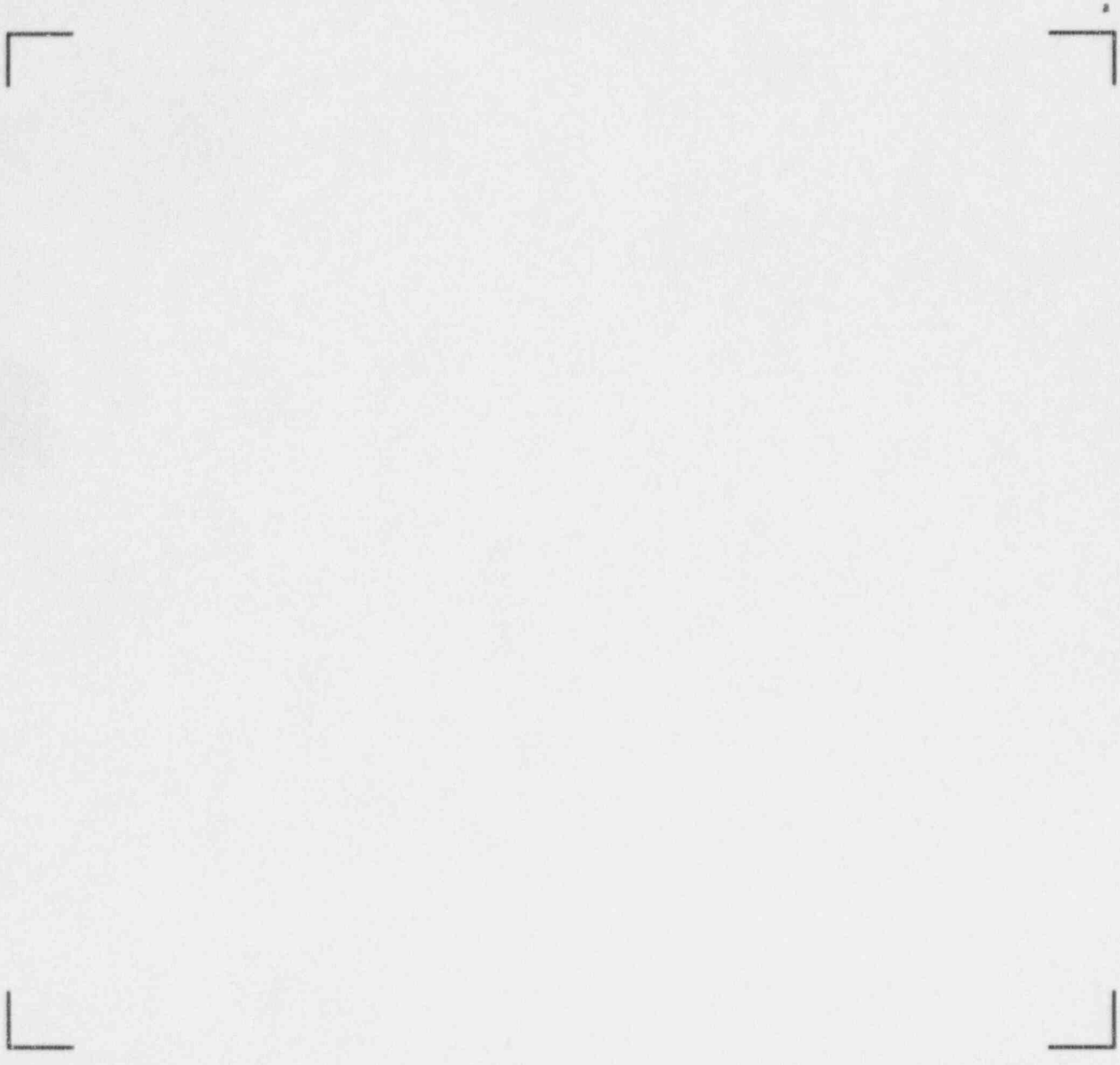

Figure 2-67 : Determination of $f_1(\Delta I)$ Reset Function

b

Figure 2-68 : $f_1(\Delta I)$ Reset Function

b

2.2.4 DNB Power Shape Verification

The axial power distributions which occur in the core are the result of many different factors. The operation of a previous cycle, the loading pattern of the current cycle, the core control strategy, and control rod pattern and rod insertion limits impact the axial power distribution. For this reason, verification that the reference shapes used to establish the DNB axial offset limits bound the actual shapes which might occur on a cycle specific basis.

The current core control strategy for the WCG Station is Relaxed Axial Offset Control (RAOC). The RAOC power shapes verification process fall into two categories:

1. The power of inlet temperature versus axial offset envelope defined by the reference power shapes must bound all power shapes which could occur at the core limits at any point during a cycle. These shapes are referred to as accident shapes or the Condition II shapes.

2. The reference axial power shape used in the DNB analysis of the limiting accident initiated from full-power normal operation, and that does not trip on OTΔT, must bound all expected full-power normal operation shapes. These shapes are referred to as the Condition I shapes. For transients in the category of Westinghouse V5H with IFMs fuel design with the WRB-2 critical heat flux correlation, WCNOC will use the axial power shape shown in Figure 2-69 as the reference shape for DNB analysis.

Section 2.1.3 presented a detailed discussion of the nuclear calculations performed in the RAOC procedure. Summarized, the RAOC procedure is;

b

Verification of the normal operation shapes is performed at the limiting condition, with respect to DNBR, from the most limiting transient which does not trip on OTΔT. Typically, this statepoint

is taken from the complete loss of flow transient. The minimum DNBR for each of the Condition I shapes is calculated and compared to the DNB results obtained with the reference shape. Typical results from Condition I shape verification are shown in Figure 2-70. The solid line in the figure represents the minimum DNBR obtained with the reference power shape at the limiting thermal condition which defines the Condition I power shape acceptance criteria.

Verification of the accident shapes is performed at 118% and 80% power at the same thermal conditions used to establish the DNB axial offset envelopes. For each accident shape generated by the Nuclear Design group, the allowable power level which yield the safety analysis limit DNBR is calculated and compared to the envelope of allowable power versus axial offset generated with the reference shapes (see Figure 2-71 and Figure 2-72). Any violations of the axial offset envelope must be resolved with the Nuclear Design group or by adopting more restrictive axial offset limits.

Figure 2-69 : WCAP-9500 Non-OTΔT Reference Power Shape (Axial Offset = +6.85%)

b

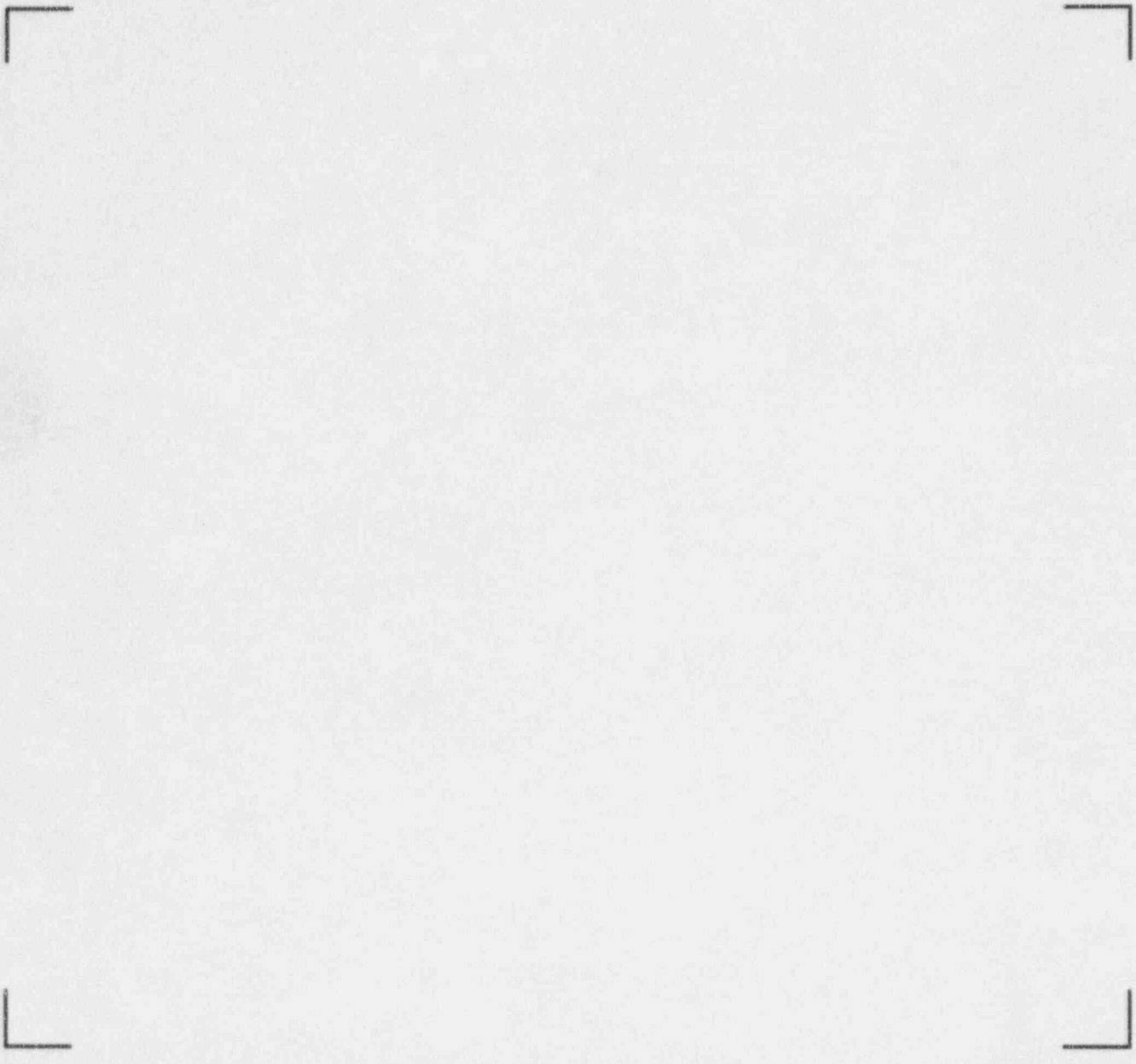

Figure 2-70 : Verification of Condition I Power Shapes

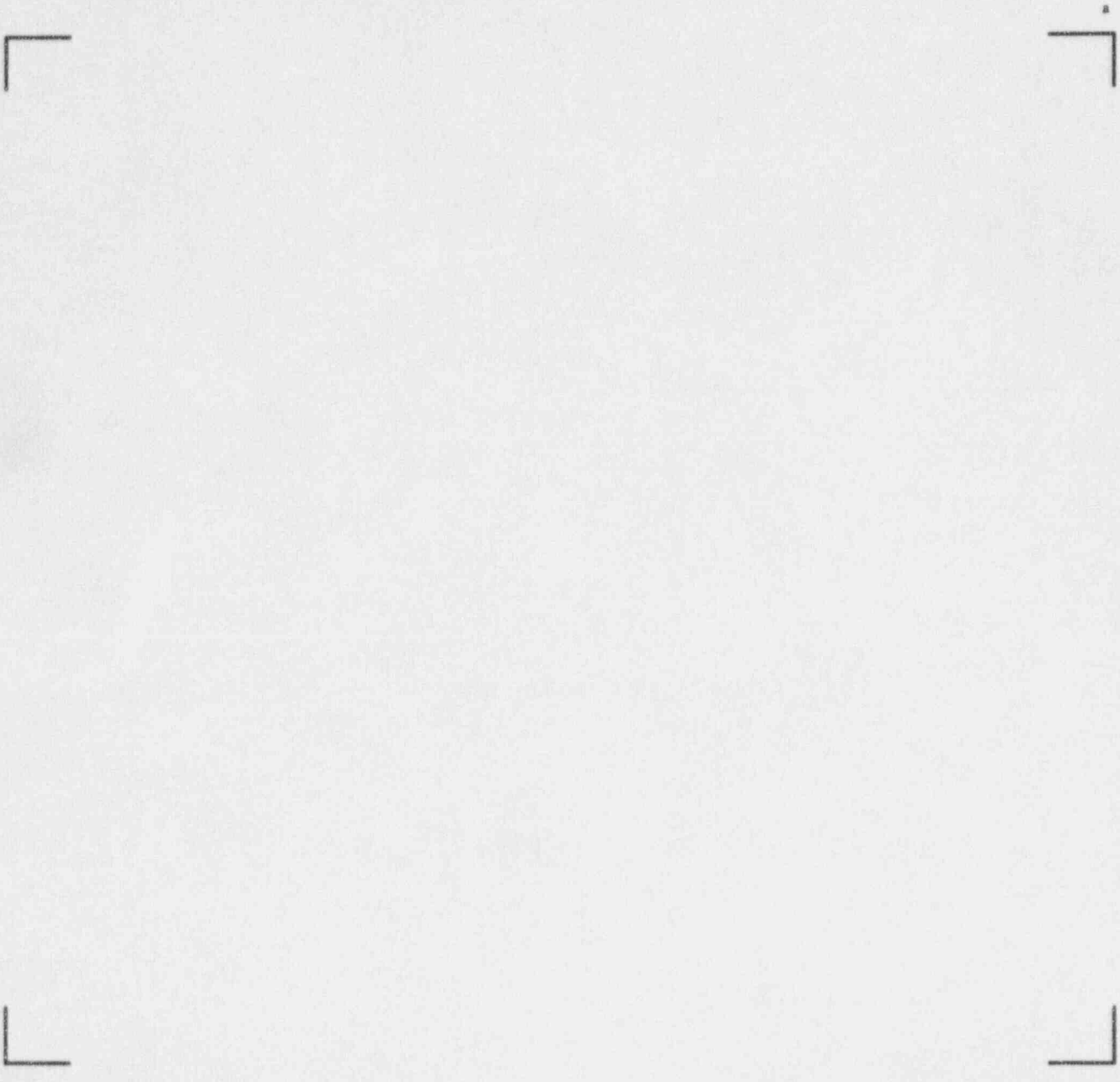

Figure 2-71 : Verification of Condition II Power Shapes - 118% Power Envelope

a

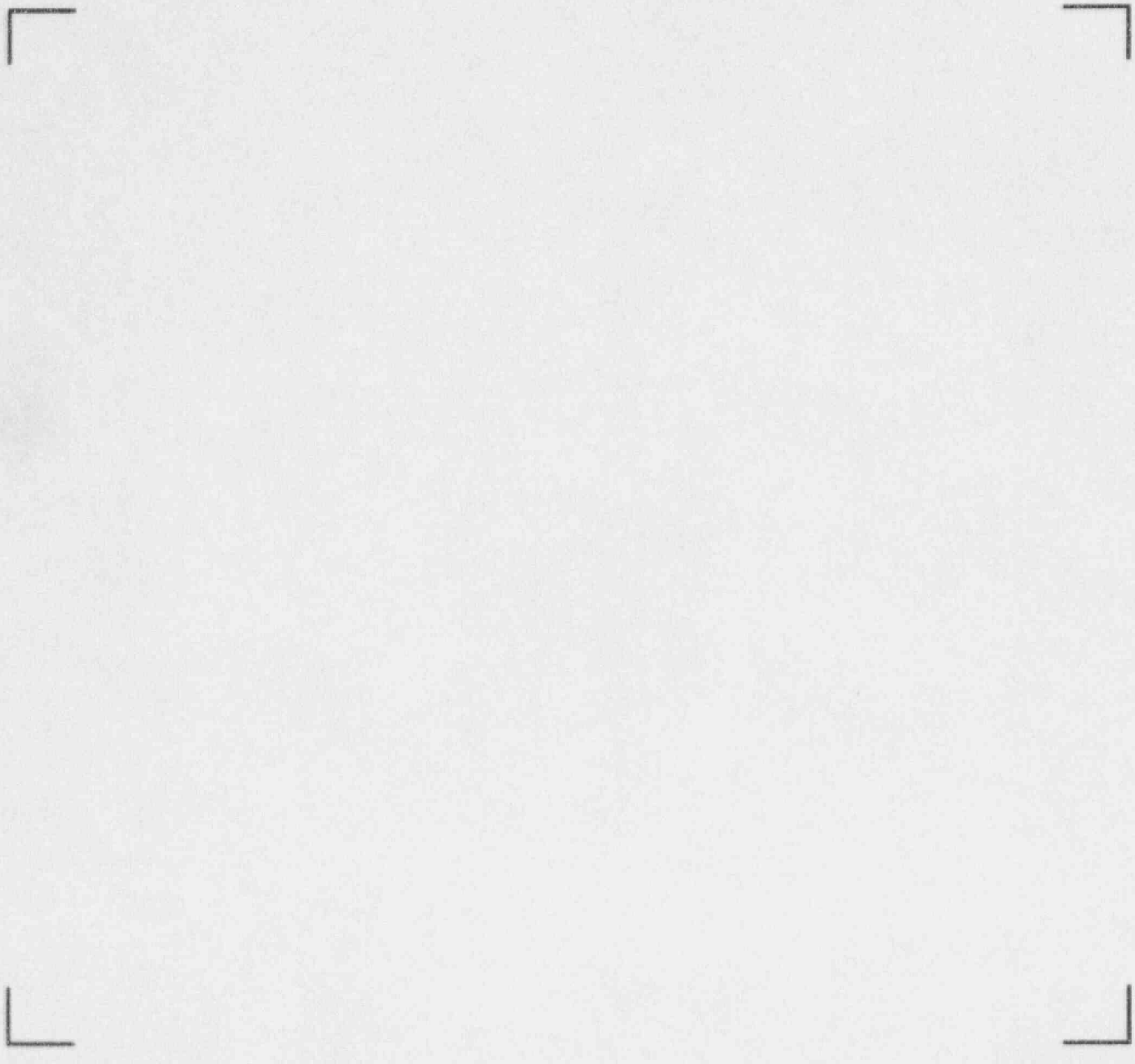

Figure 2-72 : Verification of Condition II Power Shapes - 80% Power Envelope

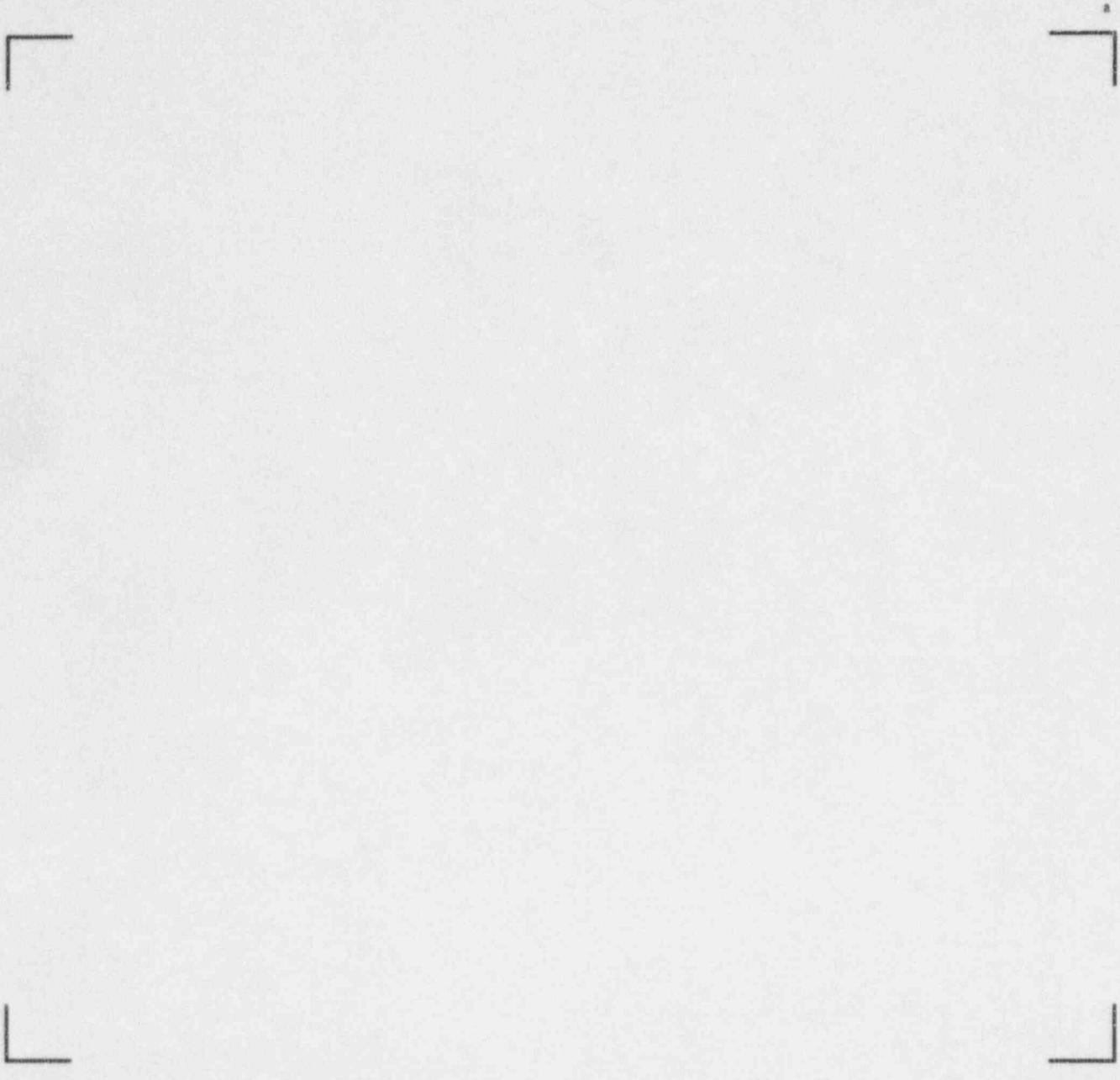

2.2.5 Reload Safety Analysis Integration

A reload design requires an examination of each accident and establishing the bounding values of the key safety parameters affected by the reload. The reference analysis for a given accident is an analysis performed for a previous cycle. Different accidents may be re-analyzed during different cycles. The bounding parameters from the reference safety analysis form the basis for evaluating the reload design. For each reload cycle, the bounding values from the reference analysis are compared to the parameter values for the reload design. If all key safety parameters for the reload cycle are found to be bounded by the parameter values used in the reference analysis, the reference analysis remains valid. However, should any key safety parameter from the reload core be determined to be out of bounds with respect to the reference analysis, a re-evaluation of the affected accident is performed.

The relationship of the core thermal-hydraulic design to the nuclear design has been detailed earlier in this evaluation. However, there are several other classes of analyses which are the responsibility of the Core Thermal-Hydraulic Design group. These include a core hydraulic compatibility evaluation, fuel rod design, and transient DNBR calculations. A summary of these analyses, their critical or limiting parameters, and integration of the core thermal-hydraulic design in the plant safety analysis is provided in the sections below. Both the classes of analyses performed, as well as the methods employed, are unchanged from those previously reviewed and approved.

2.2.5.1 Hydraulic Evaluation

The hydraulic evaluation of the reload core requires a review of the fuel assembly design (e.g., nozzles, grids, fuel rods, etc.) which is to be inserted into the core. The reload design is compared with the design of the resident fuel assemblies to be reinserted in the core. This comparison is made to ensure that the new fuel assemblies are hydraulically compatible with the fuel assemblies remaining in the core. In general, the reload fuel assembly design will be identical to the previous fuel assembly design. However, when changes in fuel assembly designs do occur, evaluations are performed to establish any transition core penalties required. The best estimate flow rate and mechanical design flow rate are considered in evaluating the core pressure drop and fuel assembly hydraulic load respectively. These evaluations are performed to verify the conservatism of the core pressure drop and hydraulic load upon which the fuel assembly hold down springs are designed.

2.2.5.2 Thermal and Hydraulic Key Safety Parameters

A list of thermal and hydraulic key safety parameters, along with their limiting direction, is given in Table 2-21. The core power, system pressure, inlet temperature, thermal design flow rate, and core bypass flow rate are defined during the design initialization phase of the reload design process. The design radial power distribution for steady state operation and design axial power shape are also defined during the initialization phase. These parameters are usually identical to the previous cycle design. The critical heat flux correlation to be used in DNB evaluations is also defined during the design initialization phase. Fuel density and sintering temperature are important to assess the effects of fuel densification. Changes in any of the above parameters identified during the design initialization phase are evaluated in the determination of the key safety parameters.

2.2.5.3 Fuel Temperatures

Fuel temperatures for safety analysis are computed for each first of a kind core design. Computed quantities include;

- Fuel centerline temperature versus kW/ft.
- Fuel average temperature versus kW/ft.
- Fuel surface temperature versus kW/ft.

Fuel temperatures are computed with approved fuel performance analysis codes and methods[50].

Fuel parameters for reload fuel are evaluated to determine if the temperatures that were computed for the reference analysis are applicable to the current reload. Fuel parameters of interest are pellet density, pellet sintering temperature, helium backfill pressure, and fuel pellet and rod dimensions. Generally, the fuel dimensions are identical to the fuel design remaining in the core. When the reference analysis is not applicable, a new fuel temperature analysis is performed.

2.2.5.4 Rod Internal Gas Pressure

The rod internal gas pressure of the lead rod in a reactor is limited to a value below that which could cause either the diametrical gap to increase due to the outward cladding creep during steady state operation or extensive DNB propagation to occur. This precludes the outward clad creep rate from exceeding the fuel solid swelling rate, ensuring that the fuel/clad diametrical gap will not reopen following contact or increase in size during steady state operation. Restricting the fuel/clad gap from opening prevents accelerated fission gas release at high burnup and precludes high burnup fuel from becoming limiting from a LOCA standpoint. Analysis has shown that this limitation satisfies the DNBR propagation design criteria[51].

2.2.5.5 Key Safety Parameters for Specific Events

This section discusses the DNB analysis for specific events. The method of analysis used in the reload evaluation of specific events may be used instead of using the traditional method of statistical approach to DNB analysis as previously described.

The DNB analysis of the loss of flow accident considers the parameters listed in Table 2-22, as well as the time dependent heat flux and flow variations. The design radial power distribution is utilized, in conjunction with a conservative outlet peaked axial power distribution, in a transient VIPRE-01 analysis to confirm that the DNB design basis is met for this event.

The VIPRE-01 code is used to perform a DNB analysis of the locked rotor event to establish the number of rods which may experience departure from nucleate boiling. The parameters listed in Table 2-22, the design radial power distribution, and a conservative outlet peaked axial power distribution are considered in the analysis. The number of pins in DNB analysis is established by determination of the radial peaking factor, $F^N_{\Delta H}$, which yields the critical heat flux thermal design limit. A fuel census curve is then used to determine the percentage of pins in the core with rod powers greater than the $F^N_{\Delta H}$ limit.

The DNB analysis of the steam line break event is normally evaluated using a traditional DNB analysis methodology since the range of core state variables is typically outside the range of application for a statistical approach. The time dependence of the parameters listed in Table 2-22 is considered in the VIPRE-01 analysis of the steam line break event.

2.2.5.6 VIPRE-01 Computer Code

The VIPRE-01 core thermal-hydraulic analysis computer code predicts the three-dimensional velocity, pressure, and thermal energy fields and fuel rod temperatures for single and two-phase flow in pressurized water reactor cores. The code uses a finite-difference formulation of the equations for mass, energy, and momentum conservation for an interconnected array of channels. VIPRE-01 solves the system of equations making the assumption of an incompressible, thermally expandable, homogeneous flow medium. The code has no time step or channel size restrictions for stability. While the formulation of the system is homogeneous, empirical models are included to account for the effects of subcooled boiling and phase slip in two-phase flow. VIPRE-01 may be used for both steady state and transient analyses[52].

The VIPRE-01 modeling structure is based on subchannel analysis. The core, or a section of symmetry, is defined as an array of parallel flow channels with lateral connections between adjacent channels. The shape and size of the channels and their interconnections are essentially arbitrary. Extensive sensitivity studies have been performed by WCNOC to insure that the methodology used to model the core yields a limiting thermal-hydraulic environment.

Table 2-21 : Core Thermal-Hydraulic Key Safety Parameters

Parameter	Limiting Direction
Engineering Hot Channel Factors	Maximum
Fuel Temperature	Maximum
Rod Internal Pressure	Maximum
Axial Fuel Stack Shrinkage	Maximum
Core DNB Limits	Minimum
Number of Rods in DNB	Maximum

Table 2-22 : Significant DNB Parameters

Parameter	Limiting Direction
Core Power	Maximum
System Pressure	Minimum
Core Inlet Enthalpy	Maximum
Flow Rate	Minimum
Core Bypass Flow	Maximum
Radial Power Distribution, $F_{\Delta H}^{N}$	Maximum
Axial Power Distribution, F_Z	Maximum
Engineering Hot Channel Factors, F_Q^E , $F_{\Delta H}^E$	Maximum
Axial Stack Height Factor	Maximum

3. Technical Specification Changes

This section contains revisions to the affected Technical Specifications. Included are changes to Technical Specification 3/4.2.2 Heat Flux Hot Channel Factor - F_Q, Technical Specification 3/4.2.3 Nuclear Enthalpy Rise Hot Channel Factor - $F_{\Delta H}^N$, Technical Specification 6.9.1.9 - Core Operating Limits Report (COLR), and changes for the BASES for the affected Specifications.

3.1 Section 3/4.2.2 : F_Q

POWER DISTRIBUTION LIMITS

3/4.2.2 HEAT FLUX HOT CHANNEL FACTOR - $F_Q(Z)$

LIMITING CONDITION FOR OPERATION

3.2.2 $F_Q(Z)$ shall be limited by the following relationships:

$$F_Q(Z) \leq \frac{\left[F_Q^{RTP}\right]\left[K(Z)\right]}{\left[P\right]} \quad \text{for } P > 0.5, \text{ and}$$

$$F_Q(Z) \leq \frac{\left[F_Q^{RTP}\right]\left[K(Z)\right]}{\left[0.5\right]} \quad \text{for } P \leq 0.5.$$

Where:

F_Q^{RTP} = the $F_Q(Z)$ Limit at RATED THERMAL POWER (RTP), as specified in the CORE OPERATING LIMITS REPORT (COLR),

$P = \frac{\text{THERMAL POWER}}{\text{RATED THERMAL POWER}}$, and

$K(Z)$ = the normalized $F_Q(Z)$ limit as a function of core height, as specified in the COLR.

APPLICABILITY: MODE 1.

ACTION:

With $F_Q(Z)$ exceeding its limit:

a. Reduce THERMAL POWER at least 1% for each 1% $F_Q(Z)$ exceeds the limit within 15 minutes and similarly reduce the Power Range Neutron Flux-High Trip Setpoints within the next 8 hours; POWER OPERATION may proceed for up to a total of 72 hours; subsequent POWER OPERATION may proceed provided the Overpower ΔT Trip Setpoints have been reduced at least 1% for each 1% $F_Q(Z)$ exceeds the limit; and

b. Identify and correct the cause of the out-of-limit condition prior to increasing THERMAL POWER above the reduced limit required by ACTION a., above; THERMAL POWER may then be increased provided $F_Q(Z)$ is demonstrated through incore mapping to be within its limit.

POWER DISTRIBUTION LIMITS

SURVEILLANCE REQUIREMENTS

4.2.2.1 The provisions of Specification 4.0.4 are not applicable.

4.2.2.2 $F_Q(Z)$ shall be evaluated to determine if $F_Q(Z)$ is within its limit by:

a. Using the movable incore detectors to obtain a power distribution map at any THERMAL POWER greater than 5% of RATED THERMAL POWER;

b. Increasing the measured $F_Q(Z)$ component of the power distribution map by 3 % to account for manufacturing tolerances and further increasing the value by 5 % to account for measurement uncertainties. Verify that the requirements of Specification 3.3.2 are satisfied.

c. Satisfying the following relationship:

$$F_Q^M(Z) \leq \frac{\left[F_Q^{RTP}\right]\left[K(Z)\right]}{\left[P\right]\left[W(Z)\right]} \quad \text{for } P > 0.5$$

$$F_Q^M(Z) \leq \frac{\left[F_Q^{RTP}\right]\left[K(Z)\right]}{\left[W(Z)\right]\left[0.5\right]} \quad \text{for } P \leq 0.5$$

where $F_Q^M(Z)$ is the measured $F_Q(Z)$ increased by the allowances for manufacturing tolerances and measurement uncertainty, and W(Z) is the cycle dependent function that accounts for power distribution transients encountered during normal operation. This function is provided in the COLR.

d. Measuring $F_Q^M(Z)$ according to the following schedule:

1. Upon achieving equilibrium conditions after exceeding, by 10% or more of RATED THERMAL POWER, the THERMAL POWER at which $F_Q(Z)$ was last determined,* or

2. At least once per 31 Effective Full Power Days, whichever occurs first.

*During power escalation at the beginning of each cycle, THERMAL POWER may be increased until a power level for extended operation has been achieved after which a power distribution map will be obtained.

POWER DISTRIBUTION LIMITS

SURVEILLANCE REQUIREMENTS (Cont.)

e. With measurements indicating

$$\underset{\text{over z}}{\text{maximum}} \left(\frac{F_Q^M(Z)}{K(Z)} \right)$$

has increased since the previous determination of $F_Q^M(Z)$ either of the following actions shall be taken:

1. $F_Q^M(Z)$ shall be increased over that specified in 4.2.2.2 c. by an appropriate factor specified in the COLR, or

2. $F_Q^M(Z)$ shall be measured at least once per 7 Effective Full Power Days until two successive maps indicate that

$$\underset{\text{over z}}{\text{maximum}} \left(\frac{F_Q^M(Z)}{K(Z)} \right)$$ is not increasing.

f. With the relationships specified in 4.2.2.2 c. above not being satisfied:

1. Calculate the percent $F_Q^M(Z)$ exceeds its limit by the following expression:

$$\left\{ \left(\text{maximum} \left[\frac{F_Q^M(Z) \text{ X } W(Z)}{\frac{F_Q^{RTP}}{P} \text{ X } K(Z)} \right] \right) - 1 \right\} \text{ X } 100 \quad \text{for } P \geq 0.5$$

$$\left\{ \left(\text{maximum} \left[\frac{F_Q^M(Z) \text{ X } W(Z)}{\frac{F_Q^{RTP}}{0.5} \text{ X } K(Z)} \right] \right) - 1 \right\} \text{ X } 100 \quad \text{for } P < 0.5$$

2. Either one of the following actions shall be taken:

a. Within 2 hours, control the AFD to within new AFD limits which are determined by tightening both the negative and positive AFD limits of Specification 3.2.1 by 1% AFD for each percent $F_Q^M(Z)$ exceeds its limit and declare the AFD monitor alarm inoperable until the AFD alarm setpoints are changed to the modified limits, or

b. Comply with the requirements of Specification 3.2.2 for $F_Q(Z)$ exceeding its limit by the percent calculated above

g. The limits in Specification 4.2.2.2 c., 4.2.2.2 e. and 4.2.2.2 f. are not applicable in the following core plane regions as measured in percent of core height from the bottom of the fuel:

1. Lower core region from 0 to 15%, inclusive,

2. Upper core region from 85 to 100%, inclusive.

3.2 Section 3/4.2.3 $F_{\Delta H}$

POWER DISTRIBUTION LIMITS

3/4.2.3 NUCLEAR ENTHALPY RISE HOT CHANNEL FACTOR - $F^N_{\Delta H}$

LIMITING CONDITION FOR OPERATION

3.2.3 $F^N_{\Delta H}$ shall be limited by the following relationship:

$$F^N_{\Delta H} \leq F^{RTP}_{\Delta H} [1.0 + PF_{\Delta H} (1.0 - P)]$$

Where,

$F^{RTP}_{\Delta H}$ = The $F^N_{\Delta H}$ limit at RATED THERMAL POWER (RTP) specified in the CORE OPERATING LIMITS REPORT (COLR),

$PF_{\Delta H}$ = the power factor multiplier for $F^N_{\Delta H}$ specified in the COLR, and

$$P = \frac{\text{THERMAL POWER}}{\text{RATED THERMAL POWER}}$$

$F^N_{\Delta H}$ = Measured values of $F^N_{\Delta H}$ obtained by using the movable incore detectors to obtain a power distribution map. The measured values of $F^N_{\Delta H}$ shall be used since an uncertainty of 4% for incore measurement of $F^N_{\Delta H}$ has been included in the above limit.

APPLICABILITY: MODE 1.

ACTION:

With $F^N_{\Delta H}$ exceeding its limit:

a. Within 4 hours either:

1. Restore $F^N_{\Delta H}$ to within the above limit, or

2. Reduce THERMAL POWER to less than 50% of RATED THERMAL POWER and reduce the Power Range Neutron Flux - High Trip Setpoint to less than or equal to 55% of RATED THERMAL POWER within the next 4 hours.

b. Within 72 hours of initially being outside the above limit, verify through incore flux mapping that $F^N_{\Delta H}$ has been restored to within the above limit, or reduce THERMAL POWER to less than 5% of RATED THERMAL POWER within the next 6 hours.

c. Identify and correct the cause of the out-of-limit condition prior to increasing THERMAL POWER above the reduced limit required by Action a. or b., above; subsequent POWER OPERATION may proceed provided that $F^N_{\Delta H}$ is demonstrated through in-core flux mapping to be within its limit at a nominal 50% of RATED THERMAL POWER prior to exceeding this THERMAL POWER, at a nominal 75% of RATED THERMAL POWER prior to exceeding this

POWER DISTRIBUTION LIMITS

SURVEILLANCE REQUIREMENTS

THERMAL POWER and within 24 hours after attaining 95% or greater RATED THERMAL POWER.

4.2.3.1 $F^{N}_{\Delta H}$ shall be determined to be within its limit by using the movable incore detectors to obtain a power distribution map:

a. Prior to operation above 75% of RATED THERMAL POWER after each fuel loading, and

b. At least once per 31 Effective Full Power Days, and

c. The provisions of Specification 4.0.4 are not applicable.

3.3 Section 6.9.1.9 COLR

CORE OPERATING LIMITS REPORT (COLR)

6.9.1.9 Core operating limits shall be established and documented in the CORE OPERATING LIMITS REPORT (COLR) before each reload cycle or any remaining part of a reload cycle, for the following;

1. Specification 3.1.1.3: Moderator Temperature Coefficient (MTC) EOL limits.
2. Specification 3.1.3.5: Shutdown Rod Insertion Limit.
3. Specification 3.1.3.6: Control Rod Insertion Limits
4. Specification 3.2.1: Axial Flux Difference (AFD).
5. Specification 3.2.2: Heat Flux Hot Channel Factor - $F_Q(Z)$.
6. Specification 3.2.3: Nuclear Enthalpy Rise Hot Channel Factor - $F_{\Delta H}^N$.
7. Specification 3.9.1.b: Refueling Boron Concentration.

The analytical methods used to determine the core operating limits shall be those previously reviewed and approved by the NRC, specifically those described in the following documents.

a) NRC Safety Evaluation Report dated October 29, 1992 for the "Core Thermal Hydraulic Analysis Methodology for the Wolf Creek Generating Station" (ET-90-0140, ET 92-0103).

(Methodology for Specification 3.2.3 - Nuclear Enthalpy Rise Hot Channel Factor - $F_{\Delta H}^N$.

b) NRC Safety Evaluation Report dated January 17, 1989 for "Acceptance for Referencing of Licensing Topical Report WCAP-11397, Revised Thermal Design Procedure"

(Methodology for Specification 3.2.3 - Nuclear Enthalpy Rise Hot Channel Factor - $F_{\Delta H}^N$.

c) NRC Safety Evaluation Report dated September 30, 1993, for "Transient Analysis Methodology for the Wolf Creek Generating Station" (ET-91-0026, ET 92-0142, WM 93-0010, WM 93-0028).

(Methodology for Specification 3.1.1.3 - Moderator Temperature Coefficient [MTC]).

d) NRC Safety Evaluation Report dated November 26, 1993, "Acceptance for Referencing of Revised Version of Licensing Topical Report WCAP-10216-P-A, Relaxation of Constant Axial Offset Control - F_Q Surveillance Technical Specification" (TAC No. M88206).

(Methodology for Specification 3.2.2 - Heat Flux Hot Channel Factor - $F_Q(Z)$: Specification 3.1.1.3 _ Moderator Temperature Coefficient (MTC): Specification 3.1.3.5 - Shutdown Rod Insertion Limit: Specification 3.1.3.6 - Control Rod Insertion Limits: Specification 3.2.1 - Axial Flux Difference: Specification 3.2.3 Nuclear Enthalpy Rise Hot Channel Factor - $F_{\Delta H}^N$: Specification 3.9.1.b - Refueling Boron Concentration).

e) NRC Safety Evaluation Report dated March 10, 1993 for "Reload Safety Evaluation Methodology for the Wolf Creek Generating Station" (ET 92-0032, ET 93-0017).

(Methodology for Specification 3.1.3.6 - Control Rod Insertion Limits: Specification 3.2.1 - Axial Flux Difference).

f) NRC Safety Evaluation Report dated March 30, 1993 for "Revision to Technical Specifications for Cycle 7" (NA 92-0073, NA 93-0013, NA 93-0054).

(Methodology for Specification 3.2.3 - Nuclear Enthalpy Rise Hot Channel Factor - $F_{\Delta H}^N$ [Use of WRB-2 Correlation with VIPRE-01 code]).

g) NRC Safety Evaluation Report dated November 13, 1986 for "The 1981 Version of the Westinghouse ECCS Evaluation Model Using the BASH Code" (WCAP-10266-P-A, Rev. 2).

(Methodology for Specification 3.2.2 - Heat Flux Hot Channel Factor - $F_Q(Z)$).

h) NRC Safety Evaluation Report dated May 17, 1988, "Acceptance for Referencing of Westinghouse Topical Report WCAP-11596 - Qualification of the Phoenix-P/ANC Nuclear Design System for Pressurized Water Reactor Cores"

(Methodology for Specification 3.2.2 - Heat Flux Hot Channel Factor - $F_Q(Z)$: Specification 3.1.1.3 - Moderator Temperature Coefficient (MTC): Specification 3.1.3.5 - Shutdown Rod Insertion Limit: Specification 3.1.3.6 - Control Rod Insertion Limits: Specification 3.2.1 - Axial Flux Difference: Specification 3.2.3 Nuclear Enthalpy Rise Hot Channel Factor - $F_{\Delta H}^N$: Specification 3.9.1.b - Refueling Boron Concentration).

i) NRC Safety Evaluation Report dated June 23, 1986, "Acceptance for Referencing of Topical Report WCAP-10965-P and WCAP 10966-NP- ANC: A Westinghouse Advanced Nodal Computer Code"

(Methodology for Specification 3.2.2 - Heat Flux Hot Channel Factor - $F_Q(Z)$: Specification 3.1.1.3 - Moderator Temperature Coefficient (MTC): Specification 3.1.3.5 - Shutdown Rod Insertion Limit: Specification 3.1.3.6 - Control Rod Insertion Limits: Specification 3.2.1 - Axial Flux Difference: Specification 3.2.3 Nuclear Enthalpy Rise Hot Channel Factor - $F^N_{\Delta H}$: Specification 3.9.1.b - Refueling Boron Concentration).

3.4 Bases - Sections 3/4.2.2 and 3/4.2.3

The limits on heat flux hot channel factor and nuclear enthalpy rise hot channel factor insure that: (1) the design limits on peak local power density and minimum DNBR are not exceeded, and (2) in the event of a LOCA the peak fuel clad temperature will not exceed the 2200 °F ECCS acceptance criteria limit.

Each of these is measurable but will normally only be determined periodically as specified in Specifications 4.2.2 and 4.2.3. This periodic surveillance is sufficient to insure that the limits are maintained provided:

a) Control rods in a single group move together with no individual rod insertion differing by more that ± 12 steps, indicated, from the group demand position.
b) Control rod groups are sequenced with overlapping groups as described in Specification 3.1.3.6.
c) The control rod insertion limits of Specification 3.1.3.6 are maintained.
d) The axial power distribution, expressed in terms of AXIAL FLUX DIFFERENCE, is maintained within the limits.

$F^N_{\Delta H}$ will be maintained within its limits provided Conditions a) through d) above are maintained. The limits on the nuclear enthalpy rise hot channel factor, $F^N_{\Delta H}$, are specified in the COLR.

$F_Q(Z)$ and $F^N_{\Delta H}$ are measured periodically to provide assurance that they remain within their limits. A peaking margin calculation is performed, when necessary, to provide the basis for reducing THERMAL POWER or for reducing the width of the AFD limits. The hot channel factor $F^M_Q(Z)$ is measured periodically and increased by a cycle and height dependent factor, W(Z), to provide assurance that that the limit on $F_Q(Z)$ is met. W(Z) accounts for the effects of normal operation transients and is determined from expected power control maneuvers over the full range of burnup conditions in the core. The W(Z) functions are specified in the Core Operating Limits Report.

4. References

1 NUREG-1136, "Technical Specifications for Wolf Creek Generating Station, Unit No. 1," Docket STN 50-482, issued by the USNRC, Amendment 83, dated January 1995.

2 Letter from Reckley, W. D. (USNRC) to Withers, B. D. (WCNOC) dated March 26, 1993, submitting the Safety Evaluation on the Wolf Creek Nuclear Operating Corporation - Steady State Core Physics Methodology Topical Report (TAC NO. M82619).

3 Liu, Y. S., et al, "ANC: A Westinghouse Advanced Nodal Computer Code," WCAP-10965-P-A (Proprietary), December 1985.

4 Nguyen, T. W., et al, "Qualification of the PHOENIX-P / ANC Nuclear Design System for Pressurized Water Reactor Cores," WCAP-11596-P-A (Proprietary), November 1987.

5 Miller, R. W. et al., "Relaxation of Constant Axial Offset Control - F_Q Surveillance Technical Specification," WCAP-10216-P-A Revision 1A, approved version dated February 1994.

6 VIPRE-01, Mod 1, "VIPRE-01: A Thermal-Hydraulic Code for Reactor Cores," Volumes 1 through 7, NP-2511-CCM-A, Electric Power Research Institute, Palo Alto, CA.

7 Letter from Rossi, C. E. (USNRC) to Blaisdell, J. A. (UGRA), "Acceptance for Referencing of Licensing Topical Report, EPRI NP-2511-CCM, VIPRE-01: A Thermal-Hydraulic Analysis Code for Reactor Cores, Volumes 1, 2, 3, and 4," dated May 1, 1986.

8 Letter from Reckley, W. D. (USNRC) to Withers, B. D. (WCNOC), "Wolf Creek Nuclear Operating Corporation - Core Thermal-Hydraulic Analysis Methodology (TAC No. M77608)," dated October 29, 1992.

9 Kennamore, W. S. (WCNOC), Neises, G. J. (WCNOC), and Garrett, T. J. (WCNOC), "Wolf Creek Nuclear Operating Corporation : Core Thermal-Hydraulic Analysis Methodology for the Wolf Creek Generating Station," TR-90-0025 W01, dated July 1990.

10 Davidson, S. L. (Westinghouse -Editor), "Vantage 5H Fuel Assembly," WCAP-10444-A, Addendum 2-A, dated April 1988.

11 Kennamore, W. S. (WCNOC), Neises, G. J. (WCNOC), and Garrett, T. J. (WCNOC), "Wolf Creek Nuclear Operating Corporation : Core Thermal-Hydraulic Analysis Methodology for the Wolf Creek Generating Station," TR-90-0025 W01, dated July 1990, section 3.3.1.

12 Letter from Reckley, W. D. (USNRC) to Carns, N. S. (WCNOC), "Wolf Creek Generating Station - Amendment No. 69 to Facility Operating License No NPF-42," (TAC No. M85311) dated November 10, 1993.

13 Farnsworth, D. A. and Meyer, G. A., "Statistical Core Design for Mixing Vane Cores," BAW-10170P, Babcock & Wilcox Company, Lynchburg, Virginia, 1987.

14 Friedlan, A. J. (Westinghouse), "Revised Thermal Design Procedure (RTDP)," Revision 2, April 1992, Thermal-Hydarulic Engineering Services Manual, TR-90-0023 W08.

15 VIPRE-01, Mod 1, "VIPRE-01: A Thermal-Hydraulic Code for Reactor Cores," Volumes 1 through 7, NP-2511-CCM-A, Electric Power Research Institute, Palo Alto, CA, Volume 5.

16 Ibid, Volume 5, page 3-3.

17 Ibid.

18 Kennamore, W. S. (WCNOC), Neises, G. J. (WCNOC), and Garrett, T. J. (WCNOC), "Wolf Creek Nuclear Operating Corporation : Core Thermal-Hydraulic Analysis Methodology for the Wolf Creek Generating Station," TR-90-0025 W01, dated July 1990, section 3.3.9.

19 VIPRE-01, Mod 1, "VIPRE-01: A Thermal-Hydraulic Code for Reactor Cores," Volumes 1 through 7, NP-2511-CCM-A, Electric Power Research Institute, Palo Alto, CA, Volume 5, page 3-4.

20 Ibid, Volume 5, page 3-10.

21 Ibid, page 3-13.

22 Kennamore, W. S. (WCNOC), Neises, G. J. (WCNOC), and Garrett, T. J. (WCNOC), "Wolf Creek Nuclear Operating Corporation : Core Thermal-Hydraulic Analysis Methodology for the Wolf Creek Generating Station," TR-90-0025 W01, dated July 1990, section 3.1.4.

23 VIPRE-01, Mod 1, "VIPRE-01: A Thermal-Hydraulic Code for Reactor Cores," Volumes 1 through 7, NP-2511-CCM-A, Electric Power Research Institute, Palo Alto, CA, Volume 5, page 3-70.

24 Ibid, Volume 2, page 2-174.

25 Ibid, Volume 4, page 8-30.

[26] Motley, F. E. (Westinghouse) et al, "New Westinghouse Correlation WRB-1 for Predicting Critical Heat Flux in Rod Bundles with Mixing Vane Grids," WCAP-8762-P-A, dated July 1984, Table 1.

[27] Davidson, S. L. (Westinghouse) and Kramer, W. R. (Westinghouse), "Reference Core Report - Vantage 5 Fuel Assembly," WCAP-10444-P-A, dated September 1985, Tables 10-1 and 10-2.

[28] Sung, Y. X. (Westinghouse), "THINC Analysis," Revision 3, dated December 1991, Thermal-Hydraulic Design Procedure Manual, TR-90-0022 W07 Volumne 1, page 1.6-8.

[29] Olson, C. A. (Westinghouse), "Hot Channel Factors," Revision 1, dated August 1991, Thermal-Hydraulic Design Procedure Manual, TR-90-0022 W07, Volumne 1, page 1.4-12.

[30] Kennamore, W. S. (WCNOC), Neises, G. J. (WCNOC), and Garrett, T. J. (WCNOC), "Wolf Creek Nuclear Operating Corporation : Core Thermal-Hydraulic Analysis Methodology for the Wolf Creek Generating Station," TR-90-0025 W01, dated July 1990.

[31] Davidson, S. L. (Westinghouse) and Kramer, W. R. (Westinghouse), "Reference Core Report - Vantage 5 Fuel Assembly," WCAP-10444-P-A, dated September 1985, Figure A-9.

[32] Office of Nuclear Reactor Regulation, Standard Review Plan, U. S. Nuclear Regulatory Commission, NUREG-0800, Revision 1, July 1981, page 15.1.1-3.

[33] Wheeler, C. L., et al., "COBRA-IV-I: An Interim Version of COBRA for Thermal-Hydraulic Analysis of Rod Bundle Nuclear Fuel Elements and Cores," BNWL-1962 UC-32, Battelle Pacific Northwest Laboratories, Richland, Washington, 1976.

[34] Stewart, C. W., et al., "VIPRE-01: A Thermal-Hydraulic Code for Reactor Cores," NP-2511-CCM Revision 2, Battelle Pacific Northwest Laboratories, Richland, Washington, 1985.

[35] Friedland, A. J. (Westinghouse) and Ray, S. (Westinghouse), "Revised Thermal Design Procedure," WCAP-11397-P-A, approved version dated April, 1988.

[36] Chelemer, H, Boman, L. H., and Sharp, D. R., "Improved Thermal Design Procedure," WCAP-8567-P-A, February, 1989.

[37] Friedland, A. J. (Westinghouse) and Ray, S (Westinghouse),. "Revised Thermal Design Procedure," WCAP-11397-P-A, April, 1989.

[38] Chelemer, H, Boman, L. H, and Sharp, D. R., "Improved Thermal Design Procedure," WCAP-8567, dated July, 1975.

[39] Friedland, A. J. (Westinghouse) and Ray, S. (Westinghouse), "Revised Thermal Design Procedure," WCAP-11397-P-A, dated April, 1989.

[40] Freidland, A. J. (Westinghouse), "Revised Thermal Design Procedure," Revision 2, dated April, 1992, Thermal-Hydraulic Engineering Services Manual, TR-90-0023 W08, section 4.3.4.

[41] Owen, D. B., "Factors for One-Sided Tolerance Limits and for Variable Sampling Plans," SCR-607, March, 1963.

[42] Davidson, S. L. (Westinghouse) and Kramer, W. R. (Westinghouse), "Reference Core Report - Vantage 5 Fuel Assembly," WCAP-10444-P-A, dated September, 1985.

[43] Freidland, A. J. (Westinghouse), "Revised Thermal Design Procedure," Revision 2, dated April, 1992, Thermal-Hydraulic Engineering Services Manual, TR-90-0023 W08, Section 4.3.7.

[44] Ellenberger, S. L. (Westinghouse) et al, "Design Bases for the Thermal Overpower ΔT and Thermal Overtemperature ΔT Trip Functions," WCAP-8745-P-A, September, 1986.

[45] Friedland, A. J. (Westinghouse) and Ray, S. (Westinghouse), "Revised Thermal Design Procedure," WCAP-11397-P-A, dated April, 1989.

[46] Ellenberger, S. L. (Westinghouse) et al, "Design Bases for the Thermal Overpower ΔT and Thermal Overtemperature ΔT Trip Functions," WCAP-8745-P-A, September, 1986.

[47] Ibid.

[48] Ibid, page 2-2.

[49] Ibid, page 3-5.

[50] Miller, J. V., (Ed.), "Improved Analytical Models Used in Westinghouse Fuel Rod Design Computations," WCAP-8720, October, 1976.

[51] Wesley, D. A. and Firth, K. J., "TACO3 - Fuel Pin Thermal Analysis Computer Code," BAW-10162P-A, Babcock & Wilcox Fuel Company, October, 1989.

[52] "VIPRE-01: A Thermal-Hydraulic Code for Reactor Cores," Battelle, Pacific Northwest Laboratories, Richland, Washington, EPRI NP-2511-CCM-A.